Heavier Alkaline Earth and heterobimetallic s-block "ate" complexes of a di(amido)siloxane ligand: solid-state structure and dynamic solution-phase behaviour

Supplementary information

Matthew D. Haynes,[a] Andrea O'Reilly,[b] Alice J. M. Poole,[a] Aisling F. Roper,[a] Stefan Thum,[c] Louis J. Morris,[a] Martyn P. Coles,*[b] J. Robin Fulton,*[b] Sjoerd Harder,[c] Zoë R. Turner,*[a] and Dermot O'Hare,*[a]

a: Chemistry Research Laboratory, Department of Chemistry, University of Oxford, Mansfield Road, Oxford, OX1 3TA, United Kingdom. Email: zoe.turner@earth.ox.ac.uk, dermot.ohare@chem.ox.ac.uk

b: School of Chemical and Physical Sciences, Victoria University of Wellington, PO Box 600, Wellington 6012, New Zealand. E-mail: martyn.coles@vuw.ac.nz, j.robin.fulton@vuw.ac.nz

c: Universität Erlangen-Nürnberg, Egerlandstrasse 1, 91058 Erlangen, Germany; Email: sjoerd.harder@fau.de

Table of Contents

I. General Considerations

All manipulations were carried out using standard Schlenk line or drybox techniques under an atmosphere of dinitrogen or argon. Protio solvents were degassed by sparging with dinitrogen, dried by passing through a column of activated sieves (pentane, hexane, toluene, benzene) and stored over potassium mirrors, or distilled from sodium metal (thf) and stored over activated 4 Å molecular sieves, or distilled from sodium-potassium alloy (diethyl ether) and stored over a potassium mirror. Deuterated solvents were dried over potassium (C_6D_6, C_7D_8) or CaH_2 (C_4D_8O), distilled under reduced pressure and freeze-pump-thaw degassed three times prior to use.

^{1}H NMR spectra were recorded at 298 K, unless otherwise stated, on Bruker AVIII 400 nanobay or Bruker AVIII 500 or Bruker NEO 600 spectrometers. ^{13}C{^{1}H} spectra were recorded on the same spectrometers at operating frequencies of 100, 125 and 151 MHz respectively, as were ^{29}Si spectra at operating frequencies of 80, 99 and 119 MHz respectively. Two dimensional ^{1}H-^{1}H, ^{13}C-^{1}H & ^{29}Si-^{1}H correlation experiments were used, when necessary, to confirm ^{1}H and ^{13}C assignments. All NMR spectra were referenced internally to residual protio solvent (^{1}H) or solvent (^{13}C) resonances and are reported relative to tetramethylsilane (δ = 0 ppm). Chemical shifts are quoted in δ (ppm) and coupling constants in Hertz. Samples were prepared in a glove box under a dinitrogen atmosphere as pellets pressed with anhydrous potassium bromide, which was dried above 150 °C at 10^{-6} mbar for 24 hours prior to use.

Crystals were mounted on MiTeGen MicroMounts using perfluoropolyether oil and rapidly transferred to a goniometer head on a diffractometer fitted with an Oxford Cryostream open-flow nitrogen cooling device.[1] Data collections were carried out at 150 K using an Oxford Diffraction Supernova diffractometer using mirror-monochromated Cu Kα radiation (λ = 1.54178 Å) or Mo Kα radiation (λ = 0.71073 Å) and the data processed using CrysAlisPro.[2] The structures were solved using direct methods (SIR-92),[3] a flipping algorithm (SUPERFLIP),[4] or intrinsic phasing (SHELXT)[5] and refined by full-matrix least squares procedures using the WinGX software suite,[6] CRYSTALS,[7] or the SHELXL[8] refinement package implemented in Olex2.[9] Where required, interplanar distances and angles were calculated using Olex2[9] and molecular structures were generated using Ortep (with ellipsoids shown at 30% probability).[10]

FTIR spectra were measured using a Nicolet iS5 ThermoScientific spectrometer, with a background spectrum run prior to the sample and subtracted from the sample spectrum.

Elemental analyses were carried out at London Metropolitan University and Friedrich-Alexander Universität Erlangen-Nürnberg.

$^{NON\text{-}Dipp}LH_2$;[11] [($^{NON\text{-}Dipp}$L)Mg]$_2$;[12] [AeN"$_2$]$_2$ (Ae = Ca and Sr);[13] [BaN"$_2$]$_2$;[14] and [AeN"$_3$K] (Ae = Ca and Sr),[15] were prepared according to published literature procedures. [MgN"$_2$]$_2$ was purchased from Sigma-Aldrich and used as received.

II Experimental details and characterising data

[{($^{NON\text{-}Dipp}$L)Mg}$_2$(thf)] (1·thf)

Crystallisation of a sample of [($^{NON\text{-}Dipp}$L)Mg]$_2$ (129.2 mg, 0.12 mmol) by the slow evaporation of a thf/hexane solution at room temperature affords [{($^{NON\text{-}Dipp}$L)Mg}$_2$(thf)] (**1·thf**). Yield = 132.2 mg, 99%.

^{1}H NMR (500 MHz, C_6D_6:thf-d_8, 323K) δ 7.07 (d, J = 7.6, 4H, C_6H_3), 6.95 (t, J = 7.6, 2H, C_6H_3), 3.88 (br. s, 4H, C*H*Me$_2$), 3.56 (br. s, 4H, thf-*H*), 1.45 (br. s, 4H, thf-*H*), 1.33 (d, J = 6.9, 12H, CH*Me$_2$*), 1.02 (br. s, 12H, CH*Me$_2$*), 0.40 (br. s, 12H, Si*Me$_2$*). ^{13}C{^{1}H} NMR (126 MHz, C_6D_6:thf-d_8, 323K) δ 147.6, 144.5, 123.8, 121.3 (*C$_6$*H$_3$), 67.9 (thf-*C*), 27.6 (*C*HMe$_2$), 26.1 (thf-*C*), 25.8, 25.0 (CH*Me$_2$*), 3.8 (Si*Me$_2$*).

[($^{NON\text{-}Dipp}$L)Mg(thf)]$_2$ (1·thf$_2$)

Crystallisation of a sample of [($^{NON\text{-}Dipp}$L)Mg]$_2$ (125.2 mg, 0.12 mmol) by the slow evaporation of a thf solution at room temperature affords [($^{NON\text{-}Dipp}$L)Mg(thf)]$_2$ (**1·thf$_2$**). Yield = 90.2 mg, 65%.

^{1}H NMR (500 MHz, C_6D_6:thf-d_8, 333K): δ 7.01 (d, J = 7.6, 4H, C_6H_3), 6.88 (t, J = 7.6, 2H, C_6H_3), 3.89 (br. s, 4H, C*H*Me$_2$), 3.55 (br. s, 8H, thf-*H*), 1.50 (br. s, 8H, thf-*H*), 1.27 (br. d, 12H, CH*Me$_2$*), 1.01 (br. s, 12H, CH*Me$_2$*), 0.41 (br. s, 12H, Si*Me$_2$*). ^{13}C{^{1}H} NMR (126 MHz, C_6D_6:thf-d_8, 333K) δ 148.4, 144.7, 123.8, 121.1 (*C$_6$*H$_3$), 67.8 (thf-*C*), 27.5 (*C*HMe$_2$), 25.9 (thf-*C*), 25.9 (CH*Me$_2$*), 3.9 (Si*Me$_2$*).

[($^{NON\text{-}Dipp}$L)Ca]$_2$ (2)

<u>UK (Oxford) and Germany (Erlangen) procedure</u>

A solution of $^{NON\text{-}Dipp}$LH$_2$ (500 mg, 1.03 mmol, 2 eq.) in *n*-hexane (2.5 mL) was layered over a solution of [Ca{N(SiMe$_3$)$_2$}$_2$]$_2$ (372 mg, 0.52 mmol, 1 eq.) in *n*-hexane (2.5 mL). The reaction mixture was left to stand for 16 hours, resulting in the formation of colourless crystals. The solution was decanted and the crystalline solid washed with *n*-pentane (3 x 0.5 mL), then dried *in vacuo* for 1 hour. [($^{NON\text{-}Dipp}$L)Ca]$_2$·(C$_6$H$_{14}$) (383 mg, 0.34 mmol, 65% (**2**)) was isolated as a colourless crystalline solid. IR (KBr): 2963, 2928, 2866, 1424, 1254, 1038, 959, 788 cm^{-1}. Anal. calcd. for $C_{56}H_{92}Ca_2N_4O_2Si_4$·($C_6H_{14}$): C, 65.78; H, 9.44; N, 4.95. Found: C, 65.52; H, 9.29; N, 4.92. Colourless single crystals of **2** suitable for X-ray diffraction studies were grown by conducting the reaction on a smaller scale (25 mg $^{NON\text{-}Dipp}$LH$_2$) in benzene (0.5 mL) or *n*-hexane (0.5 mL).

Dissolving **2** in thf-d_8 resulted in conversion to [($^{NON\text{-}Dipp}$L)Ca(thf)$_2$] (**5**), which could be characterised by multinuclear NMR spectroscopy.^{1}H NMR (C$_4$D$_8$O, 298 K, 600 MHz): δ (ppm) = 6.83 (d, $^3J_{H\text{-}H}$ = 7.5 Hz, 8H, 3,5-C$_6$***H$_3$***), 6.49 (t, $^3J_{H\text{-}H}$ = 7.5 Hz, 4H, 4-C$_6$***H$_3$***), 3.95 (hept, $^3J_{H\text{-}H}$ = 7.0 Hz, 8H, C***H***Me$_2$), 1.12 (d, $^3J_{H\text{-}H}$ = 7.0 Hz, 48H, CH(C***H$_3$***)$_2$), 0.13 (s, 24H, Si(C***H$_3$***)$_2$). ^{13}C{^{1}H} NMR (C$_4$D$_8$O, 298 K, 151 MHz): δ (ppm) = 151.23 (1-***C$_6$***H$_3$), 142.37 (2,6-***C$_6$***H$_3$), 123.04 (3,5-***C$_6$***H$_3$), 117.28 (4-***C$_6$***H$_3$), 27.74 (***C***HMe$_2$), 25.77 (CH(***C***H$_3$)$_2$), 4.89 (Si(***C***H$_3$)$_2$). ^{29}Si NMR (C$_4$D$_8$O, 298 K, 119 MHz): δ (ppm) = –19.77 (O***Si***Me$_2$N).

NZ (Wellington) procedure

A benzene solution of $^{NON\text{-}Dipp}LH_2$ (408.8 mg, 0.84 mmol) was added to a solution of $[Ca\{N(SiMe_3)_2\}_2]_2$ (304.2 mg, 0.84 mmol) in benzene while stirring at room temperature. The reaction mixture was stirred for 2 hours to give a white suspension. The suspension was allowed to settle, and the white solid was isolated. The solid was redissolved in hot benzene colourless crystals of $[(^{NON\text{-}Dipp}L)Ca]_2$ (**2**) were obtained by slow evaporation of the solvent. Yield = 289.4 mg, 66%.

^{1}H NMR (500 MHz, C_6D_6:thf-d_8 (~5:1)): δ 7.18 (d, J = 7.4, 4H, C_6H_3) 6.92 (t, J = 7.4, 2H, C_6H_3), 4.12 (sept, J = 6.9, 4H, C*H*Me$_2$), 1.30 (d, J = 6.9, 24H, CH*Me$_2$*), 0.44 (s, 12H, Si*Me$_2$*). ^{13}C{^{1}H} NMR (126 MHz, C_6D_6:thf-d_8 (~5:1)): δ 150.2, 141.8, 122.9, 117.5 (C_6H$_3$), 27.3 (*C*HMe$_2$), 25.5 (CH*Me$_2$*), 4.8 (Si*Me$_2$*). IR (solid, cm^{-1}): 2959 (s), 2868 (m), 1620 (w), 1459 (m), 1382 (m), 1254 (s), 1043 (s), 908 (s), 788 (s), 685 (w). Anal. Calcd. for $C_{56}H_{92}Ca_2N_4O_2Si_4$ (*1045.874*): C 64.31, H 8.87, N 5.36 %; Found: C 62.61, H 8.76, N 5.35 %.

$[(^{NON\text{-}Dipp}L)Sr]_2$ (3)

UK (Oxford) and Germany (Erlangen) procedure

A solution of $^{NON\text{-}Dipp}LH_2$ (500 mg, 1.03 mmol, 2 eq.) in *n*-hexane (2.5 mL) was carefully layered over a solution of $[Sr\{N(SiMe_3)_2\}_2]_2$ (422 mg, 0.52 mmol, 1 eq.) in *n*-hexane (5 mL). The reaction mixture was left to stand for 16 hours, resulting in the formation of colourless crystals. The solution was decanted and the crystalline solid washed with *n*-pentane (3 x 0.5 mL), then dried *in vacuo* for 1 hour. $[^{NON\text{-}Dipp}LSr]_2\cdot(C_6H_{14})$ (362 mg, 0.29 mmol, 57% (**3**)) was isolated as a colourless crystalline solid. IR (KBr): 3055, 2960, 2866, 1587, 1421, 1259, 990, 781, 686 cm^{-1}. Anal. calcd. for $C_{56}H_{92}Sr_2N_4O_2Si_4\cdot(C_6H_{14})$: C, 60.97; H, 8.77; N, 4.51. Found: C, 60.50; H, 8.47; N, 4.59. Colourless single crystals of **20** suitable for X-ray diffraction studies were grown by conducting the reaction on a smaller scale (25 mg $^{NON\text{-}Dipp}LH_2$) in benzene (0.5 mL) or *n*-hexane (0.5 mL).

Dissolving **3** in thf-d_8 resulted in conversion to $[(^{NON\text{-}Dipp}L)Sr(thf)_3]$ (**6**), which could be characterised by multinuclear NMR spectroscopy. ^{1}H NMR (C_4D_8O, 298 K, 600 MHz): δ (ppm) = 6.80 (d, $^3J_{H\text{-}H}$ = 7.5 Hz, 8H, 3,5-C_6***H$_3$***), 6.42 (t, $^3J_{H\text{-}H}$ = 7.5 Hz, 4H, 4-C_6***H$_3$***), 3.98 (hept, $^3J_{H\text{-}H}$ = 6.9 Hz, 8H, C***H***Me$_2$), 1.13 (d, $^3J_{H\text{-}H}$ = 6.9 Hz, 48H, CH(C***H$_3$***)$_2$), 0.10 (s, 24H, Si(C***H$_3$***)$_2$). ^{13}C{^{1}H} NMR (C_4D_8O, 298 K, 151 MHz): δ (ppm) = 153.62 (1-***C$_6$***H$_3$), 142.10 (2,6-***C$_6$***H$_3$), 123.06 (3,5-***C$_6$***H$_3$), 116.09 (4-***C$_6$***H$_3$), 27.57 (***C***HMe$_2$), 25.90 (CH(***C***H$_3$)$_2$), 5.17 (Si(***C***H$_3$)$_2$). ^{29}Si NMR (C_4D_8O, 298 K, 119 MHz): δ (ppm) = –23.74 (O***Si***Me$_2$N).

NZ (Wellington) procedure

A solution of $^{NON\text{-}Dipp}LH_2$ (29.3 mg, 0.06 mmol) in toluene was added to a solution of $[Sr\{N(SiMe_3)_2\}_2]_2$ (24.7 mg, 0.06 mmol) in benzene while stirring at room temperature. The reaction mixture was stirred for 2 hours and filtered through celite. The solvent was reduced *in vacuo* and colourless crystals of $[(^{NON\text{-}Dipp}L)Sr]_2$ were obtained by slow evaporation at room temperature. Yield = 26.2 mg, 77%.

^{1}H NMR (500 MHz, C_6D_6:thf-d_8 (~5:1)): δ 7.14 (d, J = 7.4, 4H, C_6H_3), 6.84 (t, J = 7.4, 2H, C_6H_3), 4.15 (sept, J = 6.9, 4H, C*H*Me$_2$), 1.32 (d, J = 6.9, 24H, CH*Me$_2$*), 0.43 (s, 12H, Si*Me$_2$*). ^{13}C{^{1}H} NMR (126 MHz, C_6D_6:thf-d_8 (~5:1)): δ 153.0, 141.6, 122.9, 116.1 (C_6H$_3$), 27.2 (*C*HMe$_2$), 25.6 (CH*Me$_2$*), 5.1 (Si*Me$_2$*). IR (solid, cm^{-1}): 2950 (m), 2858 (m), 1582 (w), 1452 (m), 1415 (s), 1305 (m), 1248 (s), 1054 (m), 983 (s), 932 (s), 684 (s), 670 (m), 445 (w).

[($^{NON\text{-}Dipp}$L)Ba]$_2$ (4 and 4a)

UK (Oxford) and Germany (Erlangen) procedure

A solution of $^{NON\text{-}Dipp}LH_2$ (500 mg, 1.03 mmol, 2 eq.) in *n*-hexane (2.5 mL) was carefully layered over a solution of [Ba{N(SiMe$_3$)$_2$}$_2$]$_2$ (473 mg, 0.52 mmol, 1 eq.) in *n*-hexane (5 mL). The reaction mixture was left to stand for 48 hours, resulting in the formation of large colourless crystals. The solution was decanted and the crystals washed with cold *n*-pentane (0.5 mL), then dried *in vacuo* for 1 hour. [($^{NON\text{-}Dipp}$L)Ba]$_2$ (302 mg, 0.25 mmol, 48% (**4a**)) was isolated as a colourless crystalline solid. IR (KBr): 3043, 2957, 2863, 1411, 1341, 1249, 995, 771 cm^{-1}. Anal. calcd. for $C_{56}H_{92}Ba_2N_4O_2Si_4$: C, 54.23; H, 7.48; N, 4.52. Found: C, 54.20; H, 7.52; N, 4.46. Colourless single crystals of [($^{NON\text{-}Dipp}$L)Ba]$_2$ suitable for X-ray diffraction studies were grown by conducting the reaction on a smaller scale (25 mg $^{NON\text{-}Dipp}LH_2$) in benzene (0.5 mL) or *n*-hexane (0.5 mL) (**4** and **4a** respectively).

Dissolving **4** in thf-d_8 resulted in conversion to [($^{NON\text{-}Dipp}$L)Ba(thf)$_3$] (**7**), which could be characterised by multinuclear NMR spectroscopy. ^{1}H NMR (C_4D_8O, 298 K, 600 MHz): δ (ppm) = 6.80 (d, $^3J_{H\text{-}H}$ = 7.5 Hz, 8H, 3,5-C$_6$***H$_3$***), 6.39 (t, $^3J_{H\text{-}H}$ = 7.5 Hz, 4H, 4-C$_6$***H$_3$***), 3.97 (hept, $^3J_{H\text{-}H}$ = 7.0 Hz, 8H, C***H***Me$_2$), 1.12 (d, $^3J_{H\text{-}H}$ = 7.0 Hz, 48H, CH(C***H$_3$***)$_2$), 0.10 (s, 24H, Si(C***H$_3$***)$_2$). ^{13}C{^{1}H} NMR (C_4D_8O, 298 K, 151 MHz): δ (ppm) = 152.43 (1-***C$_6$***H$_3$), 141.60 (2,6-***C$_6$***H$_3$), 123.10 (3,5-***C$_6$***H$_3$), 115.63 (4-***C$_6$***H$_3$), 27.50 (***C***HMe$_2$), 25.99 (CH(***C***H$_3$)$_2$), 5.48 (Si(***C***H$_3$)$_2$). ^{29}Si NMR (C_4D_8O, 298 K, 119 MHz): δ (ppm) = –26.22 (O***Si***Me$_2$N).

NZ (Wellington) procedure

A solution of $^{NON\text{-}Dipp}LH_2$ (60.7 mg, 0.13 mmol) in benzene was added to a solution of [Ba{N(SiMe$_3$)$_2$}$_2$]$_2$ (57.4 mg, 0.13 mmol) in benzene while stirring at room temperature. The reaction mixture was stirred for 2 hours and filtered through celite. The solvent was reduced *in vacuo* and colourless crystals of [($^{NON\text{-}Dipp}$L)Ba]$_2$ (**4**) were obtained by slow evaporation at room temperature. Yield = 35.4 mg, 44%.

^{1}H NMR (500 MHz, C_6D_6:thf-d_8 (~5:1)) δ 7.14 (d, *J* = 7.4, 4H, C$_6$*H$_3$*), 6.81 (t, *J* = 7.4, 2H, C$_6$*H$_3$*), 4.15 (sept, *J* = 6.9, 4H, C*H*Me$_2$), 1.31 (d, *J* = 6.9, 24H, CH*Me$_2$*), 0.48 (s, 12H, Si*Me$_2$*). ^{13}C{^{1}H} NMR (126 MHz, C_6D_6:thf-d_8 (~5:1)) δ 151.5, 141.0, 123.0, 115.6 (*C$_6$*H$_3$), 27.1 (*C*HMe$_2$), 25.7 (CH*Me$_2$*), 5.4 (Si*Me$_2$*). IR (solid, cm^{-1}): 2952 (s), 2861 (m) 1647 (m), 1434 (s), 1253 (m), 1041 (m), 906 (m), 761 (s).

* Integration of the thf proton resonances indicate partial loss of coordinated thf during sample preparation.

[($^{NON\text{-}Dipp}$L)Ca(thf)$_2$] (5)

Crystallisation of [($^{NON\text{-}Dipp}$L)Ca]$_2$ (30.2 mg) from thf yields colourless crystals of [($^{NON\text{-}Dipp}$L)Ca(thf)$_2$] (**5**). Isolated yield 37.2 mg, 97%.

^{1}H NMR (500 MHz, C_6D_6:thf-d_8 (~5:1)): *δ* 7.18 (d, *J* = 7.4, 4H, C$_6$*H$_3$*) 6.91 (t, *J* = 7.4, 2H, C$_6$*H$_3$*), 4.12 (sept, *J* = 6.9, 4H, C*H*Me$_2$), 3.55 (m, 8H, thf-*H*), 1.43 (m, 8H, thf-*H*), 1.29 (d, *J* = 6.9, 24H, CH*Me$_2$*), 0.43 (s, 12H, Si*Me$_2$*). ^{13}C{^{1}H} NMR (126 MHz, C_6D_6:thf-d_8 (~5:1)): *δ* 150.2, 141.8, 122.9, 117.5 (*C$_6$*H$_3$), 67.9 (thf-*C*), 27.3 (*C*HMe$_2$), 25.8 (thf-*C*), 25.5 (CH*Me$_2$*), 4.8 (Si*Me$_2$*). Accurate elemental analysis could not be obtained. Best result: Anal. Calcd. for $C_{36}H_{62}CaN_2O_3Si_2$ (*667.151*): C 64.81, H 9.37, N 4.20 %; Found: C 62.61, H 8.76, N 5.35 %.

[($^{NON\text{-}Dipp}$L)Sr(thf)$_3$] (6)

Crystallisation of [($^{NON\text{-}Dipp}$L)Sr]$_2$ (46.2 mg) from thf yields colourless crystals of [($^{NON\text{-}Dipp}$L)Sr(thf)$_3$] (**6**). Isolated yield 53.0 mg, 83%.

^{1}H NMR (500 MHz, C_6D_6:thf-d_8 (~5:1)): δ 7.14 (d, J = 7.4, 4H, C_6H_3), 7.00 (t, J = 7.4, 2H, C_6H_3), 4.12 (sept, J = 6.9, 4H, C*H*Me$_2$), 3.54 (m, 8H, thf-*H*),* 1.46 (m, 8H, thf-*H*),* 1.28 (d, J = 6.9, 24H, CH*Me$_2$*), 0.38 (s, 12H, Si*Me$_2$*). ^{13}C{^{1}H} NMR (126 MHz, C_6D_6:thf-d_8 (~5:1)): δ 153.0, 141.6, 122.9, 116.0 (C_6H_3), 67.8 (thf-*C*), 27.1 (*C*HMe$_2$), 25.8 (thf-*C*), 25.6 (CH*Me$_2$*), 5.0 (Si*Me$_2$*). Anal. Calcd. for $C_{40}H_{70}N_2O_4Si_2Sr$ (*786.8*): C 61.06, H 8.97, N 3.56 %; Found: C 61.41, H 8.40, N 3.19 %.

* Integration of the thf proton resonances indicate partial loss of coordinated thf during sample preparation.

[($^{NON\text{-}Dipp}$L)Ba(thf)$_3$] (7)

Crystallisation of [($^{NON\text{-}Dipp}$L)Ba]$_2$ (11.4 mg) from THF yields colourless crystals of [($^{NON\text{-}Dipp}$L)Ba(thf)$_3$] (**7**). Isolated yield 11.7 mg, 76%,

^{1}H NMR (500 MHz, C_6D_6:thf-d_8 (~5:1)) δ 7.08 (d, J = 7.4, 4H, C_6H_3), 6.74 (d, J = 7.4, 2H, C_6H_3), 4.12 (sept, 4H, J = 6.9, C*H*Me$_2$), 3.54 (m, 8H, thf-*H*),* 1.46 (m, 8H, thf-*H*),* 1.27 (d, 24H, J = 6.9, CH*Me$_2$*), 0.42 (s, 12H, Si*Me$_2$*). Anal. Calcd. for $C_{32}H_{54}BaN_2O_2Si_2$ (*692.293*)*: C 55.52, H 7.86, N 4.05 %; Found: C 55.49, H 7.49, N 3.65 %.

* Calculated for mono-solvate [($^{NON\text{-}Dipp}$L)Ba(thf)] from partial loss of coordinated thf.

[Ba{N(SiMe$_3$)$_2$}$_3$K]

A Schlenk flask was charged with [Ba{N(SiMe$_3$)$_2$}$_2$]$_2$ (0.250g, 0.27 mmol, 1 eq.) and KN(SiMe$_3$)$_2$ (0.119 mg, 0.55 mmol, 2 eq.). Toluene (2 mL) and hexane (3 mL) were added, and the reaction mixture stirred for 1 hour. Storage at –30 °C for 16 hours resulted in the growth of colourless crystals, which were isolated by filtration, washed with *n*-hexane (3 x 1 mL) and dried *in vacuo* for 1 hour. [Ba{N(SiMe$_3$)$_2$}$_3$K] (216 mg, 0.33 mmol, 60%) was isolated as a white crystalline solid. ^{1}H NMR (C_6D_6, 298 K, 400MHz): δ (ppm) = 0.21 (s, 54 H, N{Si(C***H$_3$***)$_3$}$_2$).^{13}C NMR (C_6D_6, 298 K, 151 MHz): δ (ppm) = 6.39 (N{Si(***C***H$_3$)$_3$}$_2$). ^{29}Si NMR (C_6D_6, 298 K, 119 MHz): δ (ppm) = –17.43 (N(***Si***Me$_3$)$_2$). Anal. Calcd. for $C_{18}H_{54}BaKN_3Si_6$: C, 32.88; H, 8.28; N, 6.39. Found: C, 32.73; H, 8.06; N, 6.08. X-ray crystallographic data could not be obtained due to the rapid degradation of crystalline samples of [Ba{N(SiMe$_3$)$_2$}$_3$K] under a non-inert atmosphere.

Synthesis of [($^{NNO\text{-}Dipp}$L)Mg{μ-N(SiMe$_3$)$_2$}K]$_n$ (8)

A solution of KN(SiMe$_3$) (95.8 mg, 0.48 mmol) in toluene was added to a suspension of [($^{NON\text{-}Dipp}$L)Mg]$_2$ (248.1 mg, 0.24 mmol) in toluene. The reaction mixture was stirred at 60 °C for 2 days to afford a pale-yellow solution. The solution was filtered through celite, and the solvent was reduced *in vacuo*. Colourless crystals of [($^{NNO\text{-}Dipp}$L)Mg{μ-N(SiMe$_3$)$_2$}K]$_n$ (**8**) were obtained by slow evaporation at room temperature. Yield = 194.5 mg, 58%.

^{1}H NMR (500 MHz, C_7D_8, 333 K): δ 7.12 (m, 4H, C_6H_3), 7.08 (m, 1H, C_6H_3), 6.92 (m, 1H, C_6H_3), 4.16 (sept, J = 6.9, 2H, C*H*Me$_2$), 4.01 (sept, J = 6.9, 2H, C*H*Me$_2$), 1.38 (d, J = 6.9, 6H, CH*Me$_2$*), 1.36 (d, J = 6.9, 6H, CH*Me$_2$*), 1.31 (m, 12H, CH*Me$_2$*), 0.16 (s, 6H, Si*Me$_2$*), 0.04 (s, 6H, Si*Me$_2$*), 0.05 (s, 18H, NSi*Me$_3$*). ^{13}C{^{1}H} NMR (126 MHz, C_7D_8, 333 K): δ 149.0, 147.6, 145.5, 145.4, 124.5, 124.2, 123.6, 120.7 (C_6H_3), 28.4 (CH*Me$_2$*), 28.1, 27.3 (*C*HMe$_2$), 26.2, 25.3.24.6 (CH*Me$_2$*), 6.0 (NSi*Me$_3$*), 4.6, 3.9 (Si*Me$_2$*).

[($^{NON\text{-}Dipp}$L)Ca{μ-N(SiMe$_3$)$_2$}K]$_n$ (9)

A Schlenk flask was charged with [Ca{N(SiMe$_3$)$_2$}$_3$K] (1.00g, 1.78mmol, 1 eq.) and $^{NON\text{-}Dipp}$LH$_2$ (864 mg, 1.78 mmol, 1 eq.). Toluene (8 ml) was added, with stirring resulting in the precipitation of a white solid. This redissolved upon gentle heating, with crystallisation then observed upon cooling to room temperature. The crystals were isolated by filtration, washed with *n*-hexane (3 x 1 mL) and dried *in vacuo* for 1 hour. [($^{NON\text{-}Dipp}$L)Ca{μ-N(SiMe$_3$)$_2$}K]$_n$ (620 mg, 0.858 mmol, 48% (**9**)) was isolated as a white crystalline solid. Crystals suitable for an X-ray diffraction study were grown by slow cooling of a saturated benzene solution to room temperature.

^{1}H NMR (C$_7$D$_8$, 343 K, 500 MHz): δ (ppm) = 6.98 (d, $^3J_{H\text{-}H}$ = 9.8 Hz, 4H, 3,5-C$_6$***H$_3$***), 6.65 (br, 2H, 4-C$_6$***H$_3$***), 3.85 (br, 4H, C***H***Me$_2$), 1.29 (d, $^3J_{H\text{-}H}$ = 6.9 Hz, 24H, CH(C***H$_3$***)$_2$), 0.39 (s, 12H, OSi(C***H$_3$***)$_2$N), –0.13 (s, 18H, N{Si(C***H$_3$***)$_3$}$_2$). ^{13}C NMR (C$_7$D$_8$, 343 K, 126 MHz): δ (ppm) = 142.16 (1-***C$_6$***H$_3$), 128.59 (2,6-***C$_6$***H$_3$), 123.37 (3,5-***C$_6$***H$_3$), 116.88 (4-***C$_6$***H$_3$), 28.10 (***C***HMe$_2$), 25.59 (CH(***C***H$_3$)$_2$), 5.90 (N{Si(***C***H$_3$)$_3$}$_2$), 4.74 (OSi(***C***H$_3$)$_2$N). ^{29}Si NMR (C$_7$D$_8$, 343 K, 99 MHz): δ (ppm) = –12.49 (N(***Si***Me$_3$)$_2$), –14.69 (O***Si***Me$_2$N).

^{1}H NMR (C$_4$D$_8$O, 298 K, 600 MHz): δ (ppm) = 6.72 (d, $^3J_{H\text{-}H}$ = 7.5 Hz, 4H, 3,5-C$_6$***H$_3$***), 6.37 (t, $^3J_{H\text{-}H}$ = 7.4 Hz, 2H, 4-C$_6$***H$_3$***), 4.01 (hept, $^3J_{H\text{-}H}$ = 6.4 Hz, 4H, C***H***Me$_2$), 1.17 (d, $^3J_{H\text{-}H}$ = 4.5 Hz, 24H, CH(C***H$_3$***)$_2$), 0.03 (s, 12H, Si(C***H$_3$***)$_2$), –0.31 (s, 18H, N{Si(C***H$_3$***)$_3$}$_2$). ^{13}C NMR (C$_4$D$_8$O, 298 K, 151 MHz): δ (ppm) = 153.67 (1-***C$_6$***H$_3$), 142.97 (2,6-***C$_6$***H$_3$), 122.54 (3,5-***C$_6$***H$_3$), 115.89 (4-***C$_6$***H$_3$), 27.41 (***C***HMe$_2$), 26.47 (CH(***C***H$_3$)$_2$), 6.14 (N{Si(***C***H$_3$)$_3$}$_2$), 5.09 (OSi(***C***H$_3$)$_2$N). ^{29}Si NMR (C$_4$D$_8$O, 298 K, 119 MHz): δ (ppm) = –19.54 (N(***Si***Me$_3$)$_2$), –22.66 (O***Si***Me$_2$N). Anal. Calcd. for C$_{34}$H$_{64}$CaKN$_3$OSi$_4$: C, 56.53; H, 8.93; N, 5.82. Found: C, 56.63; H, 8.92; N, 5.41. IR (KBr): 3049, 2960, 2865, 1581, 1413, 1339, 1250, 1068, 944, 824 cm^{-1}.

[($^{NON\text{-}Dipp}$L)Sr{μ-N(SiMe$_3$)$_2$}K]$_n$ (10)

A Schlenk flask was charged with [Sr{N(SiMe$_3$)$_2$}$_3$K] (300 mg, 0.493 mmol, 1 eq.) and $^{NON\text{-}Dipp}$LH$_2$ (239 mg, 493 mmol, 1 eq.). Toluene (4 ml) was added, with stirring resulting in the precipitation of a white solid. This redissolved upon gentle heating, with crystallisation then observed upon cooling to room temperature. The crystals were isolated by filtration, washed with *n*-hexane (3 x 1 mL) and dried *in vacuo* for 1 hour. [($^{NON\text{-}Dipp}$L)Sr{μ-N(SiMe$_3$)$_2$}K]$_n$ (208 mg, 0.270 mmol, 55% (**10**)) was isolated as a white crystalline solid. Crystals suitable for an X-ray diffraction study were grown by slow cooling of a saturated benzene solution to room temperature.

^{1}H NMR (C$_7$D$_8$, 343 K, 600 MHz): δ (ppm) = 6.95 (d, $^3J_{H\text{-}H}$ = 7.4 Hz, 4H, 3,5-C$_6$***H$_3$***), 6.59 (t, $^3J_{H\text{-}H}$ = 7.4 Hz, 2H, 4-C$_6$***H$_3$***), 3.88 (h, $^3J_{H\text{-}H}$ = 6.7 Hz, 4H, C***H***Me$_2$), 1.27 (d, $^3J_{H\text{-}H}$ = 6.9 Hz, 24H, CH(C***H$_3$***)$_2$), 0.40 (s, 12H, OSi(C***H$_3$***)$_2$N), –0.18 (s, 18H, N(Si(C*H$_3$*)$_3$)$_2$). ^{13}C NMR (C$_7$D$_8$, 343 K, 151 MHz): δ (ppm) = 152.55 (1-***C$_6$***H$_3$), 141.82 (2,6-***C$_6$***H$_3$), 123.20 (3,5-***C$_6$***H$_3$), 115.94 (4-***C$_6$***H$_3$), 27.90 (***C***HMe$_2$), 25.54 (CH(***C***H$_3$)$_2$), 5.93 (N{Si(***C***H$_3$)$_3$}$_2$), 4.71 (OSi(***C***H$_3$)$_2$N).^{29}Si NMR (C$_7$D$_8$, 343 K, 119 MHz): δ (ppm) = –21.88 (O***Si***Me$_2$N), –22.66 (N(***Si***Me$_3$)$_2$).

^{1}H NMR (C$_4$D$_8$O, 298 K, 600 MHz): δ (ppm) = 6.72 (d, $^3J_{H\text{-}H}$ = 7.4 Hz, 4H, 3,5-C$_6$***H$_3$***), 6.32 (t, $^3J_{H\text{-}H}$ = 7.4 Hz, 2H, 4-C$_6$***H$_3$***), 4.03 (hept, $^3J_{H\text{-}H}$ = 6.9 Hz, 4H, C***H***Me$_2$), 1.15 (d, $^3J_{H\text{-}H}$ = 6.9 Hz, 24H, CH(C***H$_3$***)$_2$), 0.02 (s, 12H, OSi(C***H$_3$***)$_2$N), –0.36 (s, 18H, N{Si(C***H$_3$***)$_3$}$_2$). ^{13}C NMR (C$_4$D$_8$O, 298 K, 151 MHz): δ (ppm) = 154.41 (1-***C$_6$***H$_3$), 142.45 (2,6-***C$_6$***H$_3$), 122.55 (3,5-***C$_6$***H$_3$), 115.21 (4-***C$_6$***H$_3$), 27.43 (***C***HMe$_2$), 26.38 (CH(***C***H$_3$)$_2$), 6.27 (N{Si(***C***H$_3$)$_3$}$_2$), 5.30 (OSi(***C***H$_3$)$_2$N). ^{29}Si NMR (C$_4$D$_8$O, 298 K, 119 MHz): δ (ppm) = –17.98 (N(***Si***Me$_3$)$_2$), –25.79 (O***Si***Me$_2$N). Anal. Calcd. for C$_{34}$H$_{64}$SrKN$_3$OSi$_4$: C, 56.53; H, 8.93; N, 5.82. Found: C, 56.63; H, 8.92; N, 5.41. IR (KBr): 3040, 2954, 2866, 1580, 1417, 1249, 1076, 996, 822 cm^{-1}.

[($^{NON\text{-}Dipp}$L)Ba{μ-N(SiMe$_3$)$_2$}K]$_n$ (11)

A Schlenk flask was charged with [Ba{N(SiMe$_3$)$_2$}$_3$K] (300 mg, 0.456 mmol, 1 eq.) and $^{NON\text{-}Dipp}$LH$_2$ (221 mg, 456 mmol, 1 eq.). Toluene (3 ml) was added, and the reaction mixture stirred for 10 minutes. Storage at –30 °C for 16 hours resulted in the growth of colourless crystals, which were isolated by filtration, washed with *n*-hexane (3 x 1 mL) and dried *in vacuo* for 1 hour. [($^{NON\text{-}Dipp}$L)Ba{μ-N(SiMe$_3$)$_2$}K]$_n$ (208 mg, 0.270 mmol, 55% (**11**)) was isolated as a white crystalline solid. Crystals suitable for an X-ray diffraction study were grown by slow cooling of a saturated benzene solution to room temperature.

^{1}H NMR (C$_6$D$_6$, 298 K, 600 MHz): δ (ppm) = 7.00 (d, $^3J_{H\text{-}H}$ = 7.5 Hz, 4H, 3,5-C$_6$***H$_3$***), 6.59 (t, $^3J_{H\text{-}H}$ = 7.5 Hz, 2H, 4-C$_6$***H$_3$***), 3.88 (hept, $^3J_{H\text{-}H}$ = 6.9 Hz, 4H, C***H***Me$_2$), 1.28 (d, $^3J_{H\text{-}H}$ = 6.9 Hz, 24H, CH(C***H$_3$***)$_2$), 0.57 (s, 12H, OSi(C***H$_3$***)$_2$N), -0.15 (s, br, 18H, N{Si(C***H$_3$***)$_3$}$_2$). ^{13}C NMR (C$_6$D$_6$, 298 K, 151 MHz): δ (ppm) = 155.24 (1-***C$_6$***H$_3$), 141.14 (2,6-***C$_6$***H$_3$), 123.53 (3,5-***C$_6$***H$_3$), 114.98 (4-***C$_6$***H$_3$), 27.73 (***C***HMe$_2$), 25.54 (CH(***C***H$_3$)$_2$), 5.09 (N{Si(***C***H$_3$)$_3$}$_2$), 2.65 (OSi(***C***H$_3$)$_2$N). ^{29}Si NMR (C$_6$D$_6$, 298 K, 119 MHz): δ (ppm) = 2.33 (N(***Si***Me$_3$)$_2$), –27.35 ((O***Si***Me$_2$N).

^{1}H NMR (C$_4$D$_8$O, 263 K, 500 MHz): δ = 6.72 (d, $^3J_{H\text{-}H}$ = 7.4 Hz, 4H, 3,5-C$_6$***H$_3$***), 6.27 (t, $^3J_{H\text{-}H}$ = 7.4 Hz, 2H, 4-C$_6$***H$_3$***), 4.08 (hept, $^3J_{H\text{-}H}$ = 6.8 Hz, 4H, C***H***Me$_2$), 1.12 (d, $^3J_{H\text{-}H}$ = 6.9 Hz, 24H, CH(C*H$_3$*)$_2$), 0.03 (s, 12H, OSi(C***H$_3$***)$_2$N), –0.28 (s, 18H, N{Si(C***H$_3$***)$_3$}$_2$) ppm. ^{13}C NMR (C$_4$D$_8$O, 263 K, 125 MHz): δ = 153.86 (1-***C$_6$***H$_3$), 141.77 (2,6-***C$_6$***H$_3$), 122.54 (3,5-***C$_6$***H$_3$), 114.23 (4-***C$_6$***H$_3$), 27.22 (***C***HMe$_2$), 26.41 (CH(***C***H$_3$)$_2$), 6.19 (N{Si(***C***H$_3$)$_3$}$_2$), 5.61 (OSi(***C***H$_3$)$_2$N) ppm. ^{29}Si NMR (C$_4$D$_8$O, 263 K, 99 MHz): δ = –20.32 (N(***Si***Me$_3$)$_2$), –29.29 (O***Si***Me$_2$N) ppm. IR (KBr): 3033, 2955, 2867, 1579, 1415, 1248, 1078, 995, 882 cm^{-1}. Anal. Calcd. for C$_{34}$H$_{64}$BaKN$_3$OSi$_4$: C, 49.82; H, 7.87; N, 5.13 Found: C, 49.42; H, 7.18; N, 4.49.

III NMR Spectra

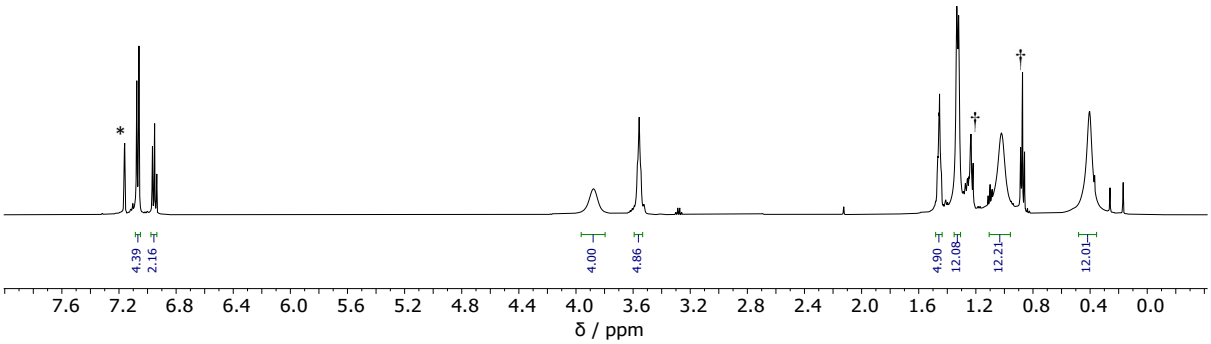

Figure S1 ^{1}H NMR spectrum (C_6D_6:C_4D_8O (~5:1), 323 K, 500 MHz) of [{($^{NON\text{-}Dipp}$L)Mg}(thf)]$_2$ (**1·thf$_2$**). † denotes n-hexane, * denotes residual protio fraction of C_6D_6.

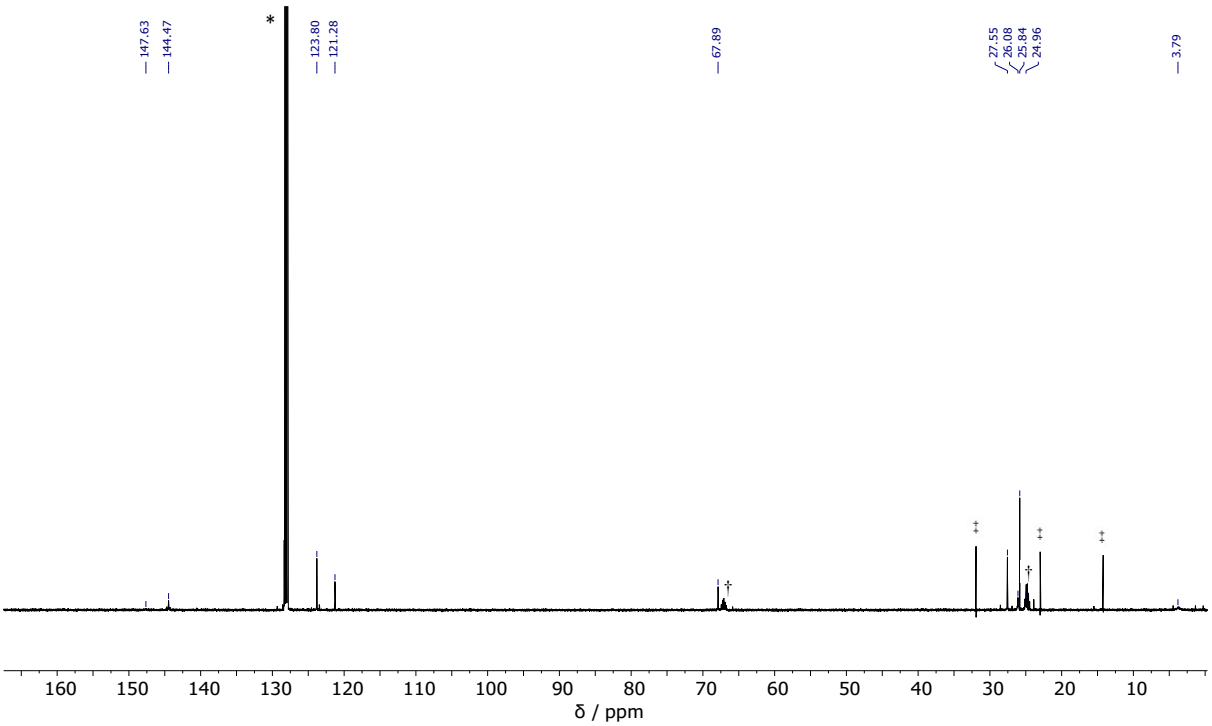

Figure S2 ^{13}C{^{1}H} NMR spectrum (C_6D_6:C_4D_8O (~5:1), 323 K, 126 MHz) of [{($^{NON\text{-}Dipp}$L)Mg}$_2$(thf)] (**1·thf$_2$**). ‡ denotes *n*-hexane, † denotes C_4D_8O, * denotes C_6D_6.

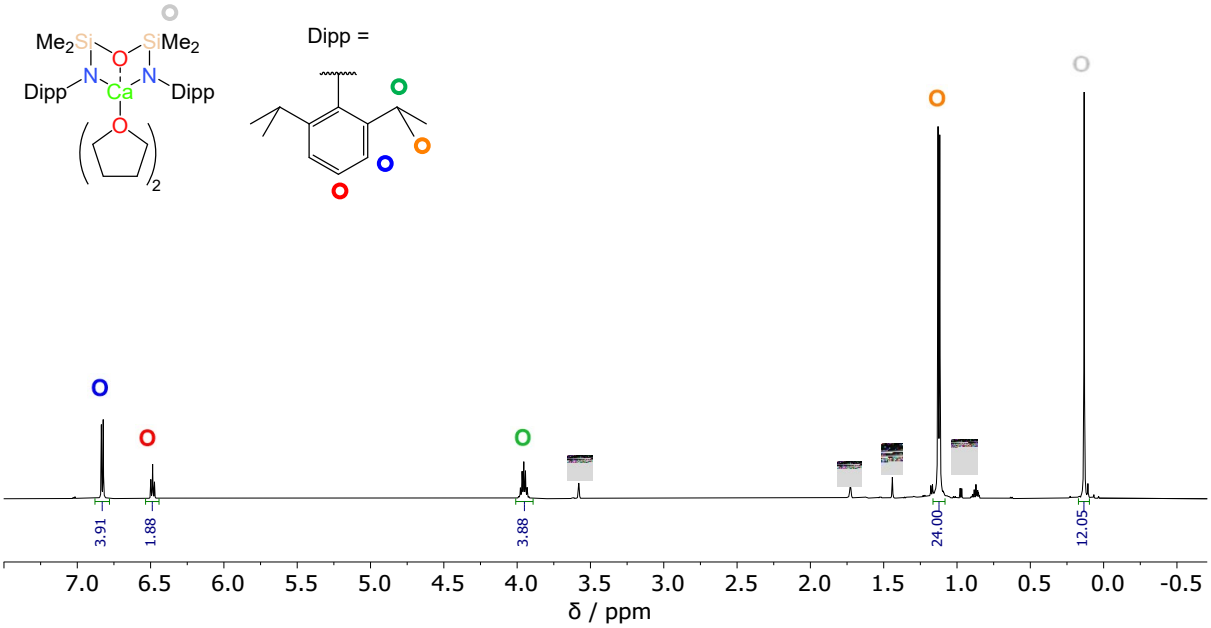

Figure S3 ^{1}H NMR spectrum (C_4D_8O, 298 K, 600 MHz) of [($^{NON\text{-}Dipp}$L)Ca(thf)$_2$] (**5**), formed when [($^{NON\text{-}Dipp}$L)Ca]$_2$ (**2**) is dissolved in thf. ‡ denotes cyclohexane, † denotes *n*-hexane, * denotes residual protio fraction of C_4D_8O.

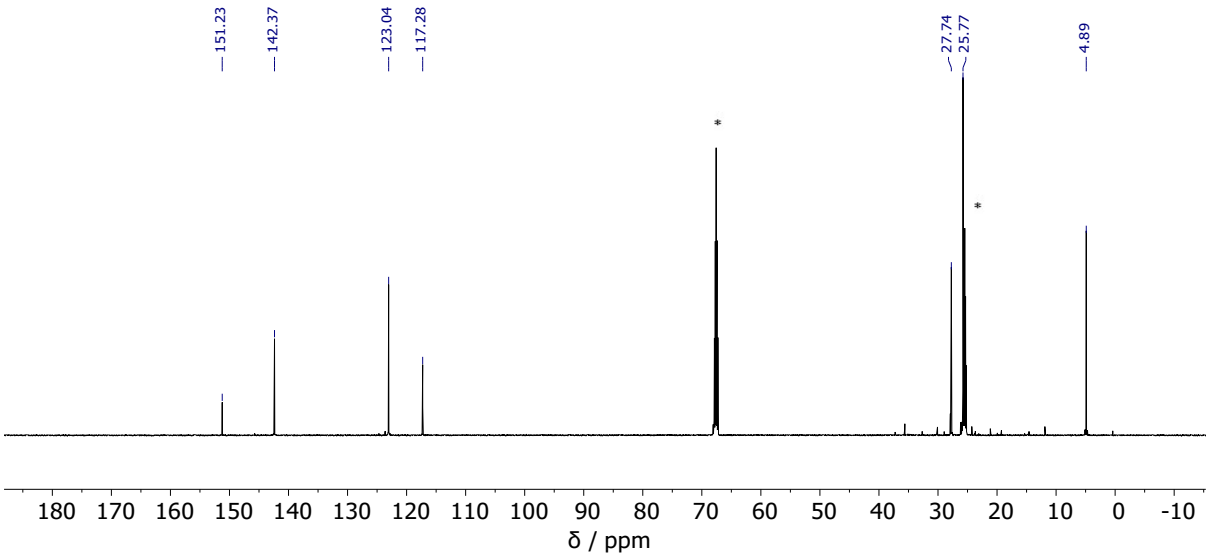

Figure S4 ^{13}C{^{1}H} NMR spectrum (C_4D_8O, 298 K, 151 MHz) of [($^{NON\text{-}Dipp}$L)Ca(thf)$_2$] (**5**), formed when [($^{NON\text{-}Dipp}$L)Ca]$_2$ (**2**) is dissolved in thf. * denotes residual protio fraction of C_4D_8O.

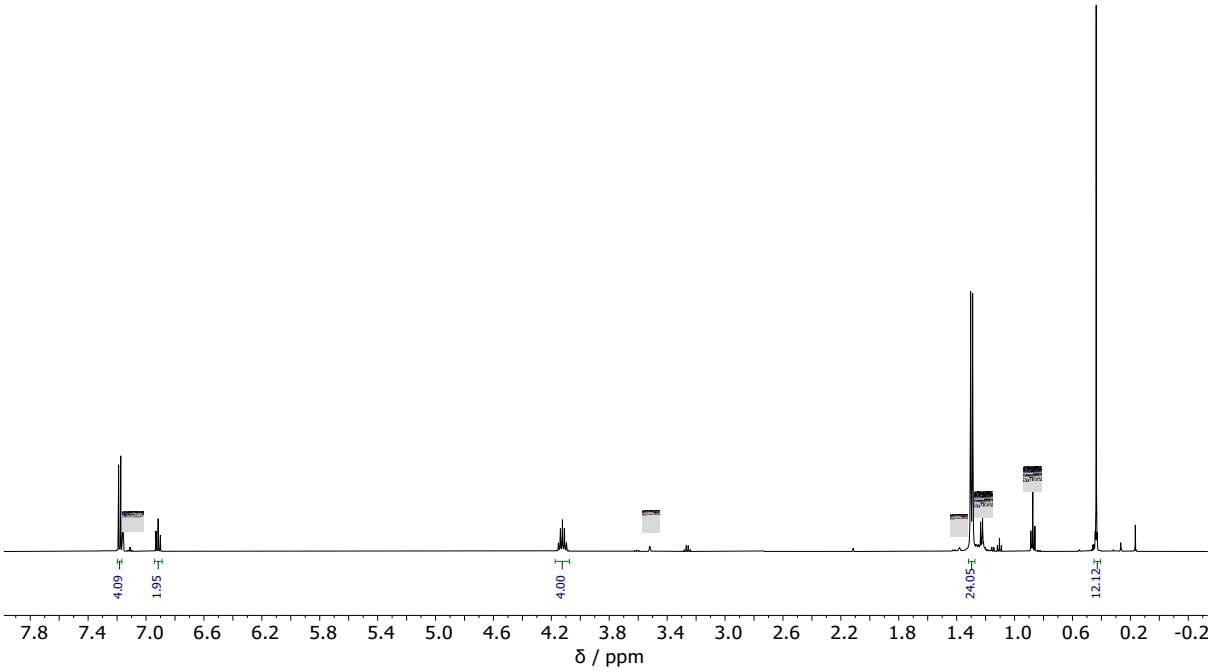

Figure S5 ^{1}H NMR spectrum (C_6D_6:C_4D_8O (~5:1), 298 K, 500 MHz) of [($^{NON\text{-}Dipp}$L)Ca]$_2$ (**2**).
‡ denotes *n*-hexane † and * denote residual protio fractions of C_4D_8O and C_6D_6 respectively.

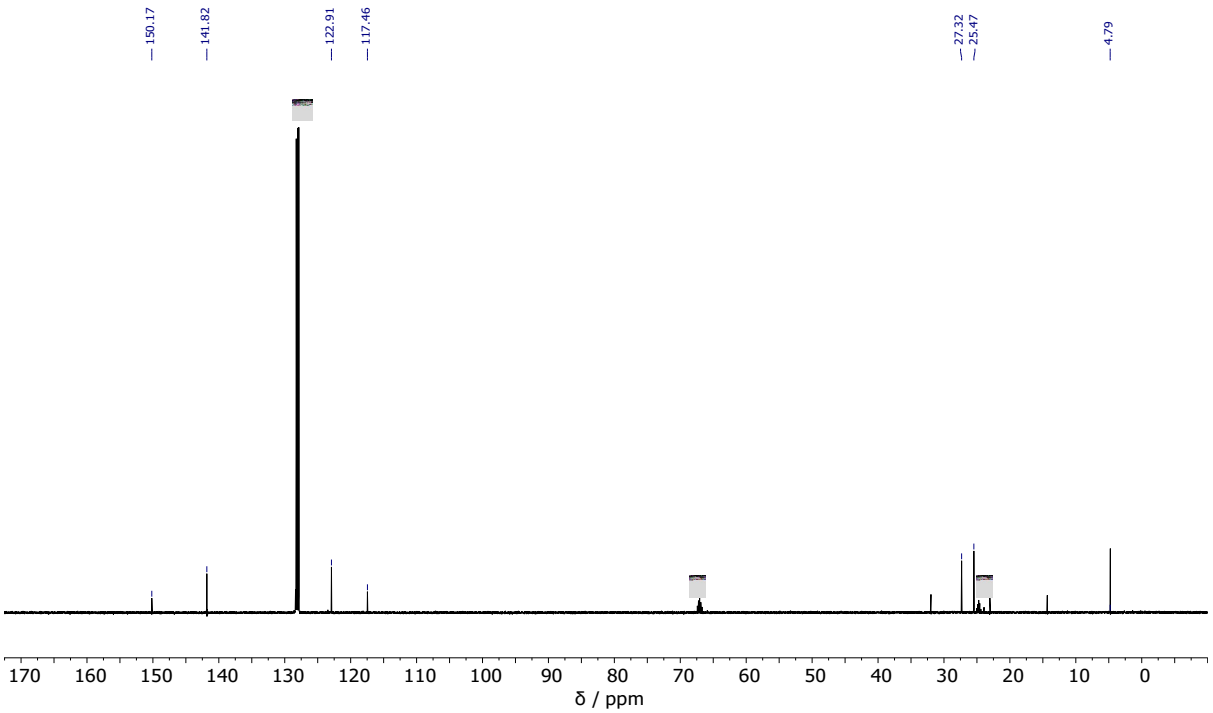

Figure S6 ^{13}C{^{1}H} NMR spectrum (C_6D_6:C_4D_8O (~5:1), 298 K, 126 MHz) of [($^{NON\text{-}Dipp}$L)Ca]$_2$ (**2**).
† and * denote C_4D_8O and C_6D_6 respectively.

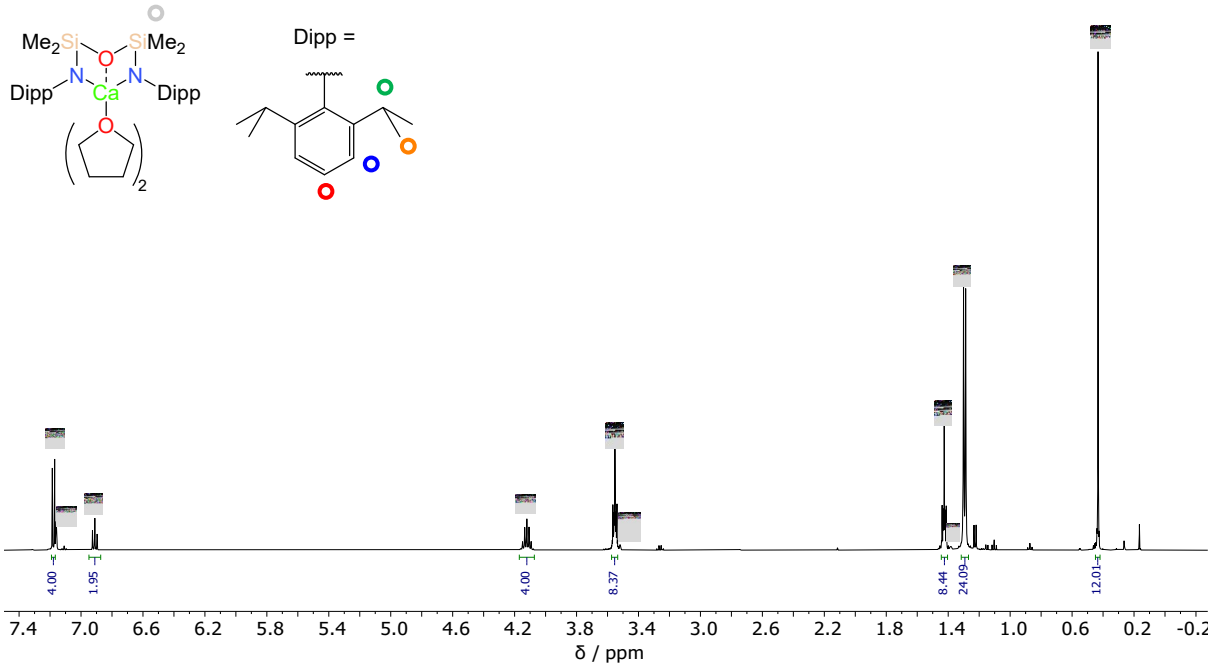

Figure S7 ^{1}H NMR spectrum (C_6D_6:C_4D_8O (~5:1), 298 K, 500 MHz) of [($^{NON\text{-}Dipp}$L)Ca(thf)$_2$] (**5**). ‡ denotes coordinated thf, † and * denote residual protio fractions of C_4D_8O and C_6D_6 respectively.

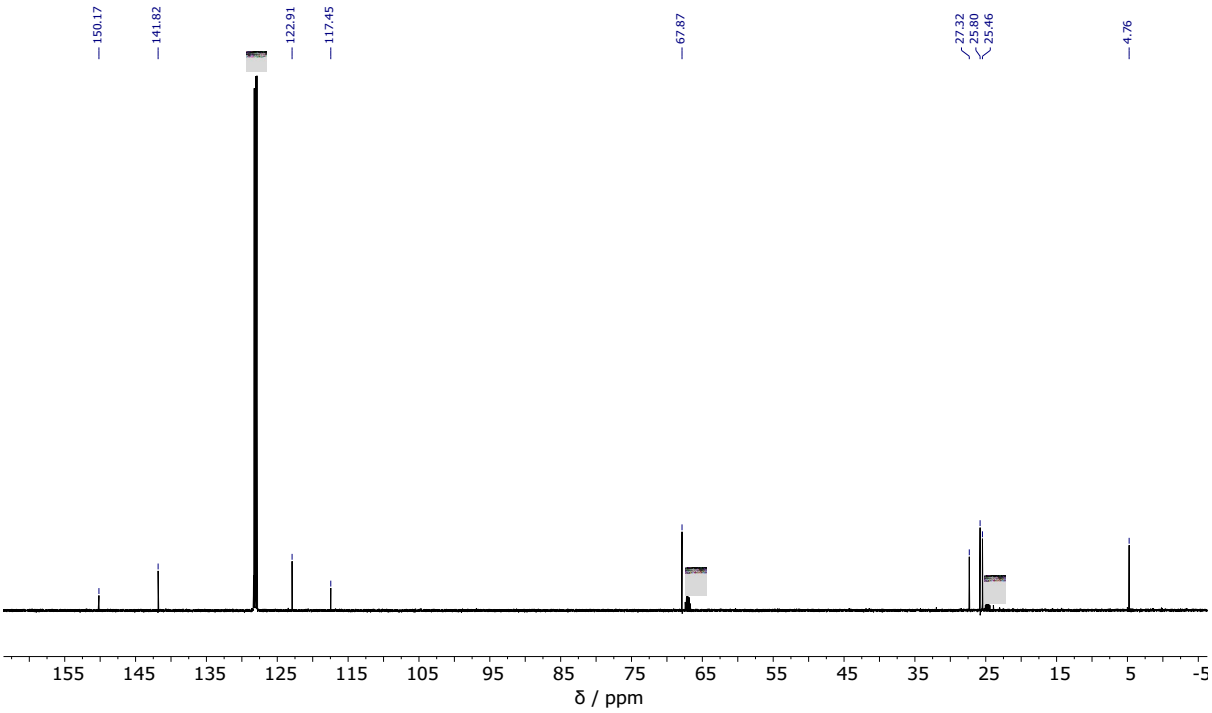

Figure S8 ^{13}C{^{1}H} NMR spectrum (C_6D_6:C_4D_8O (~5:1), 298 K, 126 MHz) of [($^{NON\text{-}Dipp}$L)Ca(thf)$_2$] (**5**). † and * denote C_4D_8O and C_6D_6 respectively.

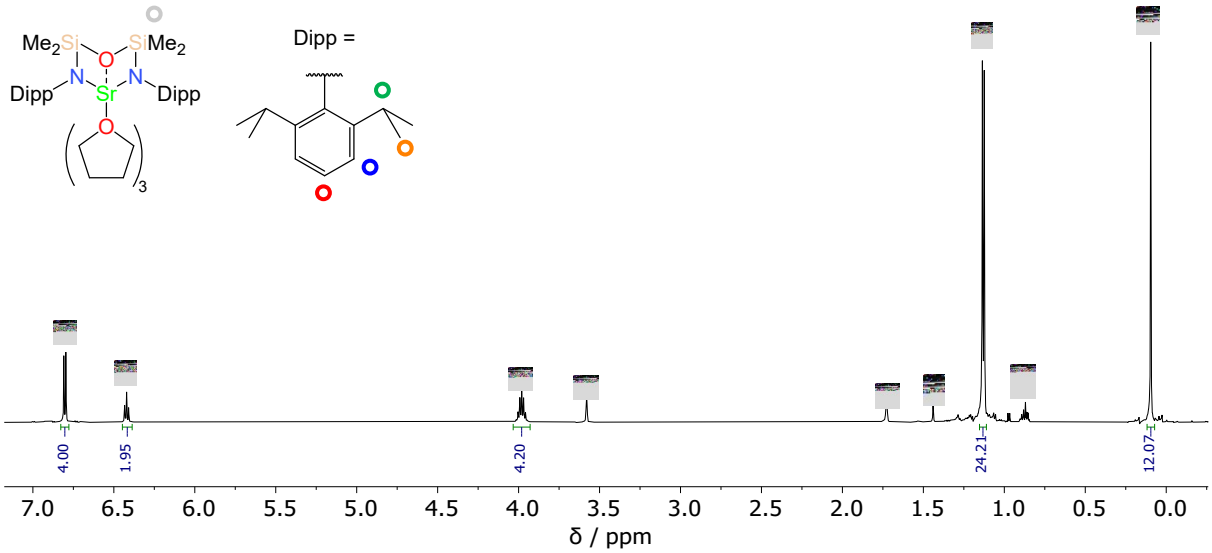

Figure S9 ^{1}H NMR spectrum (C_4D_8O, 298 K, 600 MHz) of [($^{NON\text{-}Dipp}$L)Sr(thf)$_3$] (**6**), formed when [($^{NON\text{-}Dipp}$L)Sr]$_2$ (**3**) is dissolved in thf. ‡ denotes cyclohexane, † denotes *n*-hexane, * denotes residual protio fraction of C_4D_8O.

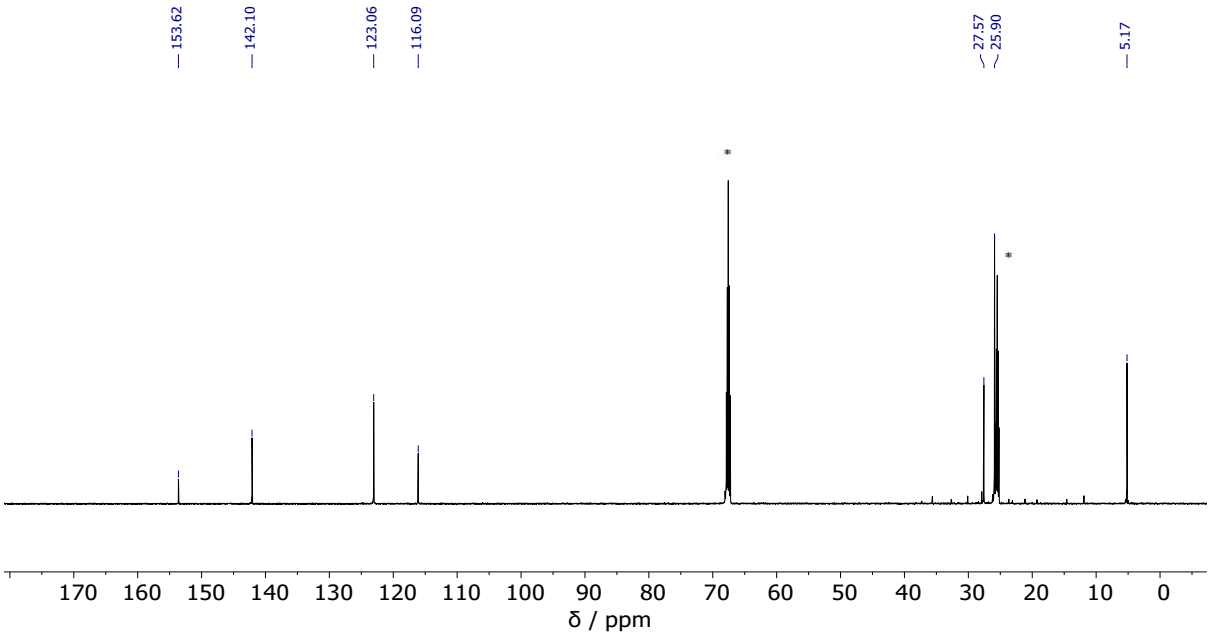

Figure S10 ^{13}C{^{1}H} NMR spectrum (C_4D_8O, 298 K, 151 MHz) of [($^{NON\text{-}Dipp}$L)Sr(thf)$_3$] (**6**), formed when [($^{NON\text{-}Dipp}$L)Sr]$_2$ (**3**) is dissolved in thf. * denotes residual protio fraction of C_4D_8O.

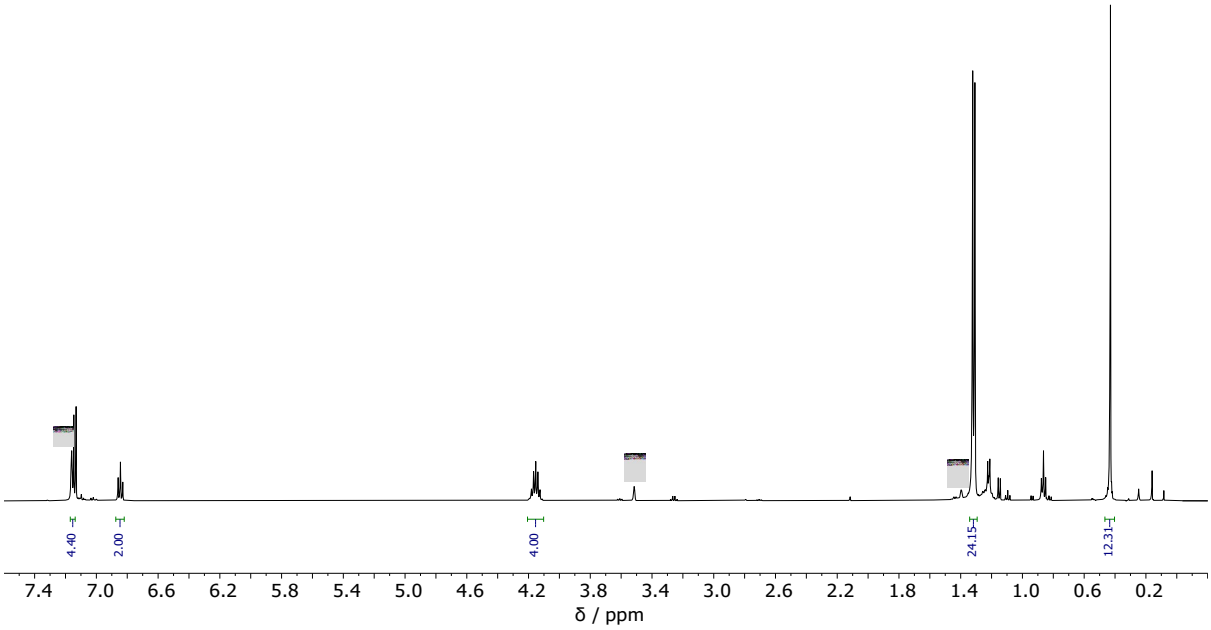

Figure S11 ^{1}H NMR spectrum (C_6D_6:C_4D_8O (~5:1), 298 K, 500 MHz) of [($^{NON\text{-}Dipp}$L)Sr]$_2$ (**3**). † and * denote residual protio fractions of C_4D_8O and C_6D_6 respectively.

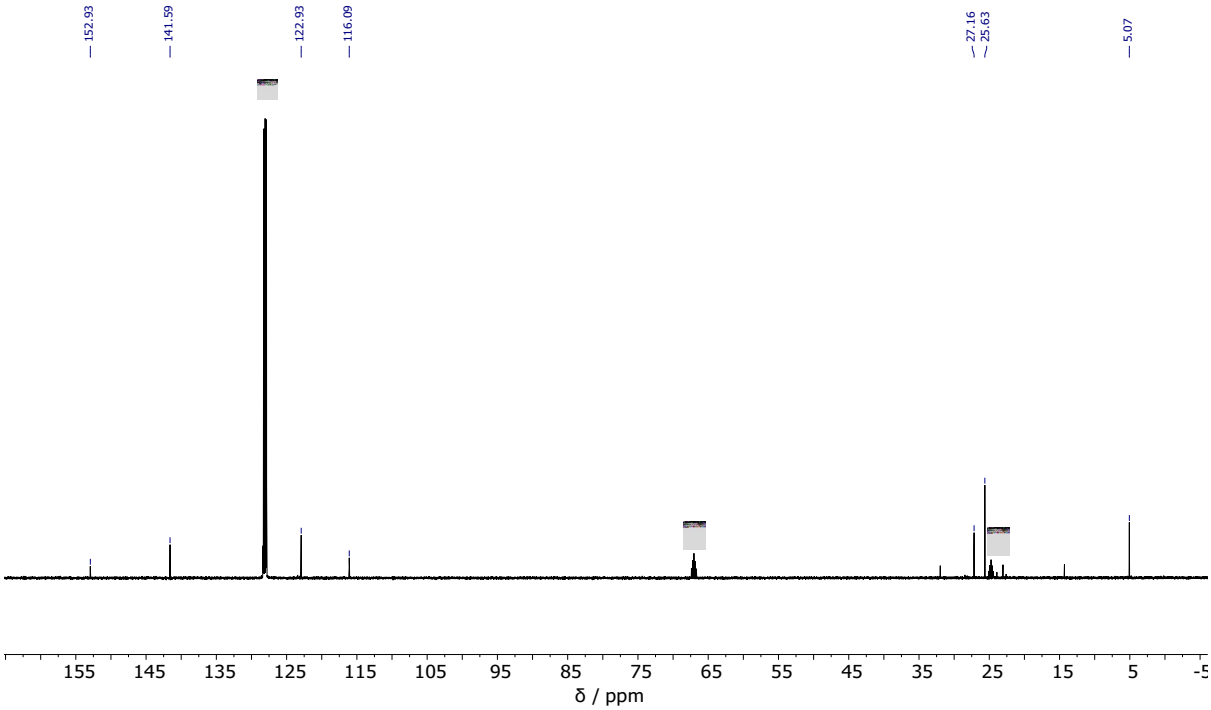

Figure S12 ^{13}C{^{1}H} NMR spectrum (C_6D_6:C_4D_8O (~5:1), 298 K, 126 MHz) of [($^{NON\text{-}Dipp}$L)Sr]$_2$ (**3**). † and * denote C_4D_8O and C_6D_6 respectively.

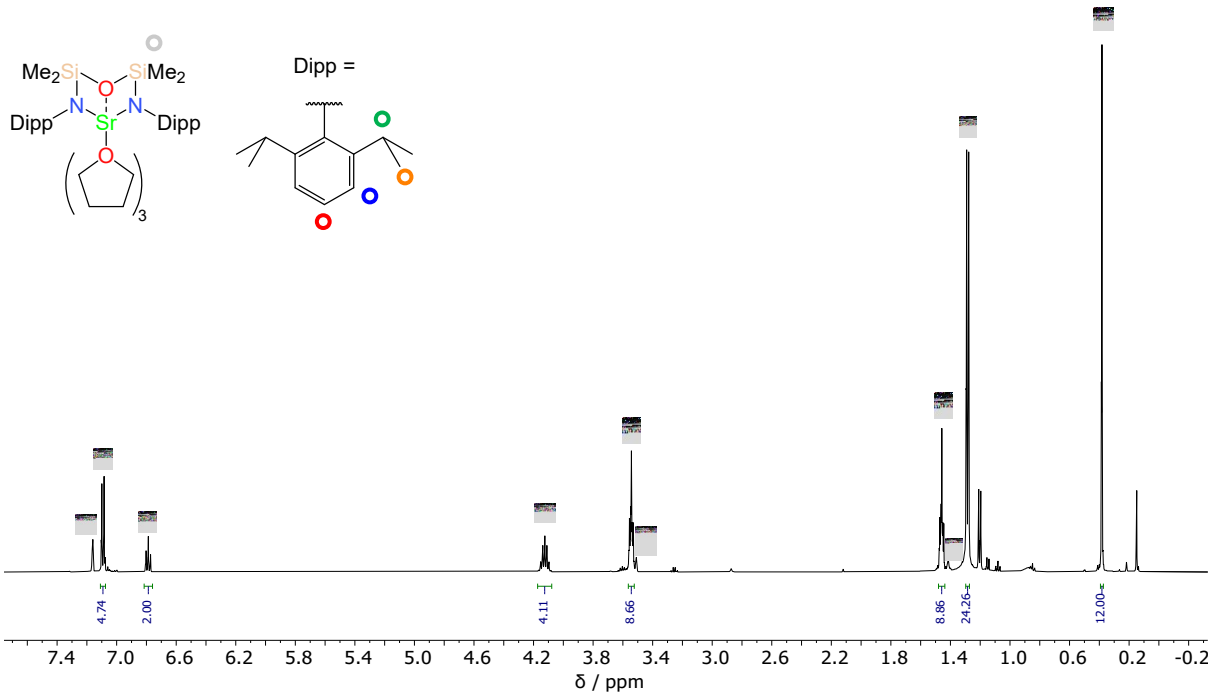

Figure S13 ^{1}H NMR spectrum (C_6D_6:C_4D_8O (~5:1), 298 K, 500 MHz) of [($^{NON\text{-}Dipp}$L)Sr(thf)$_3$] (**6**). ‡ denotes coordinated thf, † and * denote residual protio fractions of C_4D_8O and C_6D_6 respectively.

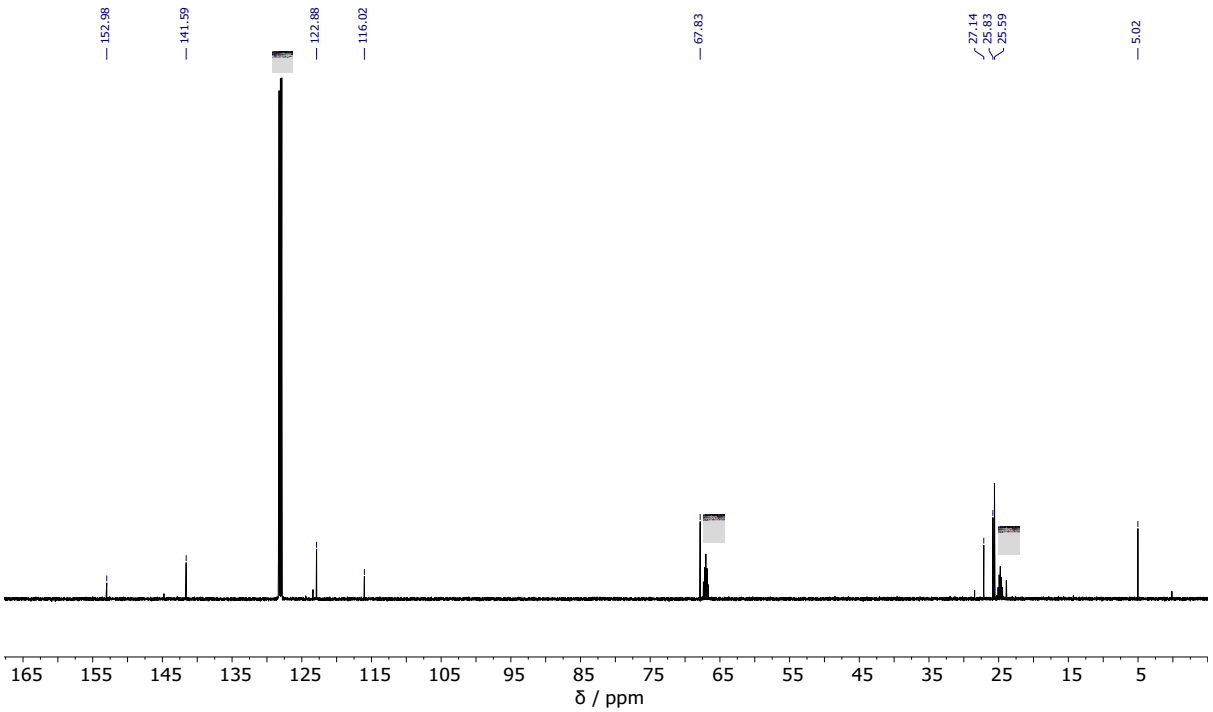

Figure S14 ^{13}C{^{1}H} NMR spectrum (C_6D_6:C_4D_8O (~5:1), 298 K, 126 MHz) of [($^{NON\text{-}Dipp}$L)Sr(thf)$_3$] (**6**). † and * denote C_4D_8O and C_6D_6 respectively.

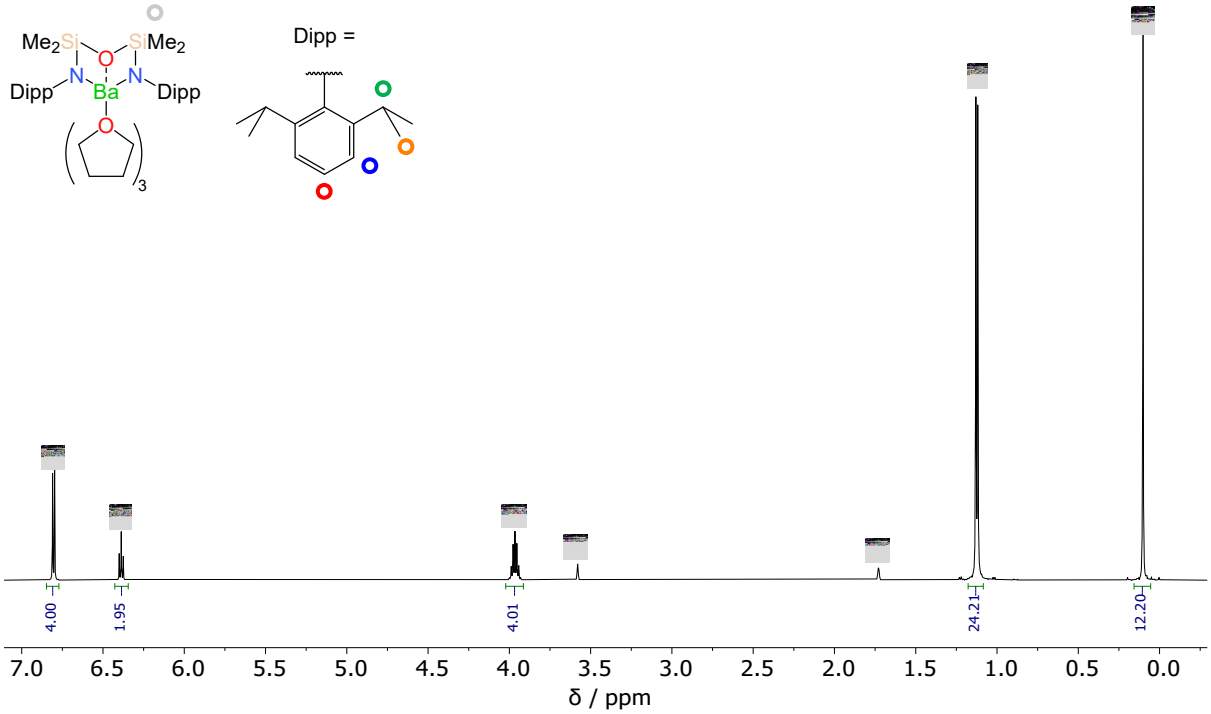

Figure S15 ^{1}H NMR spectrum (C_4D_8O, 298 K, 600 MHz) of [($^{NON\text{-}Dipp}$L)Ba(thf)$_3$] (**7**), formed when [($^{NON\text{-}Dipp}$L)Ba]$_2$ (**4a**) is dissolved in thf. * denotes residual protio fraction of C_4D_8O.

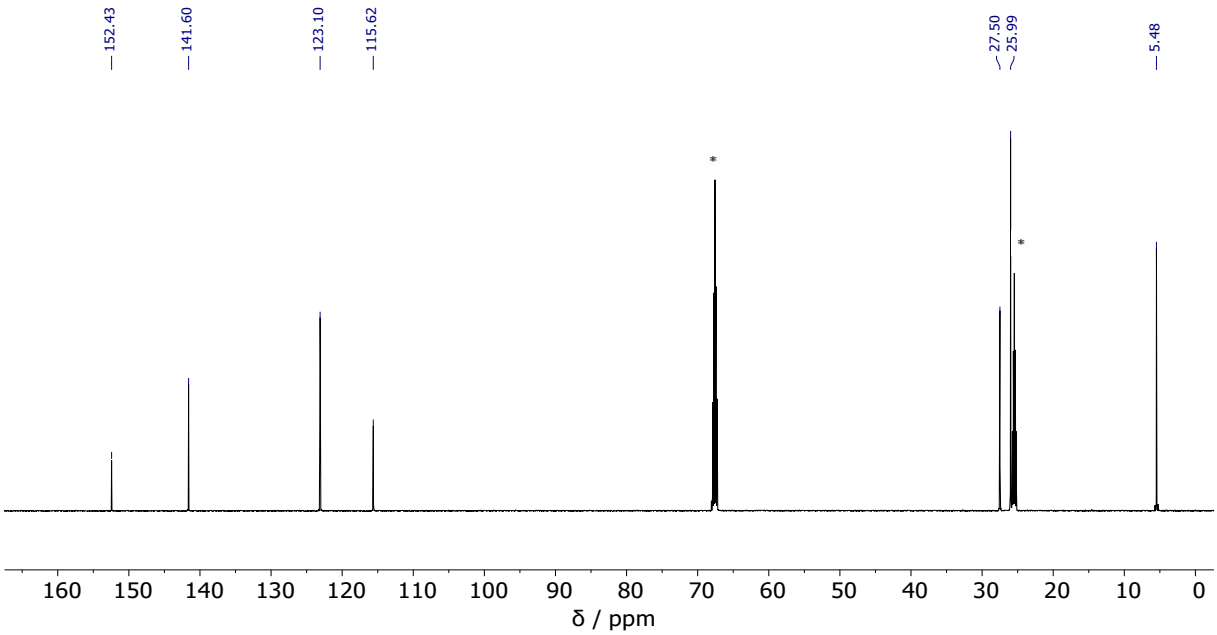

Figure S16 ^{13}C{^{1}H} NMR spectrum (C_4D_8O, 298 K, 151 MHz) of [($^{NON\text{-}Dipp}$L)Ba(thf)$_3$] (**7**), formed when [($^{NON\text{-}Dipp}$L)Ba]$_2$ (**4a**) is dissolved in thf. * denotes residual protio fraction of C_4D_8O.

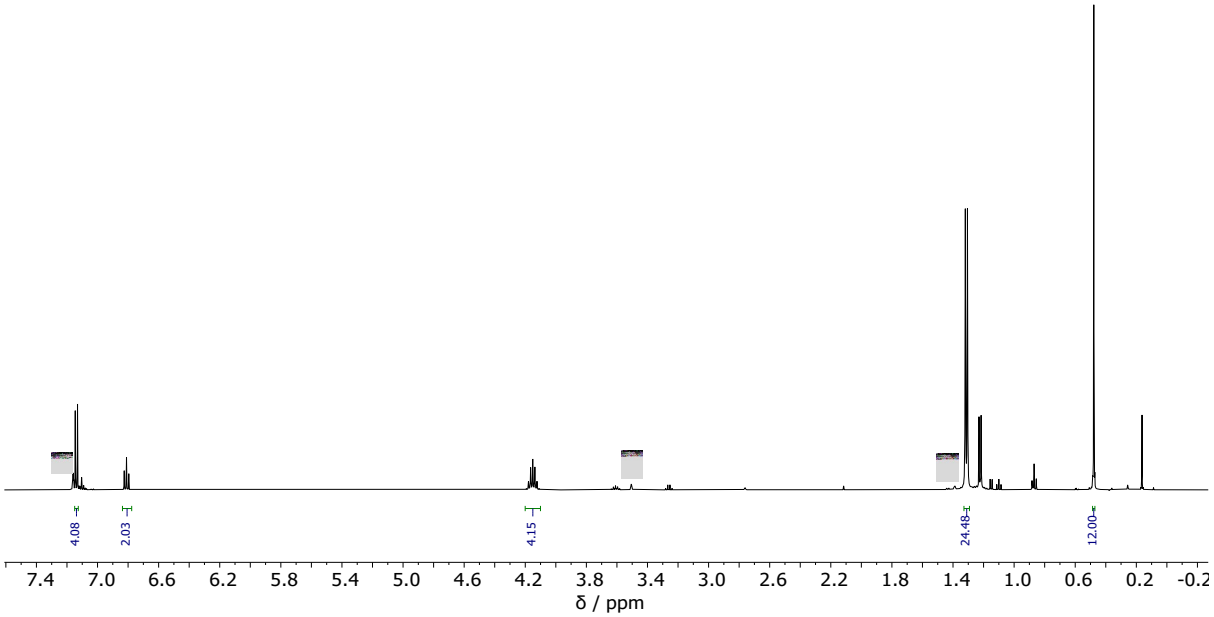

Figure S17 ^{1}H NMR spectrum (C_6D_6:C_4D_8O (~5:1), 298 K, 500 MHz) of [($^{NON\text{-}Dipp}$L)Ba]$_2$ (**4**). † and * denote residual protio fractions of C_4D_8O and C_6D_6 respectively.

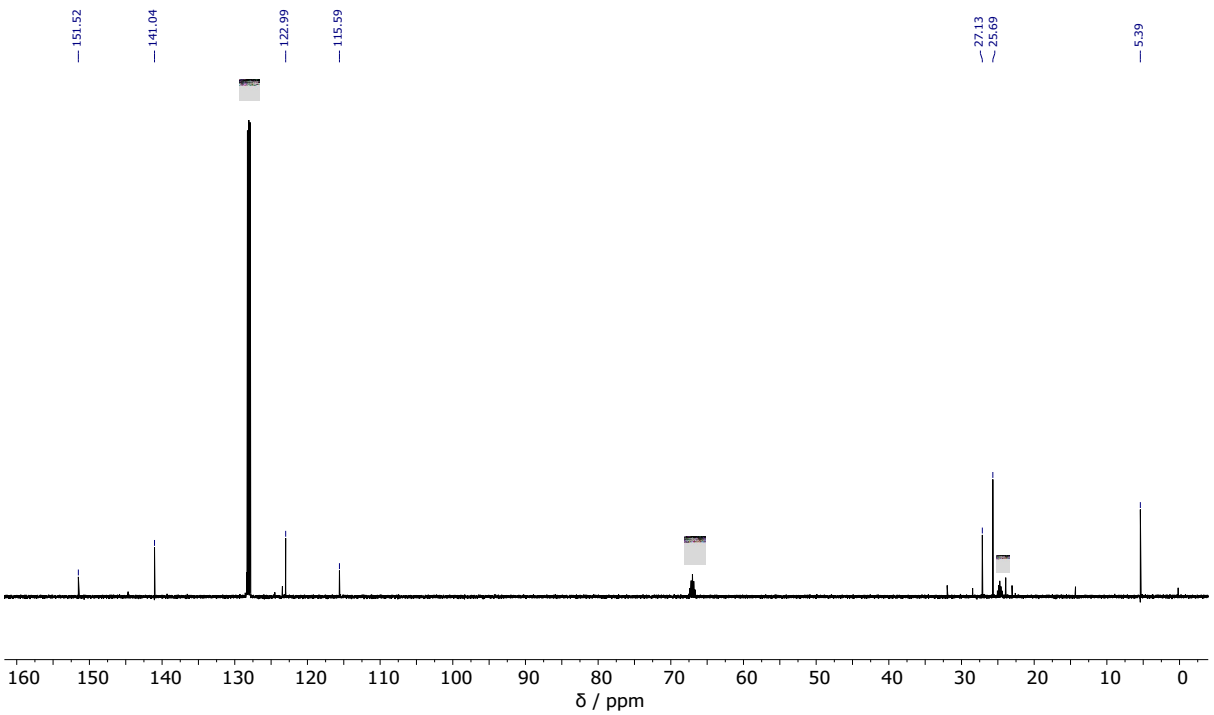

Figure S18 ^{13}C{^{1}H} NMR spectrum (C_6D_6:C_4D_8O (~5:1), 298 K, 126 MHz) of [($^{NON\text{-}Dipp}$L)Ba]$_2$ (**4**). † and * denote C_4D_8O and C_6D_6 respectively.

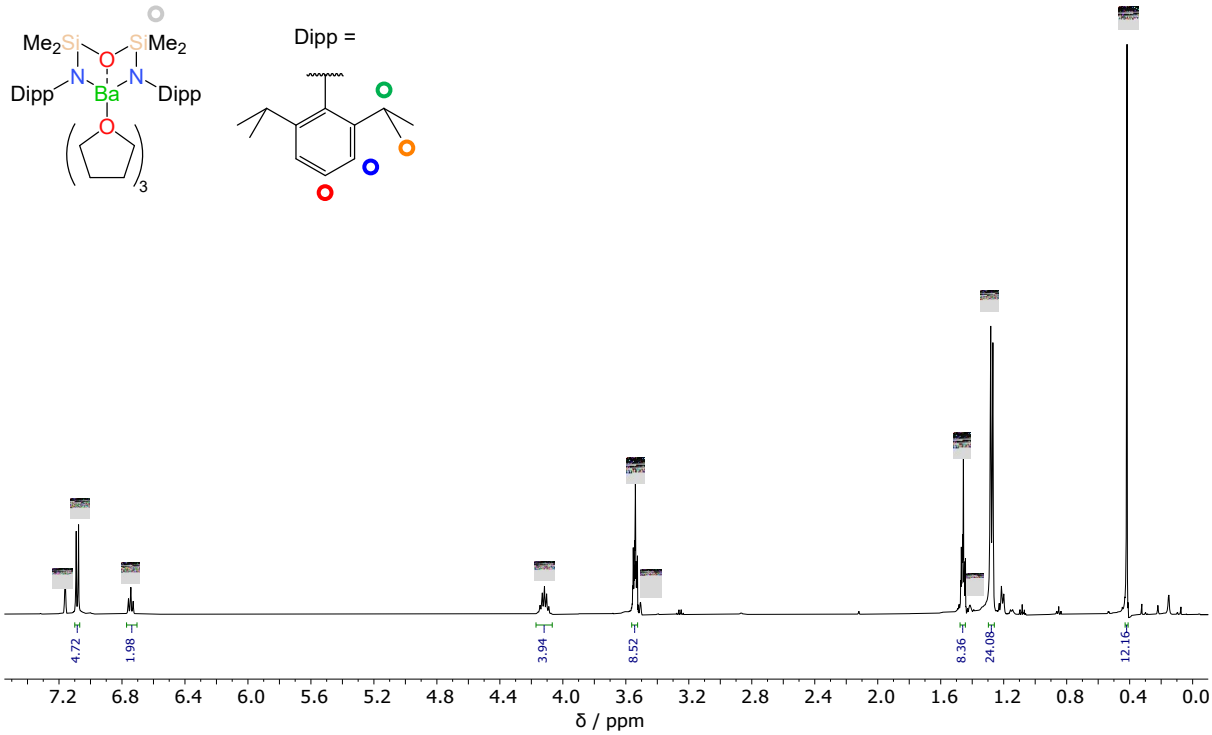

Figure S19 ^{1}H NMR spectrum (C_6D_6:C_4D_8O (~5:1), 298 K, 500 MHz) of [($^{NON\text{-}Dipp}$L)Ba(thf)$_3$] (**7**). ‡ denotes coordinated thf, † and * denote residual protio fractions of C_4D_8O and C_6D_6 respectively.

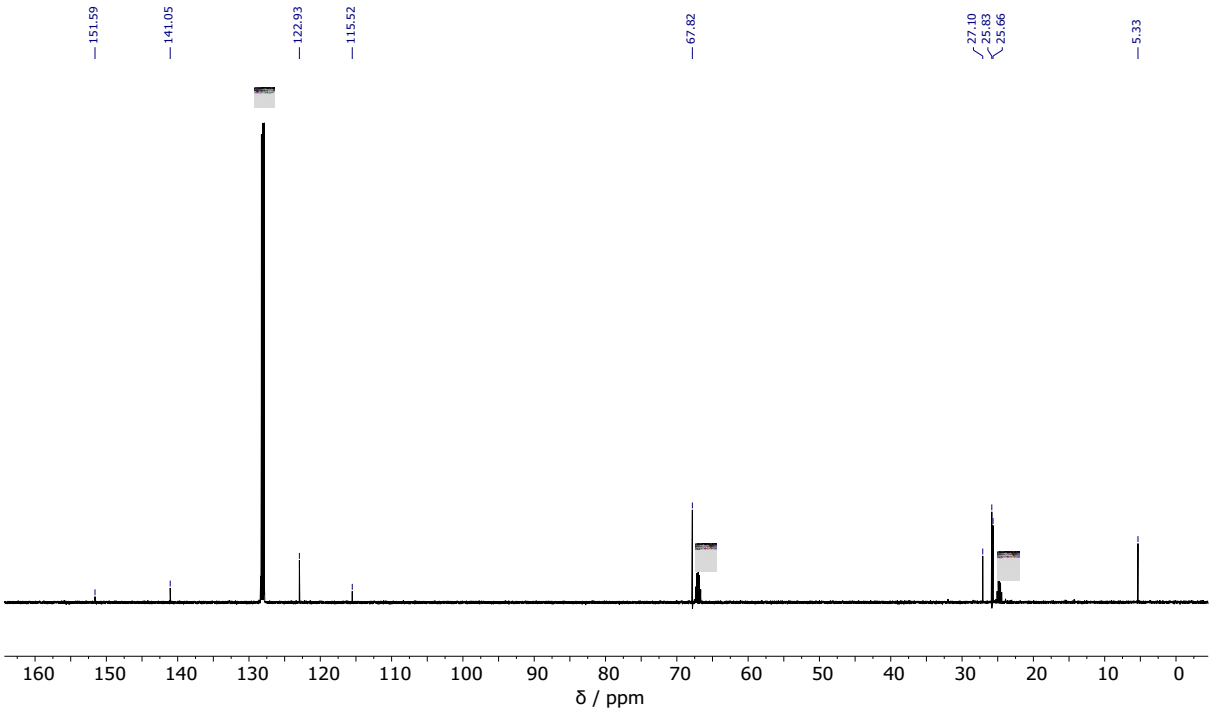

Figure S20 ^{13}C{^{1}H} NMR spectrum (C_6D_6:C_4D_8O (~5:1), 298 K, 126 MHz) of [($^{NON\text{-}Dipp}$L)Ba(thf)$_3$] (**7**). † and * denote C_4D_8O and C_6D_6 respectively.

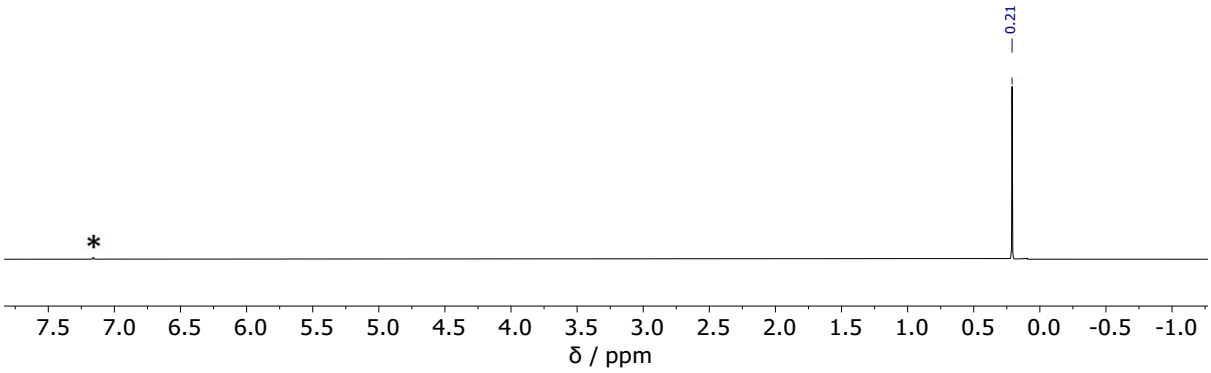

Figure S21 ^{1}H NMR spectrum (C_6D_6, 298 K, 600 MHz) of [Ba{N(SiMe$_3$)$_2$}$_3$K]. * denotes residual protio fraction of C_6D_6.

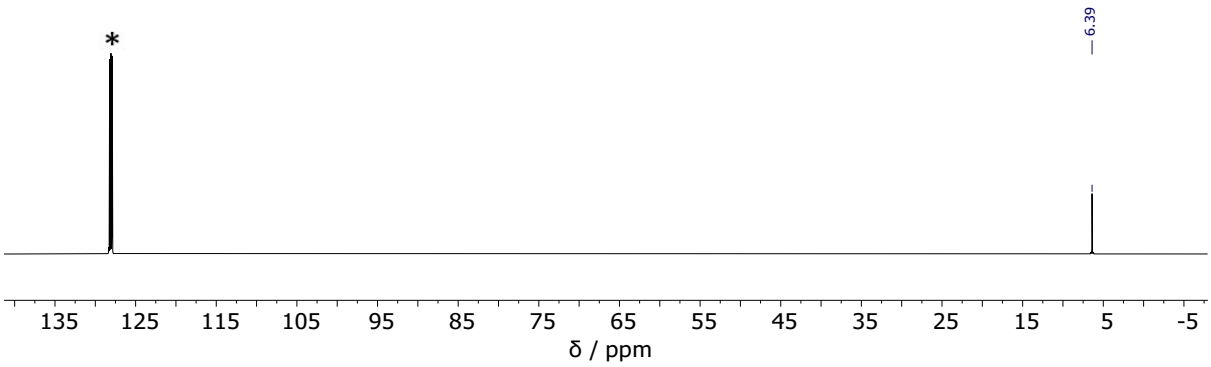

Figure S22 ^{13}C{^{1}H} NMR spectrum (C_6D_6, 298 K, 151 MHz) of [Ba{N(SiMe$_3$)$_2$}$_3$K]. * denotes residual protio fraction of C_6D_6.

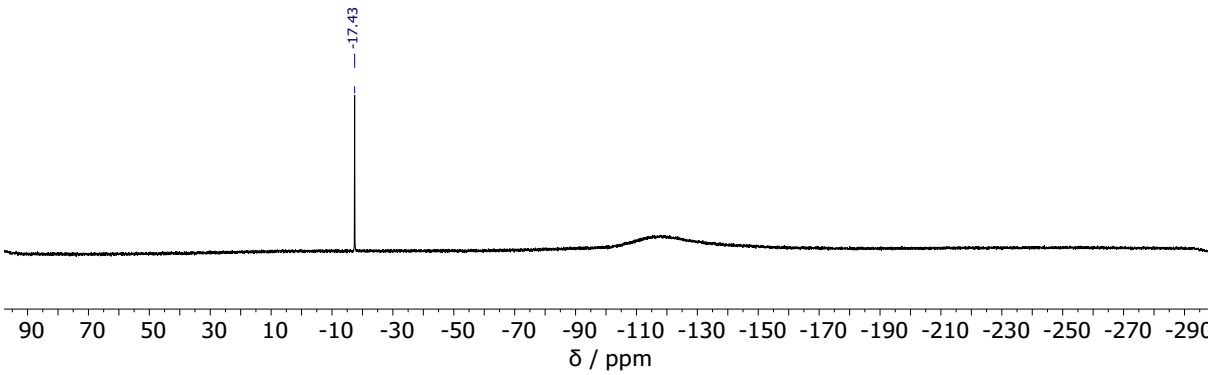

Figure S23 ^{29}Si NMR spectrum (C_6D_6, 298 K, 119 MHz) of [Ba{N(SiMe$_3$)$_2$}$_3$K].

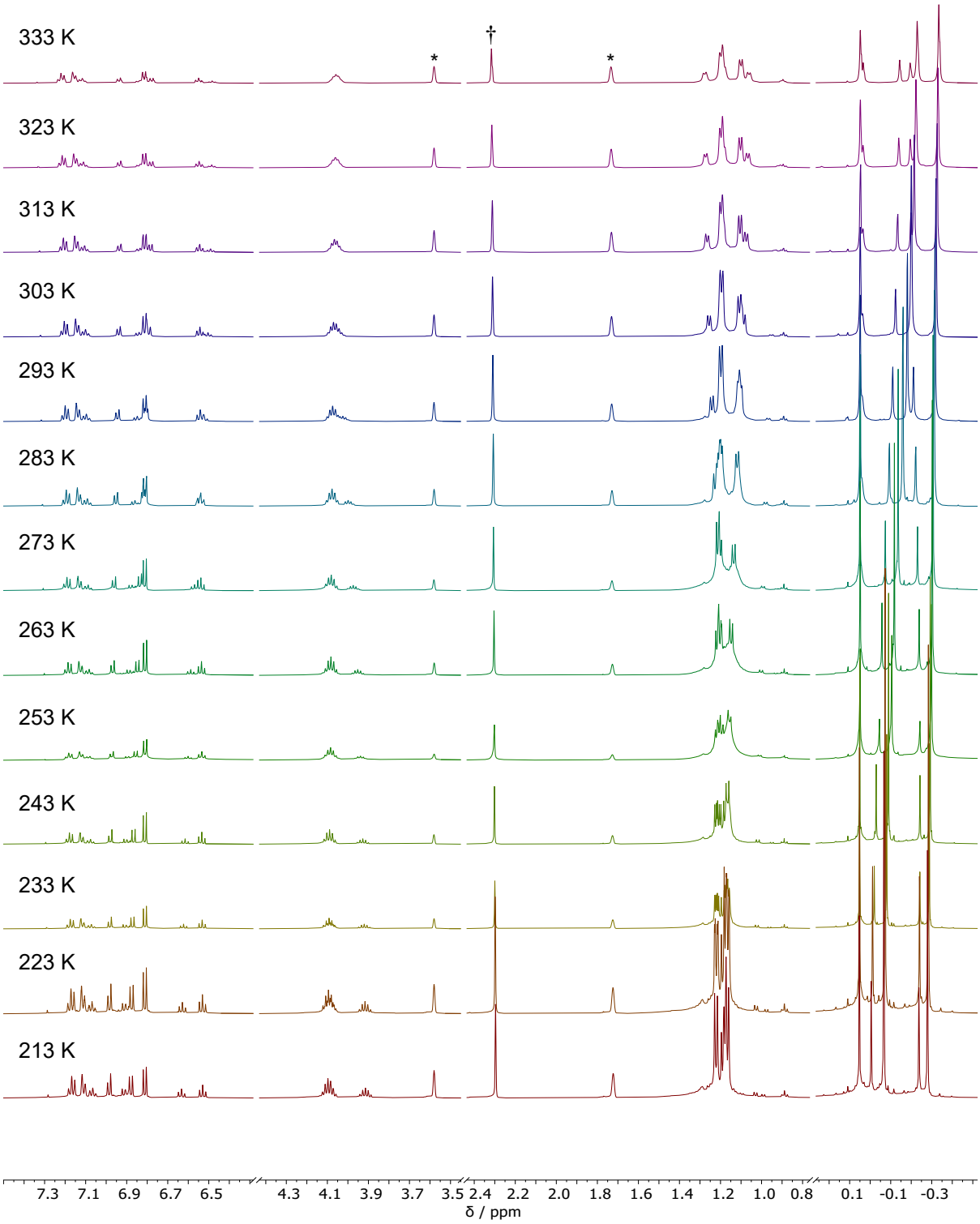

Figure S24 Variable temperature ^{1}H NMR spectra (C_4D_8O, 500 MHz) showing the complex temperature-sensitive mixture of species formed upon the dissolution of $[(^{NNO\text{-}Dipp}L)Mg(\mu\text{-}N'')K]_n$ (**8**) in thf-d_8. † denotes co-crystallised toluene, * denotes residual protio fraction of thf-d_8.

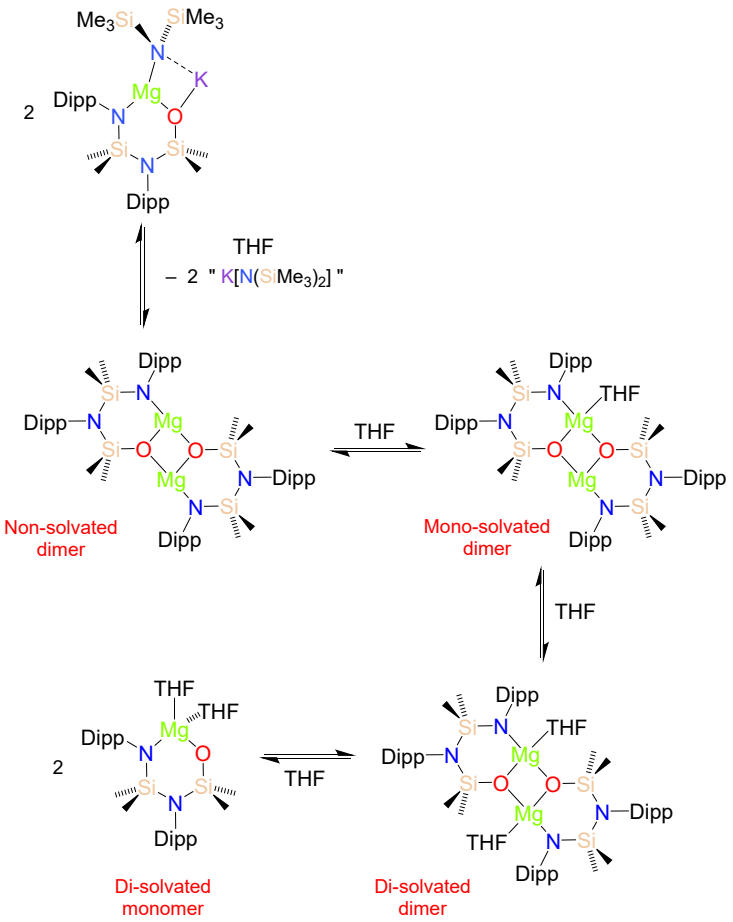

Scheme S1 Proposed solution-phase equilibrium resulting from both i) the reversible dissociation of KN" from [($^{NNO\text{-}Dipp}$L)Mg(μ-N")K] and ii) the reversible coordination of thf to dimeric and monomeric magnesium complexes supported by the [$^{NNO\text{-}Dipp}$L]$^{2-}$ligand.

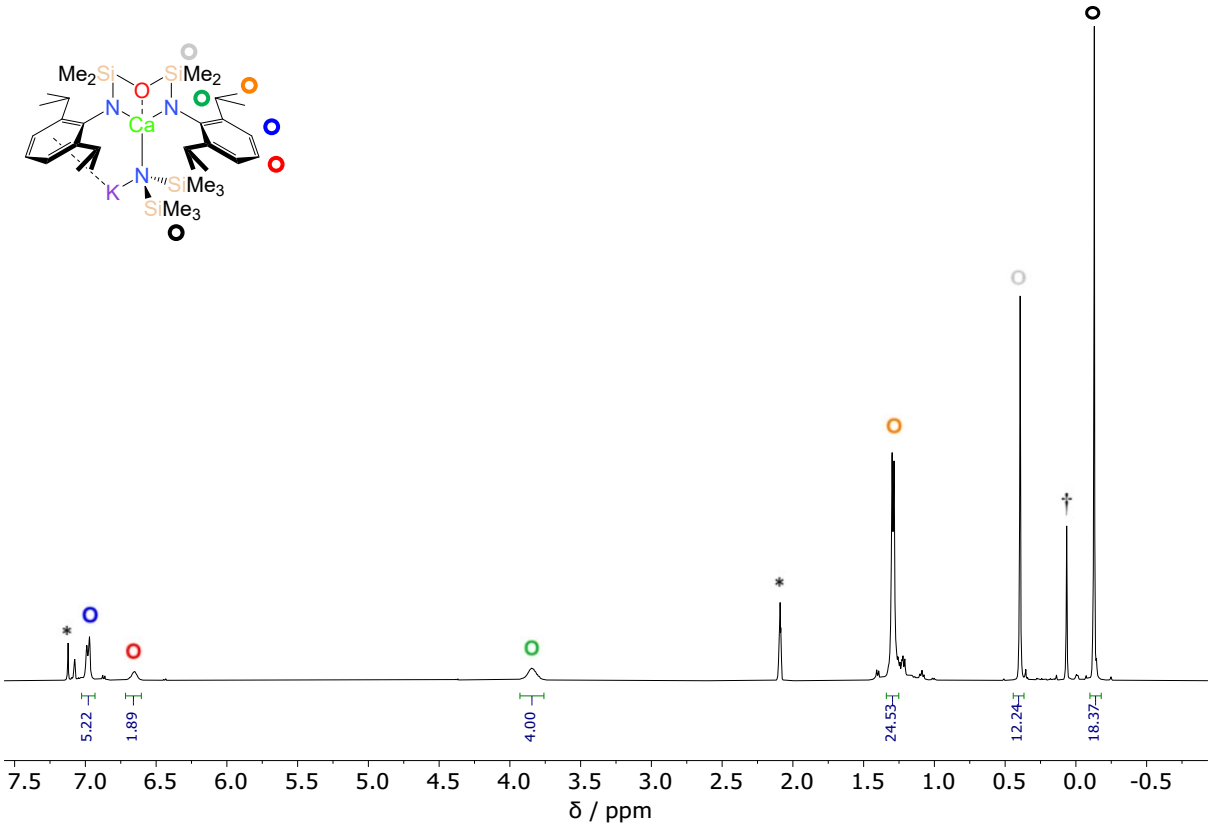

Figure S25 ^{1}H NMR spectrum (C_7D_8, 343 K, 500 MHz) of [($^{NON\text{-}Dipp}$L)Ca(μ-N")K] (**9**). † denotes KN" released by solution-phase equilibrium between [($^{NON\text{-}Dipp}$L)Ca(μ-N")K] and [($^{NON\text{-}Dipp}$L)Ca(tol)$_n$], * denotes residual protio fraction of C_7D_8.

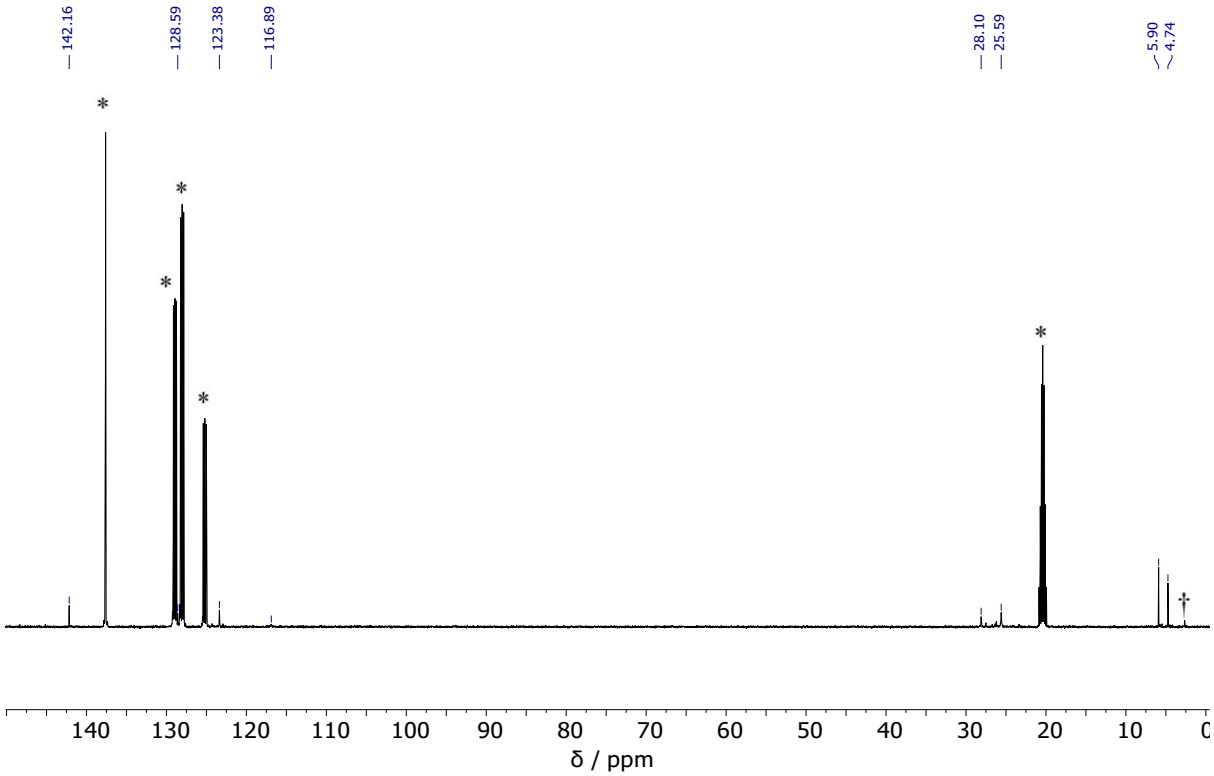

Figure S26 ^{13}C{^{1}H} NMR spectrum (C_7D_8, 343 K, 126 MHz) of [($^{NON\text{-}Dipp}$L)Ca(μ-N")K] (**9**). † denotes KN" released by solution-phase equilibrium between [($^{NON\text{-}Dipp}$L)Ca(μ-N")K] and [($^{NON\text{-}Dipp}$L)Ca], * denotes C_7D_8.

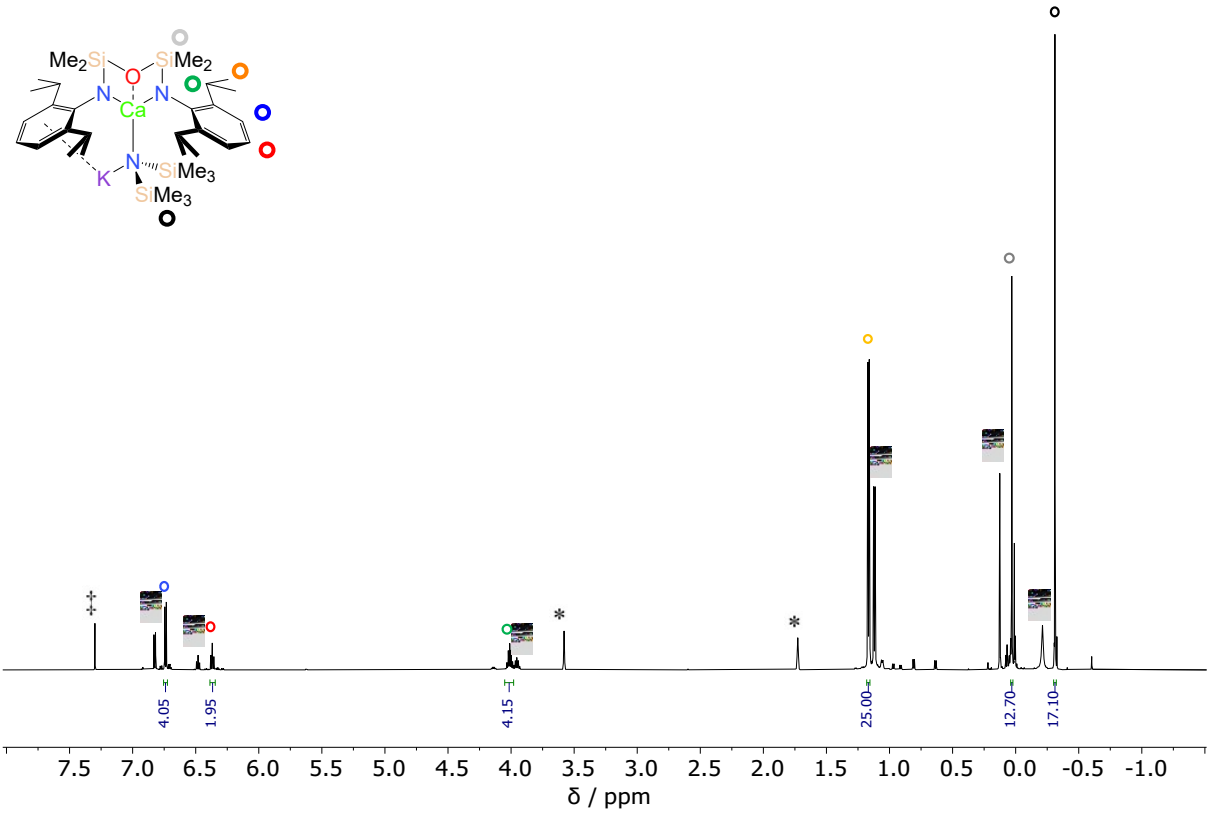

Figure S27 ^{1}H NMR spectrum (C_4D_8O, 298 K, 600 MHz) of [($^{NON\text{-}Dipp}$L)Ca(μ-N")K] (**9**). ‡ denotes co-crystallised benzene, † denotes [($^{NON\text{-}Dipp}$L)Ca(thf)$_n$] (**5**) and KN" released by a solution-phase equilibrium, * denotes residual protio fraction of C_4D_8O.

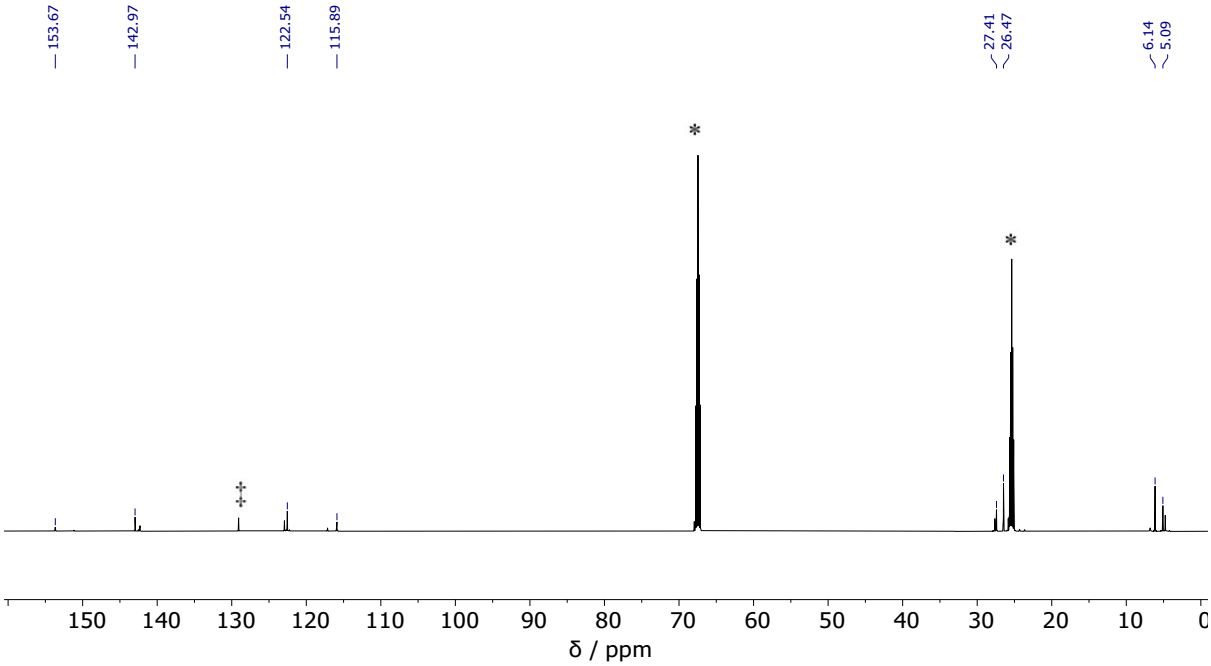

Figure S28 ^{13}C{^{1}H} NMR spectrum (C_4D_8O, 298 K, 151 MHz) of [($^{NON\text{-}Dipp}$L)Ca(μ-N")K] (**9**). Unlabelled peaks result from [($^{NON\text{-}Dipp}$L)Ca(thf)$_n$] (**5**) and KN" released by a solution-phase equilibrium. ‡ denotes co-crystallised benzene, * denotes C_4D_8O.

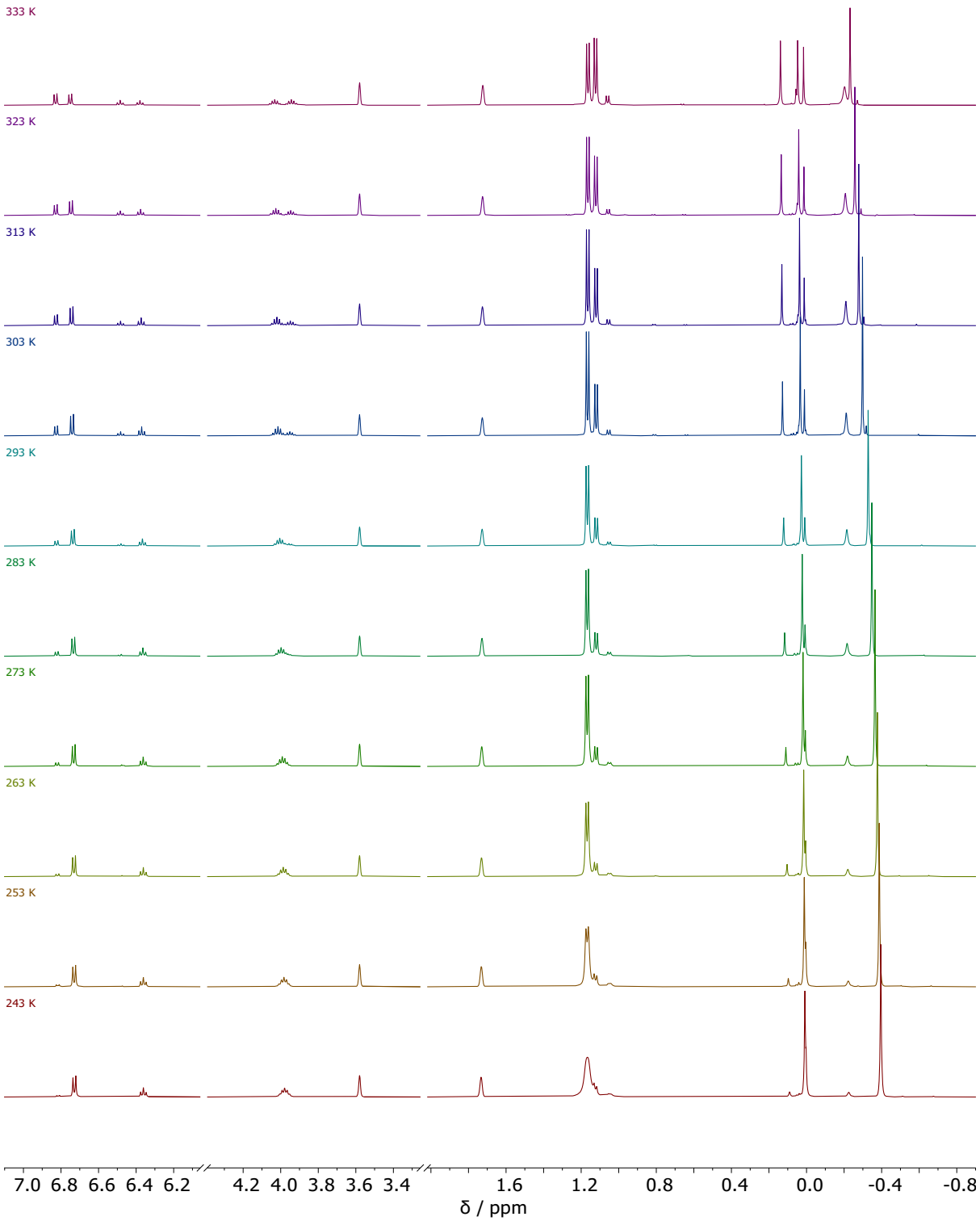

Figure S29 Variable temperature ^{1}H NMR spectra (C_4D_8O, 500 MHz) showing the temperature-sensitive equilibrium between [($^{NON\text{-}Dipp}$L)Ca(μ-N")K(thf)$_n$)] (**9^{thf}**), [($^{NON\text{-}Dipp}$L)Ca(thf)$_n$] (**5**) and KN".

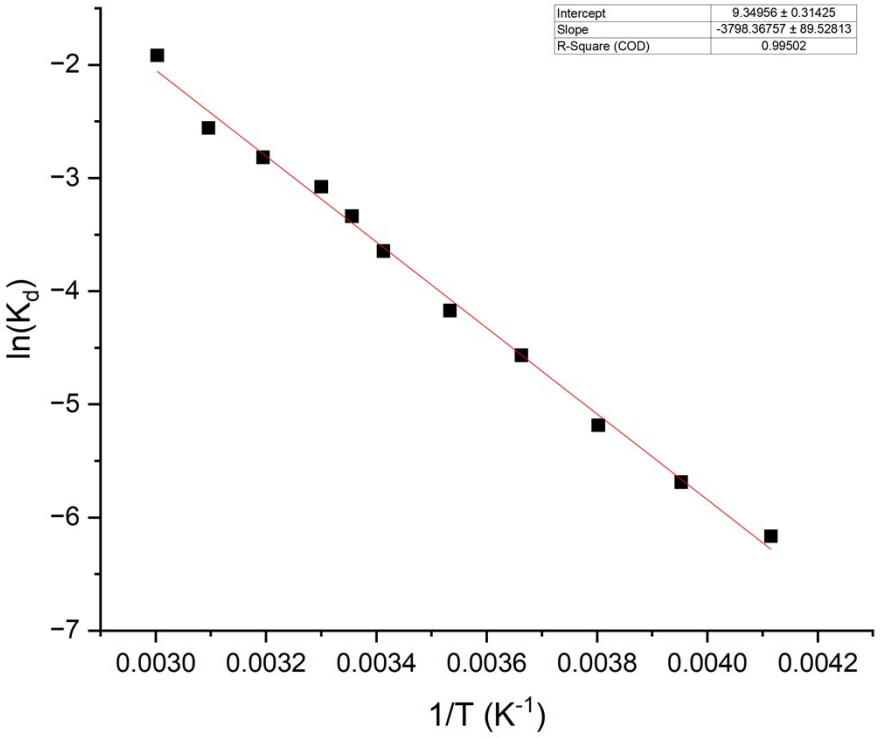

Figure S30 Van 't Hoff plot for the dissociation of [($^{NON\text{-}Dipp}$L)Ca(μ-N")K(thf)$_n$] (**9^{thf}**) into [($^{NON\text{-}Dipp}$L)Ca(thf)$_n$] (**5**) and KN".

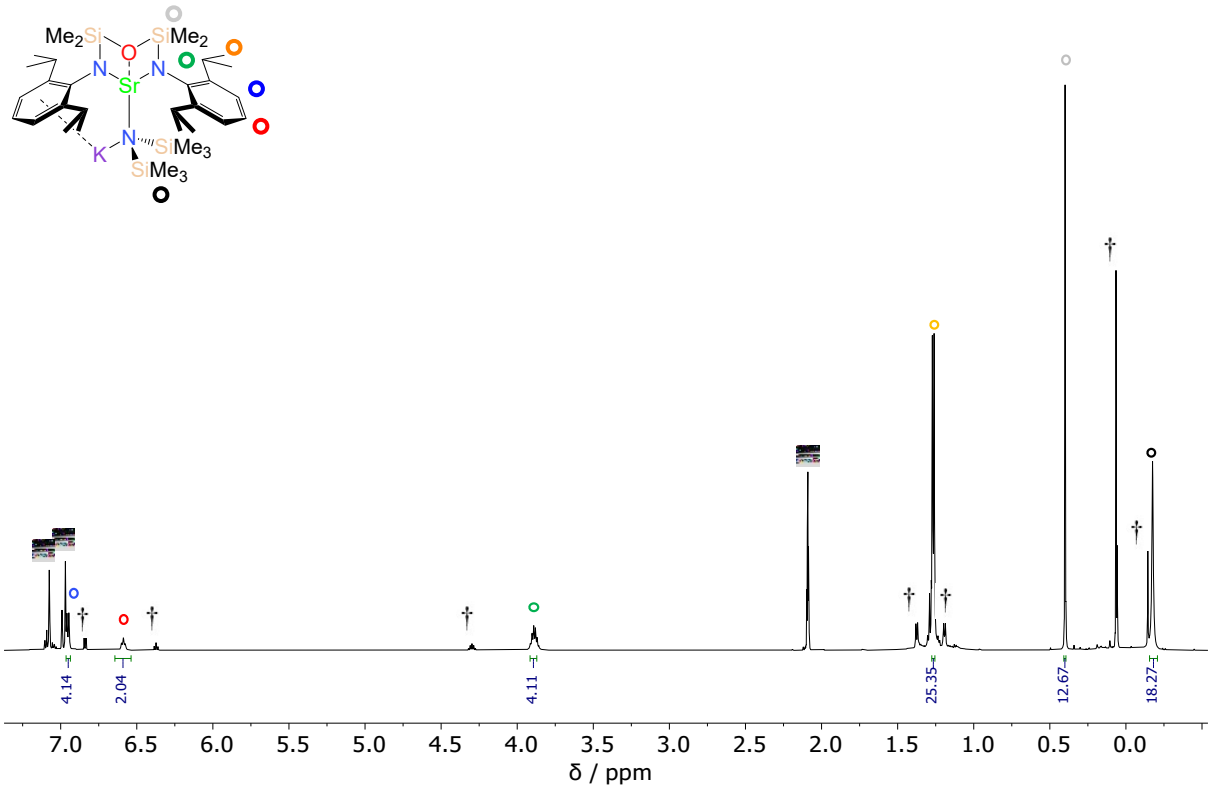

Figure S31 ^{1}H NMR spectrum (C_7D_8, 343 K, 500 MHz) of [($^{NON\text{-}Dipp}$L)Sr(μ-N")K] (**10**). † denotes KN" and [($^{NON\text{-}Dipp}$L)Sr(tol)$_n$] released by a solution-phase equilibrium, * denotes residual protio fraction of C_7D_8.

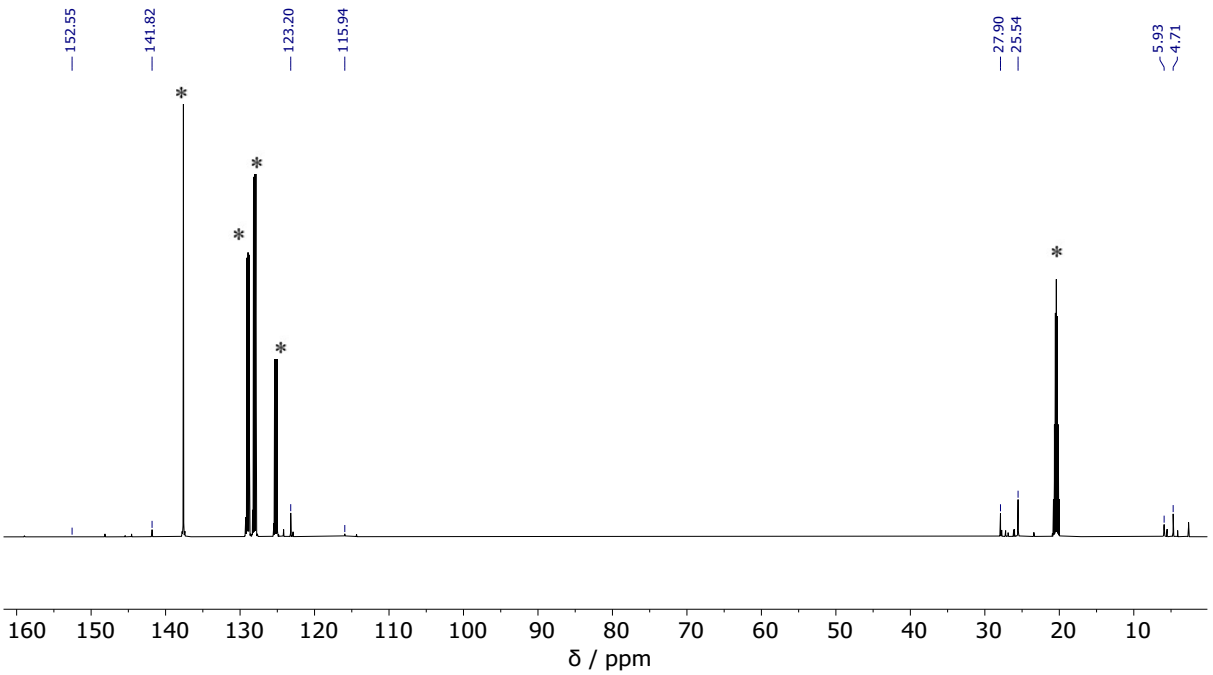

Figure S32 ^{13}C{^{1}H} NMR spectrum (C_7D_8, 343 K, 126 MHz) of [($^{NON\text{-}Dipp}$L)Sr(μ-N")K] (**10**). Unlabelled peaks result from KN" and [($^{NON\text{-}Dipp}$L)Sr(tol)$_n$] present due to solution-phase equilibrium with [($^{NON\text{-}Dipp}$L)Sr(μ-N")K], * denotes C_7D_8.

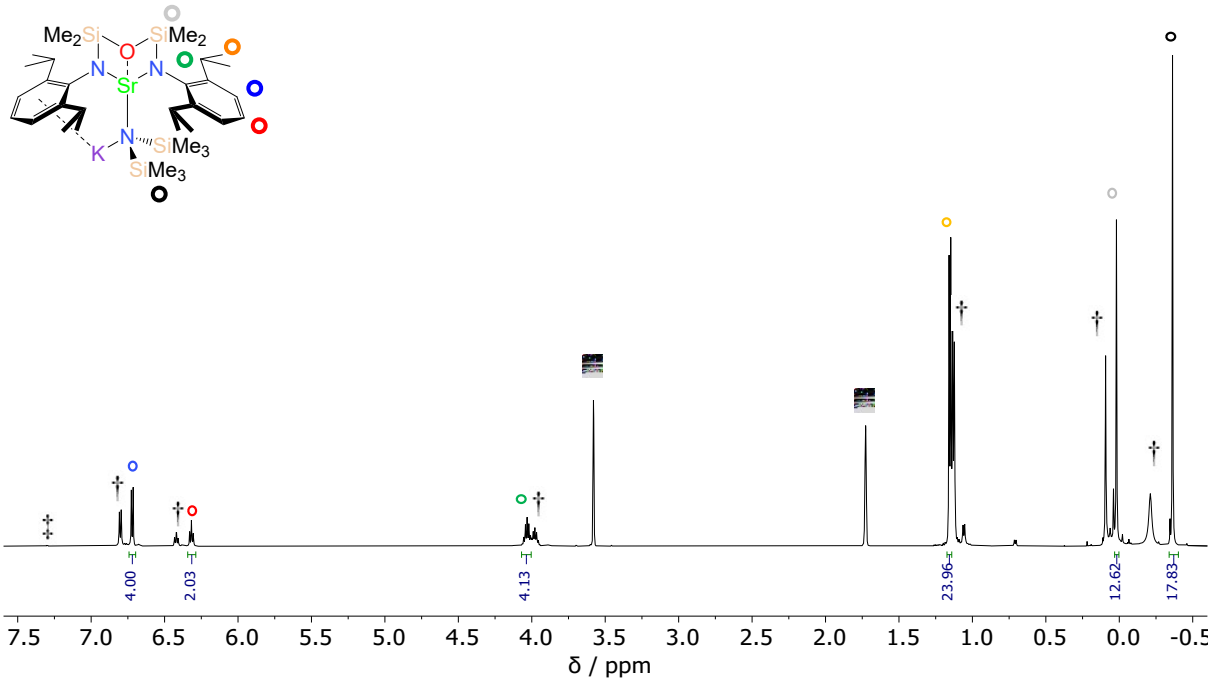

Figure S33 ^{1}H NMR spectrum (C_4D_8O, 298 K, 600 MHz) of [($^{NON\text{-}Dipp}$L)Sr(μ-N")K] (**10**). ‡ denotes co-crystallised benzene, † denotes [($^{NON\text{-}Dipp}$L)Sr(thf)$_n$] (**6**) and KN" released by a solution-phase equilibrium, * denotes residual protio fraction of C_4D_8O.

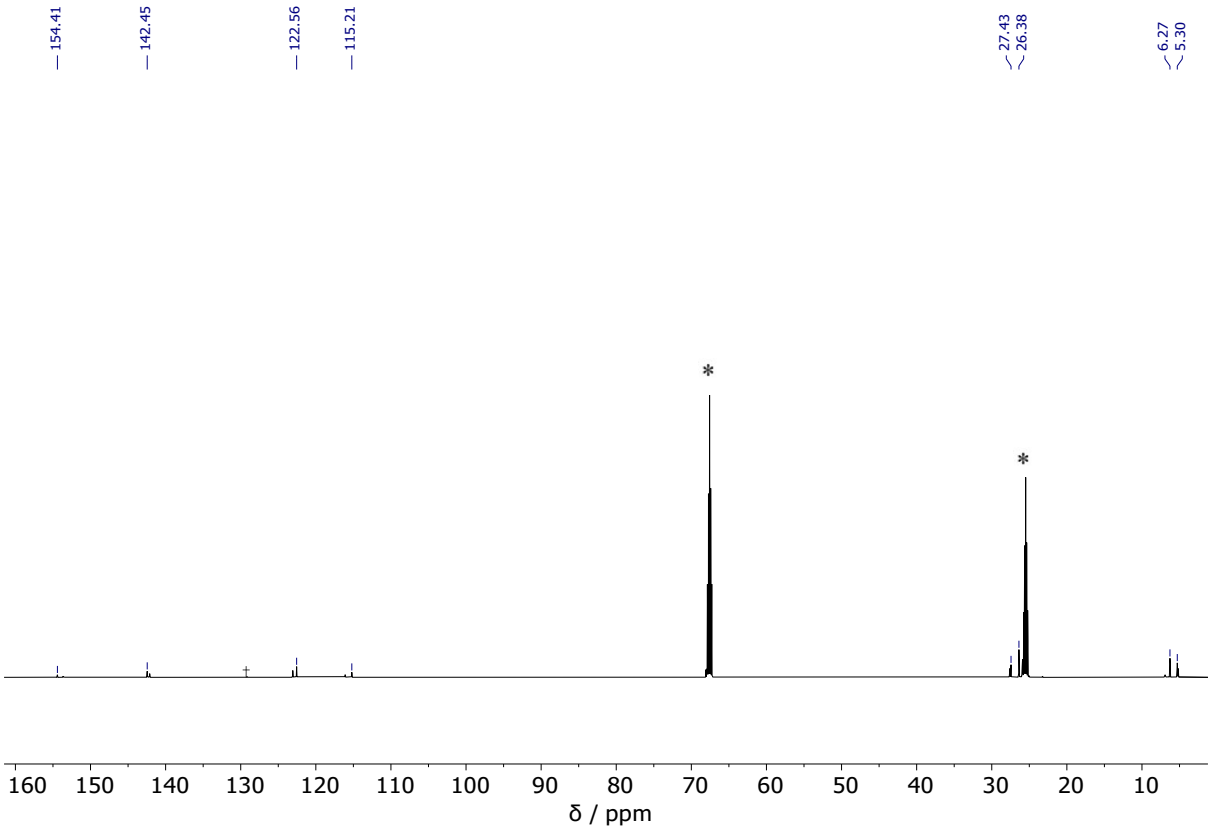

Figure S34 ^{13}C{^{1}H} NMR spectrum (C_4D_8O, 298 K, 151 MHz) of [($^{NON\text{-}Dipp}$L)Sr(μ-N")K] (**10**). Unlabelled peaks result from [($^{NON\text{-}Dipp}$L)Sr(thf)$_n$] (**6**) and KN" released by a solution-phase equilibrium. † denotes co-crystallised benzene, * denotes C_4D_8O.

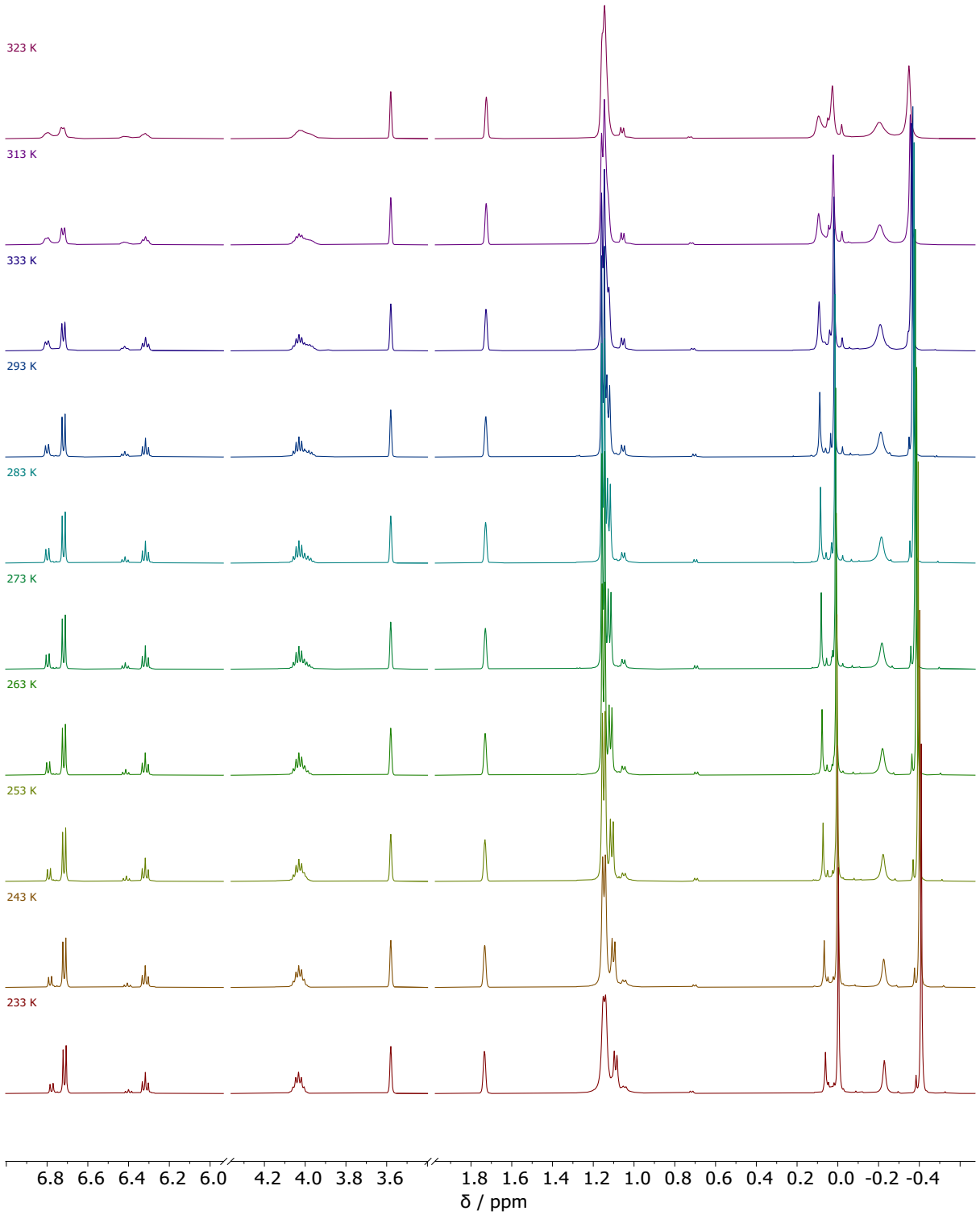

Figure S35 Variable temperature ^{1}H NMR spectra (C_4D_8O, 500 MHz) showing the temperature-sensitive equilibrium between [($^{NON\text{-}Dipp}$L)Sr(μ-N")K(thf)$_n$)] (**10^{thf}**), [($^{NON\text{-}Dipp}$L)Sr(thf)$_n$] (**6**) and KN".

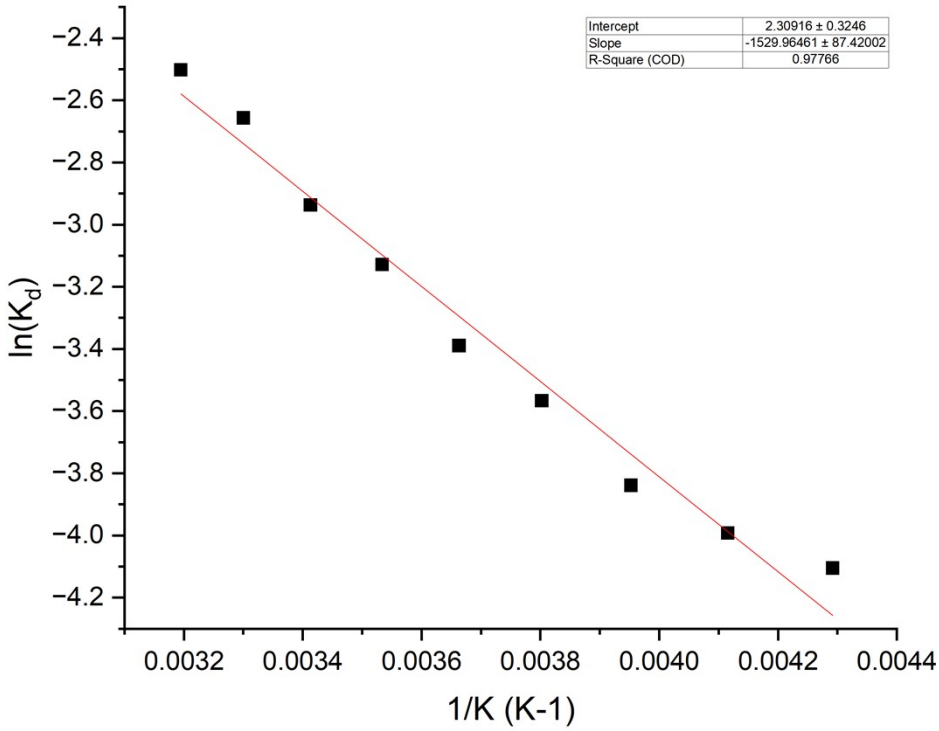

Figure S36 Van 't Hoff plot for the dissociation of [($^{NON\text{-}Dipp}$L)Sr(μ-N")K(thf)$_n$)] (**10^{thf}**) into [($^{NON\text{-}Dipp}$L)Sr(thf)$_n$] (**6**) and KN".

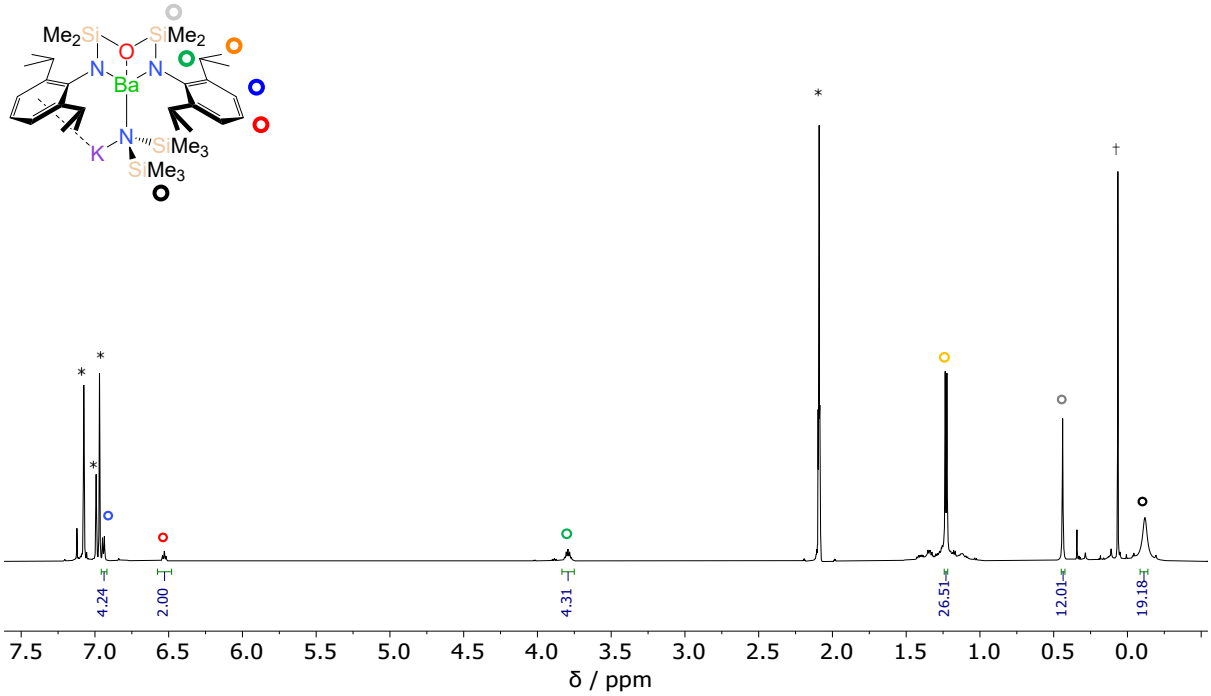

Figure S37 ^{1}H NMR spectrum (C_7D_8, 343 K, 500 MHz) of [($^{NON\text{-}Dipp}$L)Ba(μ-N")K] (**11**). † denotes residual HN", * denotes residual protio fraction of C_7D_8.

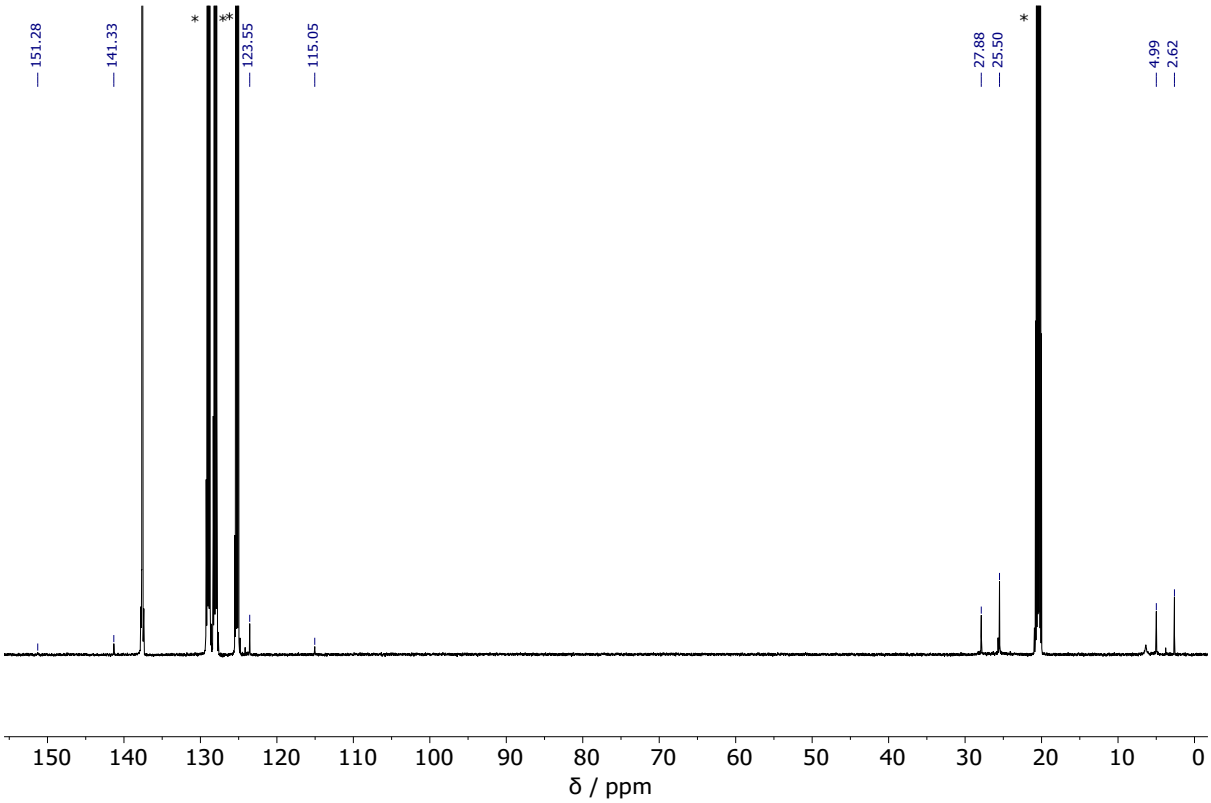

Figure S38 ^{13}C{^{1}H} NMR spectrum (C_7D_8, 343 K, 126 MHz) of [($^{NON\text{-}Dipp}$L)Ba(μ-N")K] (**11**). * denotes C_7D_8

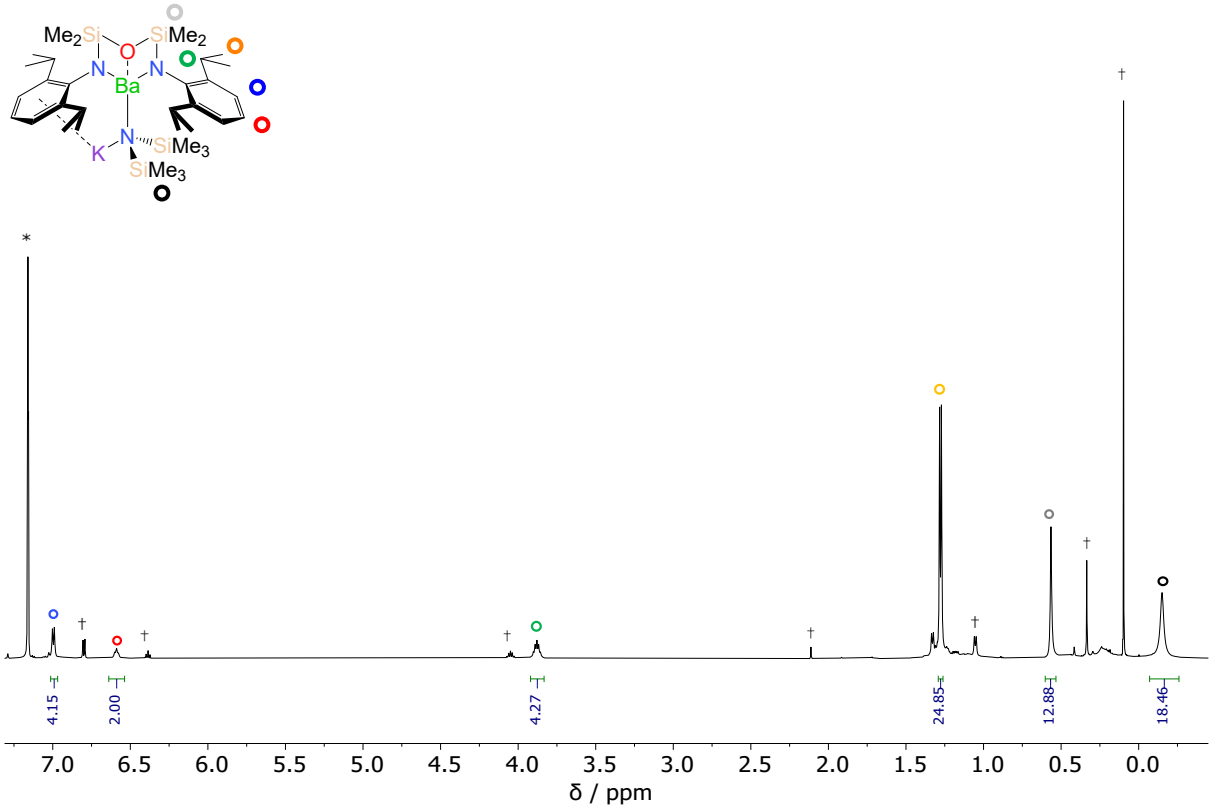

Figure S39 ^{1}H NMR spectrum (C_6D_6, 298 K, 600 MHz). of [($^{NON\text{-}Dipp}$L)Ba(μ-N")K] (**11**). † denotes KN" and [($^{NON\text{-}Dipp}$L)Ba(C_6D_6)$_n$] released by a solution-phase equilibrium, * denotes residual protio fraction of C_6D_6.

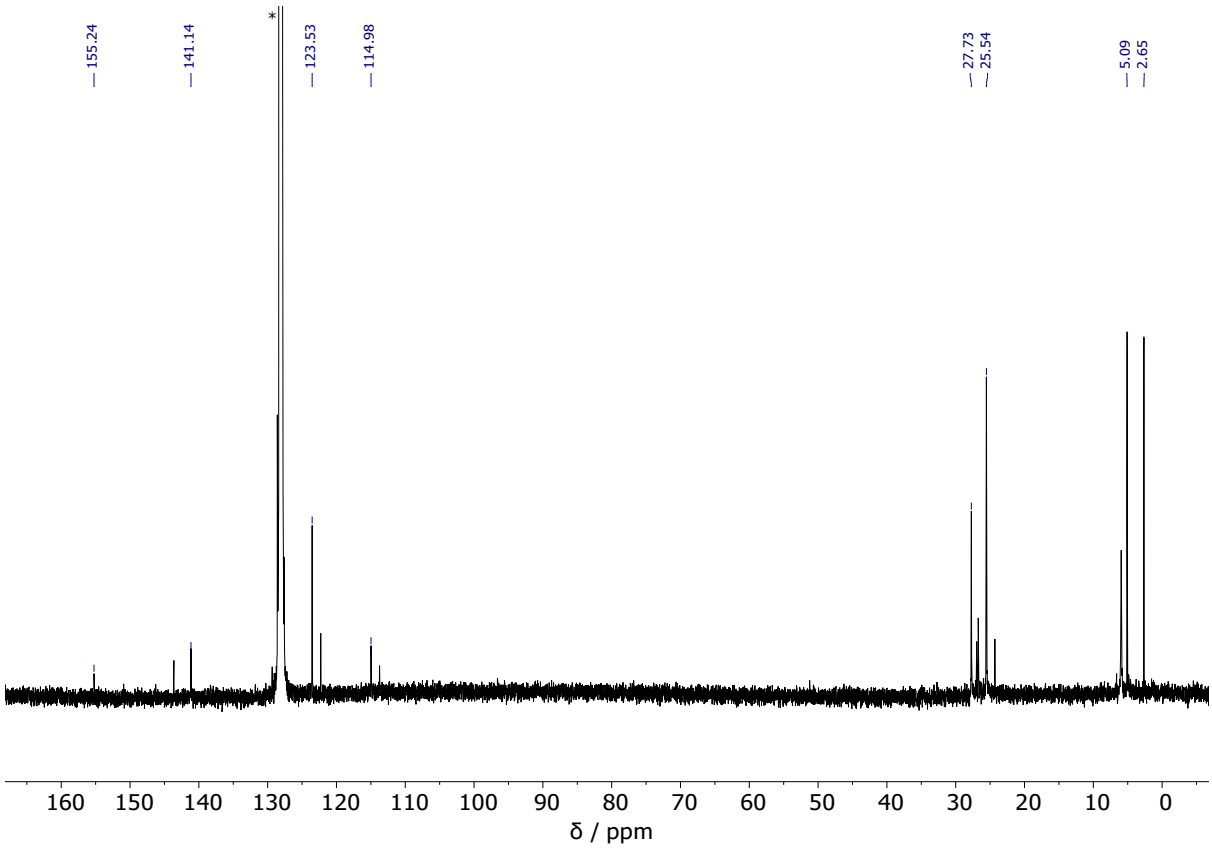

Figure S40 ^{13}C{^{1}H} NMR spectrum (C_6D_6, 298 K, 151 MHz) of [($^{NON\text{-}Dipp}$L)Ba(μ-N")K] (**11**). Unlabelled peaks result from KN" and [($^{NON\text{-}Dipp}$L)Ba(C_6D_6)$_n$] present due to a solution-phase equilibrium, * denotes C_6D_6.

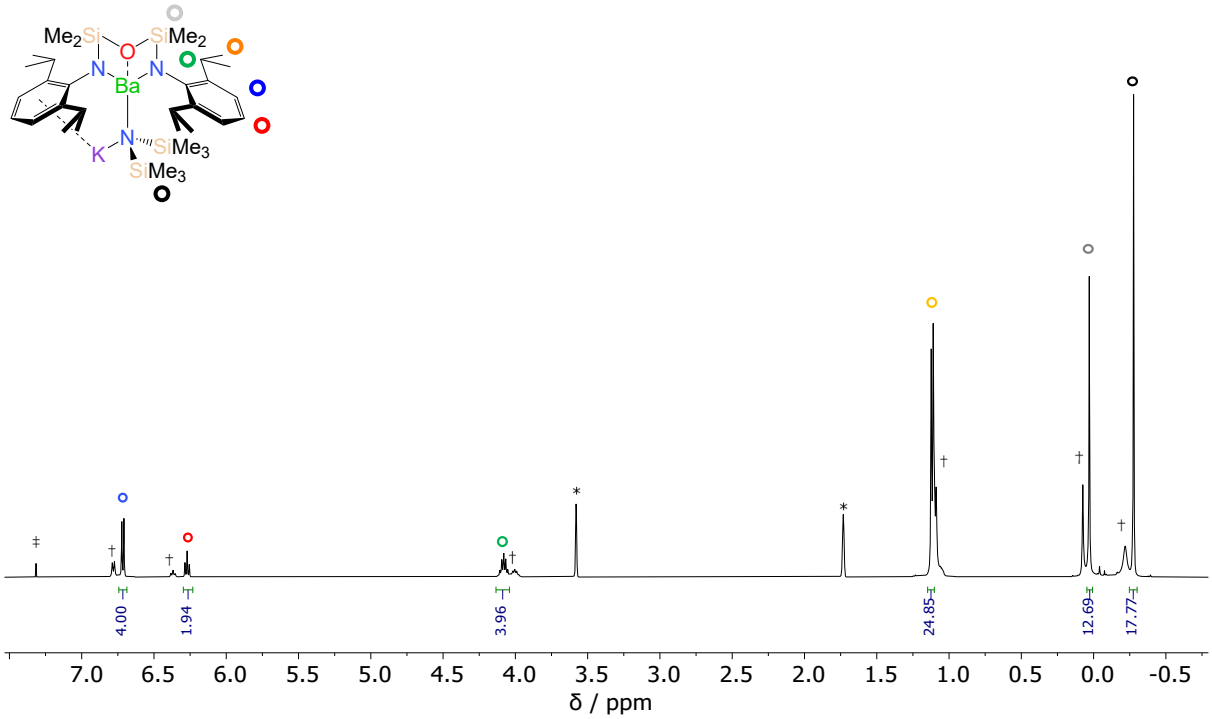

Figure S41 ^{1}H NMR spectrum (C_4D_8O, 263 K, 600 MHz) of [($^{NON\text{-}Dipp}$L)Ba(μ-N")K] (**11**). ‡ denotes co-crystallised benzene, † denotes [($^{NON\text{-}Dipp}$L)Ba(thf)$_n$] (**7**) and KN" released by a solution-phase equilibrium, * denotes residual protio fraction of C_4D_8O.

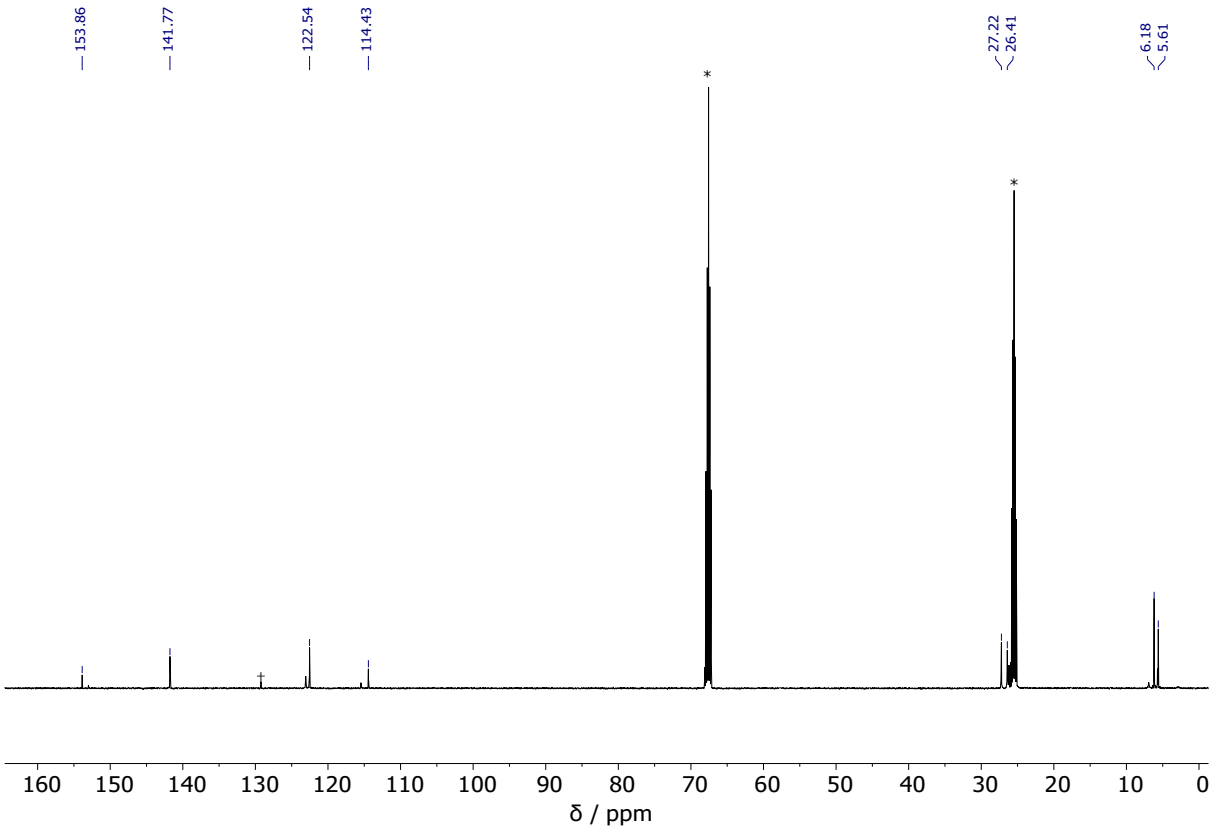

Figure S42 ^{13}C{^{1}H} NMR spectrum (C_4D_8O, 263 K, 151 MHz) of [($^{NON\text{-}Dipp}$L)Ba(μ-N")K] (**11**). Unlabelled peaks result from [($^{NON\text{-}Dipp}$L)Ba(thf)$_n$] (**7**) and KN" released by a solution-phase equilibrium. † denotes co-crystallised benzene, * denotes C_4D_8O.

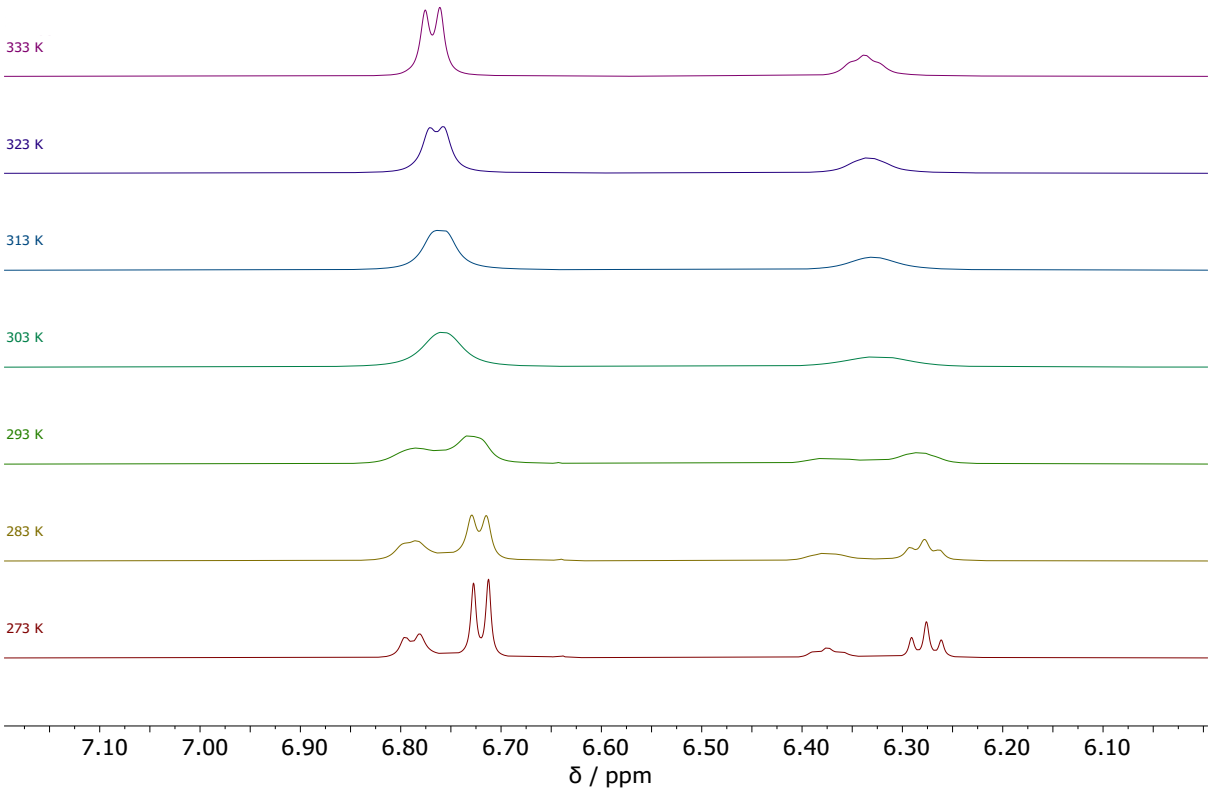

Figure S43 Aromatic regions of variable temperature ^{1}H NMR spectra (C_4D_8O, 500 MHz) showing the coalescence of signals assigned as [($^{NON\text{-}Dipp}$L)Ba(μ-N")K(thf)$_n$)] (**11^{thf}**), [($^{NON\text{-}Dipp}$L)Ba(thf)$_n$] (**7**).

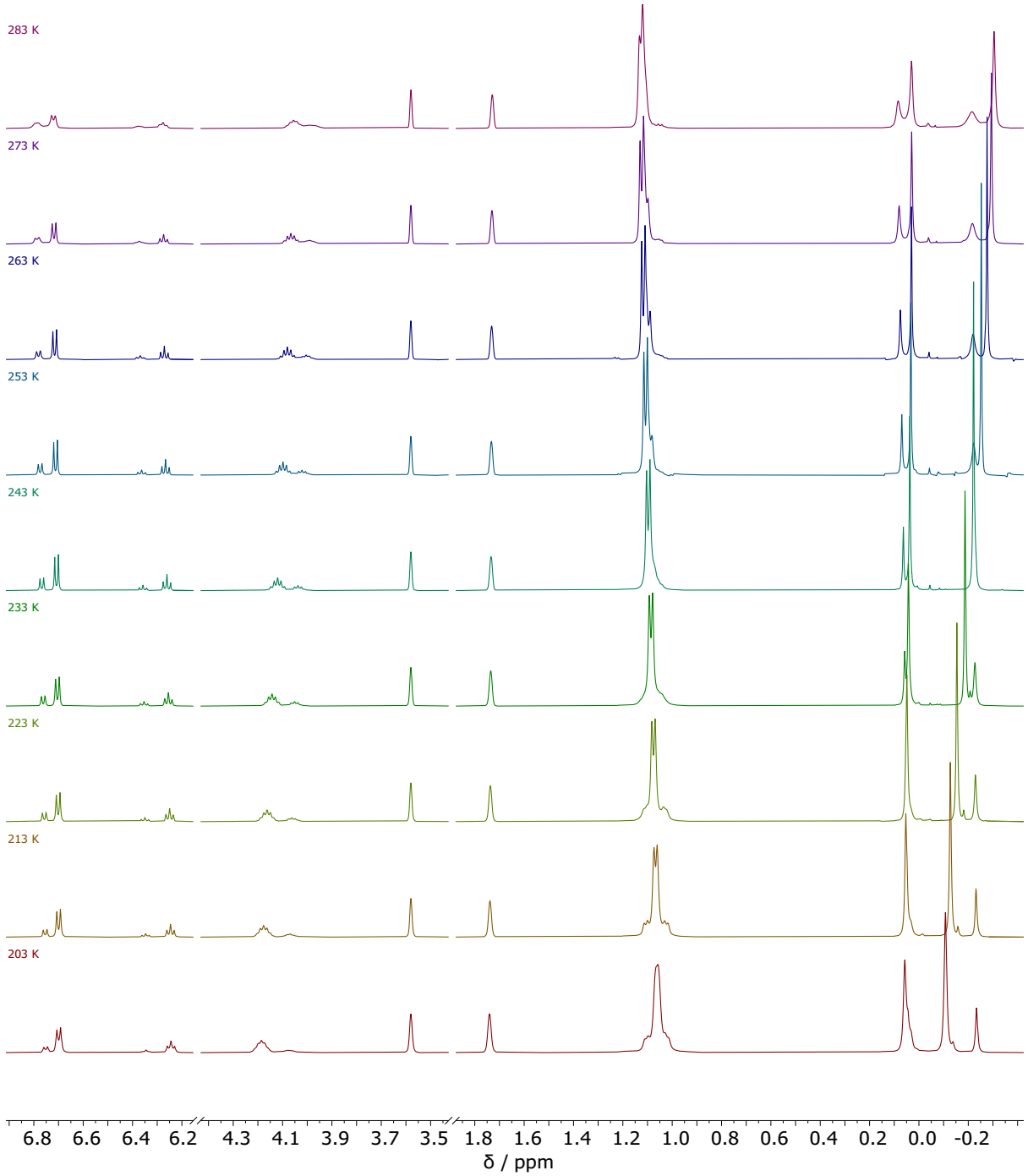

Figure S44 Variable temperature ^{1}H NMR spectra (C_4D_8O, 500 MHz) showing the temperature-sensitive equilibrium between [($^{NON\text{-}Dipp}$L)Ba(μ-N")K(thf)$_n$)] (**11^{thf}**), [($^{NON\text{-}Dipp}$L)Ba(thf)$_n$] (**7**) and KN".

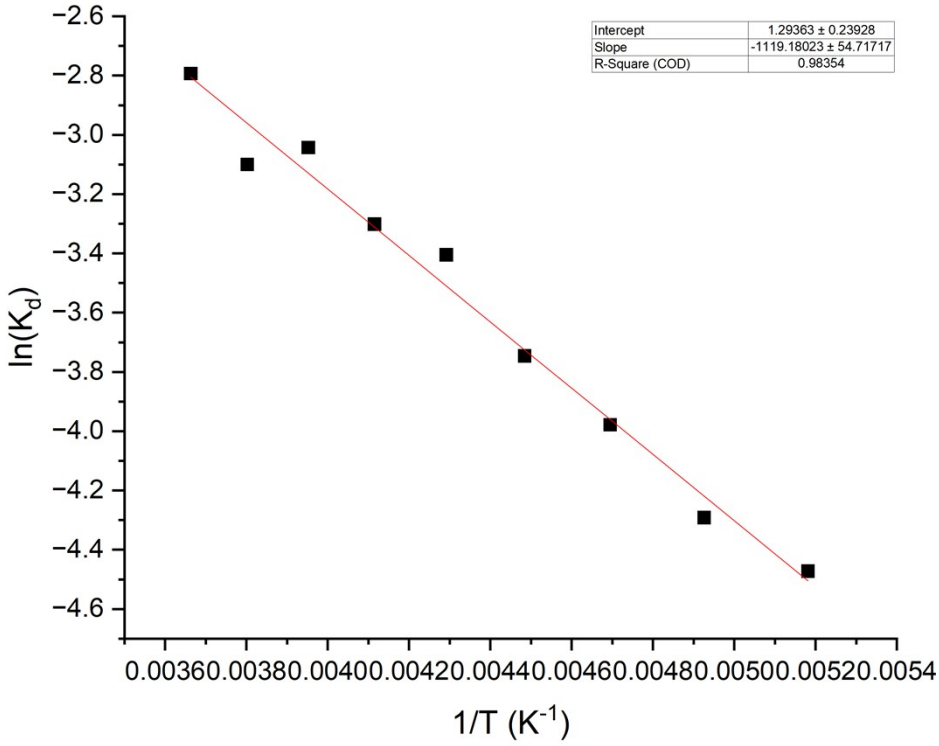

Figure S45 Van 't Hoff plot for the dissociation of [($^{NON\text{-}Dipp}$L)Ba(μ-N")K(thf)$_n$)] (**11^{thf}**) into [($^{NON\text{-}Dipp}$L)Ba(thf)$_n$] (**7**) and KN".

Table S1 Thermodynamic data extracted from Van 't Hoff plots in **Figures S30**, **S36** and **S44**.

Equilibrium	**Ae**	ΔH / kJ mol^{-1}	ΔS / J K^{-1} mol^{-1}	$\Delta G_{298\ K}$ / kJ mol^{-1}
9^{thf}/5	Ca	31.58	77.74	8.413
10^{thf}/6	Sr	12.72	19.20	6.998
11^{thf}/7	Ba	9.69	12.60	5.928

III Crystallographic Data

Table S2 Selected experimental crystallographic data.

Complex	**[{($^{NON\text{-}Dipp}$L)Mg}$_2$(thf)] (1·thf)**	**[($^{NON\text{-}Dipp}$L)Mg(thf)]$_2$ (1·thf$_2$)**
	Crystal data	
Chemical formula	$C_{66}H_{114}Mg_2N_4O_3Si_4 \cdot 0.5(C_6H_6)$	$C_{64}H_{108}Mg_2N_4O_4Si_4 \cdot 3(C_4H_8O)$
M_r	1211.64	1374.83
Crystal system, space group	Monoclinic, $P2_1/n$	Monoclinic, $P2_1/n$
Temperature (K)	119.99(10)	149.99(10)
a, b, c (Å)	13.29922(14), 35.7370(3), 15.62092(17)	21.3834(3), 13.93371(15), 27.2300(3)
α, β, γ (°)	90, 103.0217(10), 90	90, 102.0079(12), 90
V (Å^3)	7233.30(12)	7935.64(16)
Z	4	4
Radiation type	Cu $K\alpha$	Cu $K\alpha$
μ (mm^{-1})	1.27	1.252
Crystal size (mm)	0.373 × 0.212 × 0.157	0.23 × 0.119 × 0.085
	Data Collection	
Diffractometer	SuperNova, Dual, Cu at home/near, EosS2	SuperNova, Dual, Cu at home/near, EosS2

Absorption correction	Gaussian CrysAlisPro 1.171.40.53 (Rigaku Oxford Diffraction, 2019) Numerical absorption correction based on gaussian integration over a multifaceted crystal model. Empirical absorption correction using spherical harmonics, implemented in SCALE3 ABSPACK scaling algorithm.	Gaussian CrysAlisPro 1.171.40.53 (Rigaku Oxford Diffraction, 2019). Numerical absorption correction based on gaussian integration over a multifaceted crystal model. Empirical absorption correction using spherical harmonics, implemented in SCALE3 ABSPACK scaling algorithm.
T_{min}, T_{max}	0.577, 1.000	0.666, 1.000
No. of measured, independent and observed [$I > 2\sigma(I)$] reflections	52183, 14216, 13055	55164, 15587, 13191
R_{int}	0.0236	0.0307
Refinement		
$R[F^2 > 2\sigma(F^2)]$, $wR(F^2)$, S	0.0528, 0.1514, 1.032	0.0337, 0.0911, 1.042
No. of reflections	14216	15587
No. of parameters	716	746
No. of restraints	-	-
$(\Delta/\sigma)_{max}$	-	-
$\Delta\rho_{max}$, $\Delta\rho_{min}$ (e Å^{-3})	1.118, -0.77	0.971, -0.326
Absolute structure	-	-
Absolute structure parameter	-	-

Complex	**[($^{NON\text{-}Dipp}$L)Ca]$_2$·C$_6$H$_6$ (2)**	**[($^{NON\text{-}Dipp}$L)Sr]$_2$·C$_6$H$_6$ (3)**	**[($^{NON\text{-}Dipp}$L)Ba]$_2$·C$_6$H$_6$ (4)**
Crystal data			
Chemical formula	$C_{56}H_{92}Ca_2N_4O_2Si_4 \cdot C_6H_6$	$C_{56}H_{92}N_4O_2Si_4Sr_2 \cdot C_6H_6$	$C_{56}H_{92}Ba_2N_4O_2Si_4 \cdot C_6H_6$
M_r	1123.96	1219.04	1318.48
Crystal system, space group	Monoclinic, *C*2/*c*	Monoclinic, *C*2/*c*	Monoclinic, *C*2/*c*
Temperature (K)	150	150	150
a, *b*, *c* (Å)	30.8158 (2), 10.5849 (1), 19.6876 (2)	30.63227 (12), 10.88063 (5), 19.72812 (8)	29.62654 (9), 11.41698 (4), 20.02024 (7)
α, *β*, *γ* (°)	90, 94.094 (1), 90	90, 92.7130 (4), 90	90, 93.5715 (3), 90
V (Å^3)	6405.36 (10)	6567.98 (5)	6758.61 (4)
Z	4	4	4
Radiation type	Cu *K*α	Cu *K*α	Cu *K*α
μ (mm^{-1})	2.59	3.16	9.99
Crystal size (mm)	0.24 × 0.22 × 0.09	0.2 × 0.18 × 0.03	0.27 × 0.18 × 0.15
Data Collection			
Diffractometer	SuperNova, Dual, Cu at home/near, Atlas	SuperNova, Dual, Cu at home/near, Atlas	SuperNova, Dual, Cu at home/near, Atlas
Absorption correction	Multi-scan *CrysAlis PRO* 1.171.42.72a (Rigaku Oxford Diffraction, 2022) Empirical absorption correction using spherical harmonics, implemented in SCALE3 ABSPACK scaling algorithm.	Multi-scan *CrysAlis PRO* 1.171.42.72a (Rigaku Oxford Diffraction, 2022) Empirical absorption correction using spherical harmonics, implemented in SCALE3 ABSPACK scaling algorithm.	Gaussian *CrysAlis PRO* 1.171.41.93a (Rigaku Oxford Diffraction, 2020) Numerical absorption correction based on gaussian integration over a multifaceted crystal model Empirical absorption correction using spherical harmonics, implemented in SCALE3 ABSPACK scaling algorithm.

T_{min}, T_{max}	0.641, 1.000	0.642, 1.000	0.497, 1.000
No. of measured, independent and observed [$I > 2\sigma(I)$] reflections	86957, 6721, 6368	84520, 6865, 6399	89686, 7053, 6907
R_{int}	0.035	0.032	0.036
Refinement			
$R[F^2 > 2\sigma(F^2)]$, $wR(F^2)$, S	0.027, 0.077, 1.05	0.021, 0.057, 1.05	0.018, 0.046, 1.03
No. of reflections	6721	6865	7053
No. of parameters	346	353	350
No. of restraints	-	-	30
$(\Delta/\sigma)_{max}$	-	-	-
$\Delta\rho_{max}$, $\Delta\rho_{min}$ (e Å^{-3})	0.26, -0.27	0.46, -0.44	0.57, -0.70
Absolute structure	-	-	-
Absolute structure parameter	-	-	-

Complex	**[($^{NON\text{-}Dipp}$L)Ca]$_2$·C$_6$H$_{14}$ (2)**	**[($^{NON\text{-}Dipp}$L)Sr]$_2$·C$_6$H$_{14}$ (3)**	**[($^{NON\text{-}Dipp}$L)Ba]$_2$ (4a)**
		Crystal data	
Chemical formula	$C_{56}H_{92}Ca_2N_4O_2Si_4 \cdot C_6H_{14}$	$C_{56}H_{92}N_4O_2Si_4Sr_2 \cdot C_6H_{14}$	$C_{56}H_{92}Ba_2N_4O_2Si_4$
M_r	1132.02	1227.10	1240.37
Crystal system, space group	Monoclinic, *C*2/*c*	Monoclinic, *C*2/*c*	Monoclinic, *C*2/*c*
Temperature (K)	150	150	150
a, *b*, *c* (Å)	31.405 (3), 10.7081 (9), 19.7961 (13)	31.1544 (2), 10.9816 (1), 19.7810 (1)	18.5088 (2), 17.9946 (2), 19.4082 (3)
α, *β*, *γ* (°)	90, 92.787 (8), 90	90, 93.440 (1), 90	90, 109.429 (1), 90
V (Å^3)	6649.3 (10)	6755.38 (8)	6095.96 (14)
Z	4	4	4
Radiation type	Cu *K*α	Cu *K*α	Cu *K*α
μ (mm^{-1})	2.49	3.07	11.04
Crystal size (mm)	0.15 × 0.06 × 0.04	0.15 × 0.13 × 0.05	0.18 × 0.16 × 0.12
		Data Collection	
Diffractometer	SuperNova, Dual, Cu at home/near, Atlas	SuperNova, Dual, Cu at home/near, Atlas	SuperNova, Dual, Cu at home/near, Atlas
Absorption correction	Multi-scan *CrysAlis PRO* 1.171.43.95a (Rigaku Oxford Diffraction, 2023) Empirical absorption correction using spherical harmonics, implemented in SCALE3 ABSPACK scaling algorithm.	Multi-scan *CrysAlis PRO* 1.171.43.95a (Rigaku Oxford Diffraction, 2023) Empirical absorption correction using spherical harmonics, implemented in SCALE3 ABSPACK scaling algorithm.	Multi-scan *CrysAlis PRO* 1.171.43.95a (Rigaku Oxford Diffraction, 2023) Empirical absorption correction using spherical harmonics, implemented in SCALE3 ABSPACK scaling algorithm.
T_{min}, T_{max}	0.696, 1.000	0.807, 1.000	0.573, 1.000

No. of measured, independent and observed [$I > 2\sigma(I)$] reflections	40355, 6929, 4365	76112, 7046, 6211	71967, 6380, 6225
R_{int}	0.105	0.035	0.045
Refinement			
$R[F^2 > 2\sigma(F^2)]$, $wR(F^2)$, S	0.058, 0.184, 1.02	0.029, 0.079, 1.06	0.019, 0.051, 1.06
No. of reflections	6929	7046	6380
No. of parameters	347	319	319
No. of restraints	-	-	-
$(\Delta/\sigma)_{max}$	-	-	-
$\Delta\rho_{max}$, $\Delta\rho_{min}$ (e Å^{-3})	0.35, −0.40	0.75, −0.65	0.90, −0.81
Absolute structure	-	-	-
Absolute structure parameter	-	-	-

Complex	**[($^{NON\text{-}Dipp}$L)Ca(thf)$_2$] (5)**	**[($^{NON\text{-}Dipp}$L)Sr(thf)$_3$] (6)**	**[($^{NON\text{-}Dipp}$L)Ba(thf)$_3$] (7)**
		Crystal data	
Chemical formula	$C_{36}H_{62}CaN_2O_3Si_2$	$C_{40}H_{70}N_2O_4Si_2Sr$	$C_{40}H_{70}BaN_2O_4Si_2$
M_r	667.13	786.78	836.5
Crystal system, space group	Monoclinic, $P2_1/c$	Monoclinic, $P2_1$	Orthorhombic, $Pca2_1$
Temperature (K)	120.01(11)	120.00(10)	119.99(10)
a, b, c (Å)	10.30216(17), 20.9676(4), 18.5303(3)	10.86671(12), 18.7432(2), 11.11722(12)	17.2911(2), 14.4444(2), 17.4395(3)
α, β, γ (°)	90, 93.4268(16), 90	90, 107.5561(12), 90	90, 90, 90
V (Å^3)	3995.62(12)	2158.86(4)	4355.70(11)
Z	4	2	4
Radiation type	Cu $K\alpha$	Cu $K\alpha$	Cu $K\alpha$
μ (mm^{-1})	2.181	2.561	7.913
Crystal size (mm)	0.297 × 0.112 × 0074	0.158 × 0.098 × 0.079	0.213 × 0.141 × 0.0.107
		Data Collection	
Diffractometer	SuperNova, Dual, Cu at home/near, EosS2	SuperNova, Dual, Cu at home/near, EosS2	SuperNova, Dual, Cu at home/near, EosS2
Absorption correction	Gaussian CrysAlisPro 1.171.40.53 (Rigaku Oxford Diffraction, 2019). Numerical absorption correction based on gaussian integration over a multifaceted crystal model. Empirical absorption correction using spherical	Gaussian CrysAlisPro 1.171.40.53 (Rigaku Oxford Diffraction, 2019). Numerical absorption correction based on gaussian integration over a multifaceted crystal model. Empirical absorption correction using spherical	Gaussian CrysAlisPro 1.171.40.53 (Rigaku Oxford Diffraction, 2019). Numerical absorption correction based on gaussian integration over a multifaceted crystal model. Empirical absorption correction using spherical

	harmonics, implemented in SCALE3 ABSPACK scaling algorithm.	harmonics, implemented in SCALE3 ABSPACK scaling algorithm.	harmonics, implemented in SCALE3 ABSPACK scaling algorithm
T_{min}, T_{max}	0.626, 1.000	0.764, 1.000	0.36, 0.74
No. of measured, independent and observed [$I > 2\sigma(I)$] reflections	27707, 7859, 6876	12925, 6637 , 6507	17670, 7245, 7043
R_{int}	0.0317	0.0374	0.0632
Refinement			
$R[F^2 > 2\sigma(F^2)]$, $wR(F^2)$, S	0.0369, 0.0985, 1.03	0.027, 0.067, 1.022	0.0206, 0.0505, 1.024
No. of reflections	7859	6637	7245
No. of parameters	487	455	454
No. of restraints	27	10	1
$(\Delta/\sigma)_{max}$	-	-	-
$\Delta\rho_{max}$, $\Delta\rho_{min}$ (e Å^{-3})	0.506, -0.381	0.477, -0.307	0.386, -0.417
Absolute structure	-	-	-
Absolute structure parameter	-	-	-

Complex	**[($^{NNO\text{-}Dipp}$L)Mg(μ-N")K]$_n$ (8)**
Crystal data	
Chemical formula	$C_{34}H_{64}KMgN_3OSi_4 \cdot C_7H_8$
M_r	798.78
Crystal system, space group	Monoclinic, $P2_1/n$
Temperature (K)	150
a, b, c (Å)	16.55505 (12), 18.14500 (12), 17.16341 (13)
α, β, γ (°)	112.3390 (9)
V (Å^3)	4768.81 (6)
Z	4
Radiation type	Cu $K\alpha$
μ (mm^{-1})	2.30
Crystal size (mm)	0.39 × 0.18 × 0.13
Data collection	
Diffractometer	SuperNova, Dual, Cu at home/near, EosS2
Absorption correction	Gaussian *CrysAlis PRO* 1.171.40.53 (Rigaku Oxford Diffraction, 2019) Numerical absorption correction based on gaussian integration over a multifaceted crystal model Empirical absorption correction using spherical harmonics, implemented in SCALE3 ABSPACK scaling algorithm.
T_{min}, T_{max}	0.356, 1

No. of measured, independent and observed [$I > 2\sigma(I)$] reflections	33934, 9383, 8611
R_{int}	0.025
Refinement	
$R[F^2 > 2\sigma(F^2)]$, $wR(F^2)$, S	0.034, 0.092, 1.03
No. of reflections	9383
No. of parameters	479
No. of restraints	0
$(\Delta/\sigma)_{max}$	-
$\Delta\rho_{max}$, $\Delta\rho_{min}$ (e Å^{-3})	0.84, −0.34
Absolute structure	-
Absolute structure parameter	-

Complex	**[($^{NON\text{-}Dipp}$L)Ca(μ-N")K]$_n$ (9)**	**[($^{NON\text{-}Dipp}$L)Sr(μ-N")K]$_n$ (10)**	**[($^{NON\text{-}Dipp}$L)Ba(μ-N")K]$_n$ (11)**

Crystal data			
Chemical formula	$C_{68}H_{128}Ca_2K_2N_6O_2Si_8 \cdot 0.5(C_6H_6)$	$C_{34}H_{64}KN_3OSi_4Sr$	$C_{68}H_{128}Ba_2K_2N_6O_2Si_8$
M_r	1483.89	769.96	1639.36
Crystal system, space group	Triclinic, *P*1	Orthorhombic, $Pna2_1$	Monoclinic, $P2_1$
Temperature (K)	150	150	150
a, *b*, *c* (Å)	11.5062 (3), 19.0448 (6), 20.7624 (6)	24.5555 (2), 20.6930 (2), 16.8114 (2)	20.7134 (1), 16.9120 (1), 24.6169 (1)
α, *β*, *γ* (°)	88.998 (2), 80.120 (2), 75.017 (3)	90, 90, 90	90.29
V (Å^3)	4328.1 (2)	8542.33 (15)	8623.31 (7)
Z	2	8	4
Radiation type	Cu *K*α	Cu *K*α	Cu *K*α
μ (mm^{-1})	3.39	3.91	9.30
Crystal size (mm)	0.21 × 0.16 × 0.12	0.4 × 0.08 × 0.07	0.15 × 0.12 × 0.10
Data Collection			
Diffractometer	SuperNova, Dual, Cu at home/near, Atlas	SuperNova, Dual, Cu at home/near, Atlas	SuperNova, Dual, Cu at home/near, Atlas
Absorption correction	Gaussian *CrysAlis PRO* 1.171.42.72a (Rigaku Oxford Diffraction, 2022) Numerical absorption correction based on gaussian integration over a multifaceted crystal model Empirical absorption correction using spherical harmonics, implemented in SCALE3 ABSPACK scaling algorithm.	Multi-scan *CrysAlis PRO* 1.171.42.72a (Rigaku Oxford Diffraction, 2022) Empirical absorption correction using spherical harmonics, implemented in SCALE3 ABSPACK scaling algorithm.	Multi-scan *CrysAlis PRO* 1.171.43.90 (Rigaku Oxford Diffraction, 2023) Empirical absorption correction using spherical harmonics, implemented in SCALE3 ABSPACK scaling algorithm.
T_{min}, T_{max}	0.633, 0.820	0.431, 1.000	0.544, 1.000

No. of measured, independent and observed [$I > 2\sigma(I)$] reflections	49068, 17878, 14246	84481, 16314, 15086	123918, 34960, 33165
R_{int}	0.050	0.048	0.040
Refinement			
$R[F^2 > 2\sigma(F^2)]$, $wR(F^2)$, S	0.043, 0.123, 1.04	0.031, 0.075, 1.06	0.050, 0.136, 1.07
No. of reflections	17878	16314	34960
No. of parameters	883	872	1703
No. of restraints	116	29	2
$(\Delta/\sigma)_{max}$	-	-	-
$\Delta\rho_{max}$, $\Delta\rho_{min}$ (e Å^{-3})	0.49, −0.37	0.38, −0.26	2.70, −2.17
Absolute structure	-	Refined as an inversion twin.	Refined as an inversion twin.
Absolute structure parameter	-	0.326 (12)	0.147 (4)

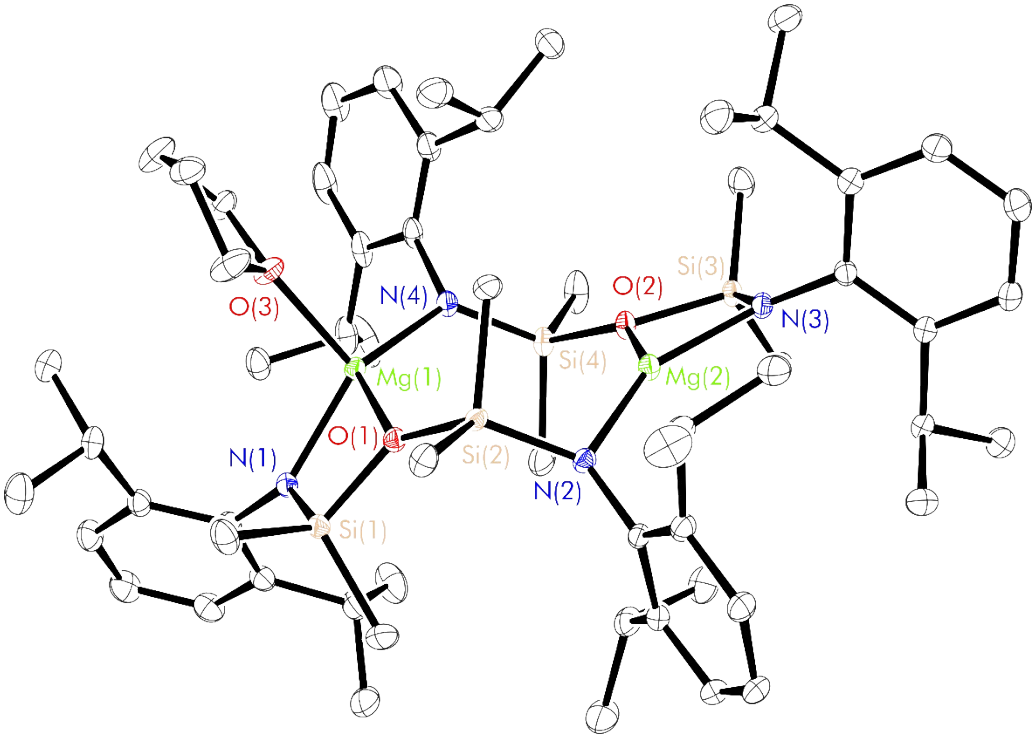

Figure S47 Thermal displacement ellipsoid drawing (30% probability) of [{($^{NON\text{-}Dipp}$L)Mg}$_2$(thf)] (**1·thf**). All hydrogen atoms omitted for clarity.

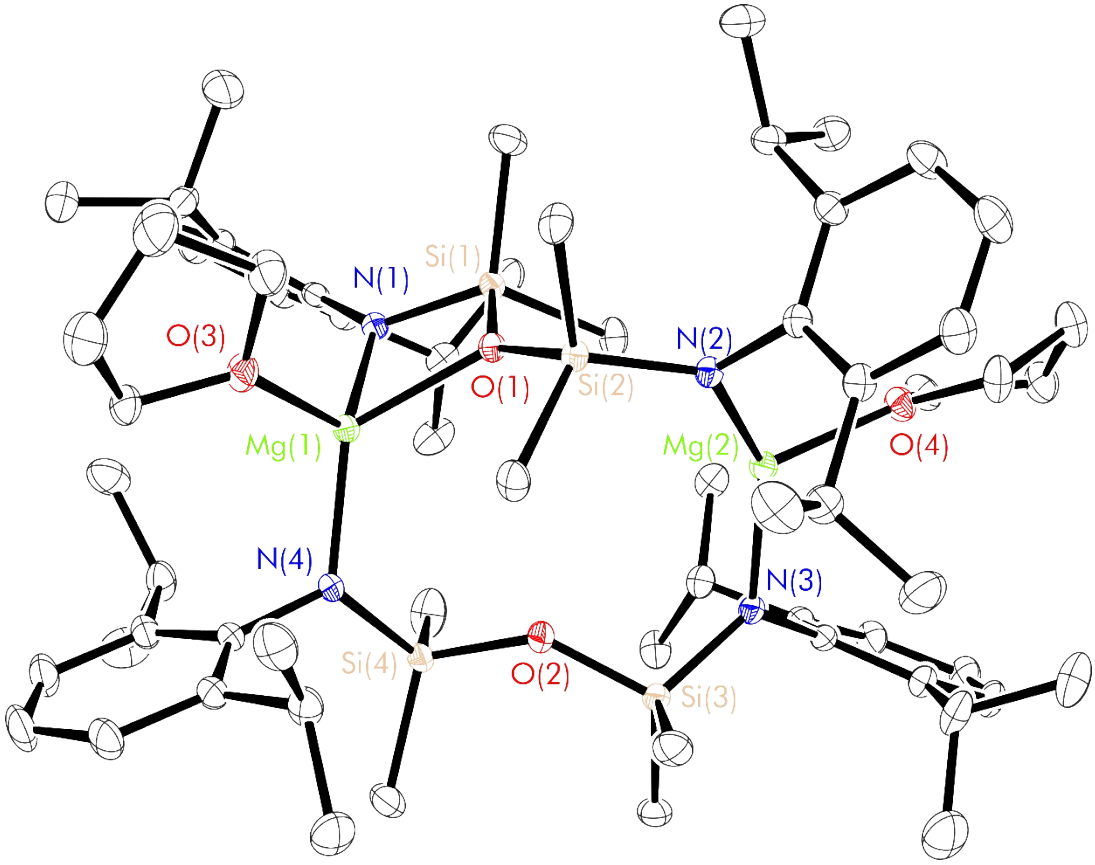

Figure S46 Thermal displacement ellipsoid drawing (30% probability) of [($^{NON\text{-}Dipp}$L)Mg(thf)]$_2$ (**1·thf$_2$**). All hydrogen atoms omitted for clarity.

Table S3 Experimental metrical parameters (bond lengths in Å and angles in °) for [{($^{NON\text{-}Dipp}$L)Mg}$_2$(thf)] (**1·thf**) and [($^{NON\text{-}Dipp}$L)Mg(thf)]$_2$ (**1·thf$_2$**). Angles denoted * not included in sum totals.

Parameter	**1·thf**	**1·thf$_2$**
Mg(1)-N(1)	2.035(2)	2.0626(9)
Mg(1)-N(4)	2.019(2)	2.000(1)
Mg(1)-O(1)	2.128(2)	2.133(1)
Mg(1)-O(3)	2.051(2)	2.046(1)
Mg(2)-N(3)	1.950(2)	1.992(1)
Mg(2)-N(2)	1.969(2)	2.003(1)
Mg(2)-O(2)	2.040(2)	3.549(1)
Mg(2)-O(4)	-	2.018(1)
Mg(1)-Mg(2)	4.6000(9)	5.2386(7)
N(1)-Mg(1)-N(4)	140.32(8)	128.61(5)
N(1)-Mg(1)-O(1)	75.04(7)	74.83(4)
N(1)-Mg(1)-O(3)	107.88(7)	115.74(4)
N(4)-Mg(1)-O(1)	118.20(7)	124.09(4)
N(4)-Mg(1)-O(3)	104.82(7)	107.52(4)
O(1)-Mg(1)-O(3)	103.42(7)	99.91(4)
ΣX-Mg(1)-X	649.68(18)	650.70(10)
N(2)-Mg(2)-N(3)	147.95(8)	141.68(5)
N(2)-Mg(2)-O(2)	131.37(7)	47.66(3)*
N(2)-Mg(2)-O(4)	-	108.53(4)
N(3)-Mg(2)-O(2)	77.56(7)	111.91(4)*
N(3)-Mg(2)-O(4)	-	107.05(4)
ΣX-Mg(2)-X	356.88(13)	357.26(8)

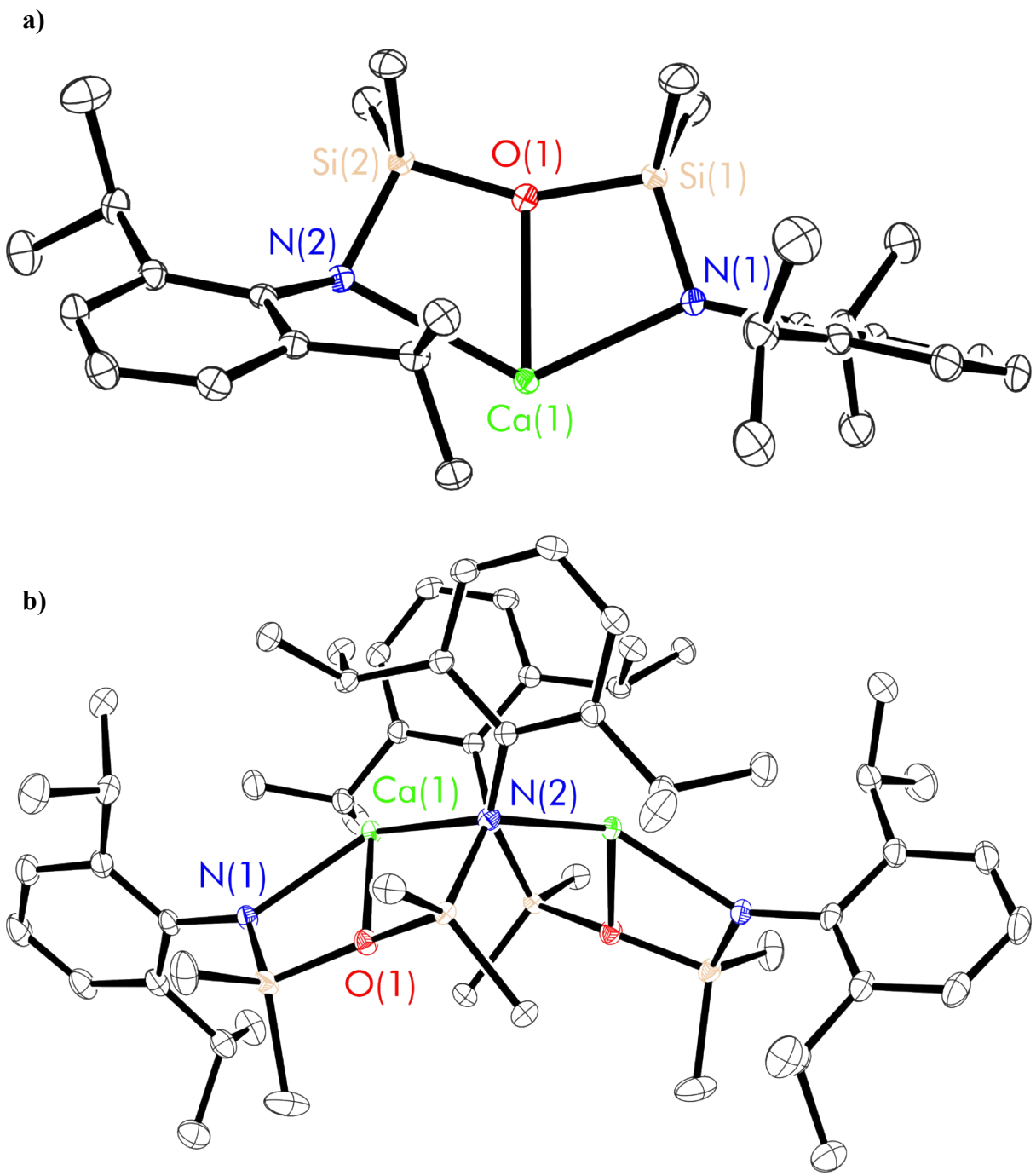

Figure S48 Thermal displacement ellipsoid drawing (30% probability) of $[(^{NON\text{-}Dipp}L)Ca]_2$ (**2**) grown from benzene; **a)** asymmetric unit **b)** full dimeric structure generated by a (–X+1, Y, –Z+1/2) symmetry operation. All hydrogen atoms omitted for clarity.

Table S4 Experimental metrical parameters (bond lengths in Å and angles in °) for $[(^{NON\text{-}Dipp}L)Ca]_2$ (**2**) crystallised from benzene and *n*-hexane. * refers to symmetry related atoms.

Parameter	$[(^{NON\text{-}Dipp}L)Ca]_2 \cdot C_6H_6$	$[(^{NON\text{-}Dipp}L)Ca]_2 \cdot C_6H_{14}$
Ca(1)-N(1)	2.340(1)	2.349(3)
Ca(1)-N(2)	2.686(1)	2.700(3)
Ca(1)-N(2)*	2.3787(9)	2.386(3)
Ca(1)-O(1)	2.3494(8)	2.344(2)
Ca(1)-C(17)*	3.000(1)	3.009(3)
Ca(1)-C(18)*	3.269(1)	3.268(3)
N(1)-Si(1)	1.684(1)	1.685(3)
N(2)-Si(2)	1.698(1)	1.701(2)
O(1)-Si(1)	1.6694(9)	1.673(3)
O(1)-Si(2)	1.6542(9)	1.657(3)
Ca(1)-Ca(1)*	3.7151(8)	3.7311(9)
N(1)-Ca(1)-N(2)	126.01(3)	125.5(1)
N(1)-Ca(1)-N(2)*	134.41(4)	135.8(1)
N(2)-Ca(1)-N(2)*	85.31(3)	85.32(9)
N(1)-Ca(1)-O(1)	65.77(3)	65.82(9)
N(2)-Ca(1)-O(1)	61.91(3)	61.95(8)
N(2)-Ca(1)-O(1)*	120.43(3)	119.65(9)
Σ{∠Ca(1)}	593.84(8)	594.04(23)
Si(1)-O(1)-Ca(1)	97.70(4)	97.8(1)
Si(2)-O(1)-Ca(1)	104.94(4)	105.2(1)
Si(1)-O(1)-Si(2)	151.14(5)	148.9(2)
Σ{∠O(1)}	353.78(7)	351.90(24)
C(5)-N(1)-Ca(1)	141.05(7)	139.1(2)
C(5)-N(1)-Si(1)	120.61(8)	123.1(3)
Ca(1)-N(1)-Si(1)	97.62(5)	97.3(1)
Σ{∠N(1)}	359.28(12)	359.50(37)
Ca(1)-N(2)-Ca(1)*	94.16(3)	94.18(9)
Ca(1)-N(2)-C(17)	121.44(6)	121.4(2)
Ca(1)-N(2)-Si(2)	91.01(4)	90.6(1)
Ca(1)-N(2)-C(17)*	101.34(6)	101.3(2)
Ca(1)-N(2)-Si(2)*	121.89(5)	120.6(1)
C(17)-N(2)-Si(2)	124.11(7)	125.5(2)
Σ{∠N(2)}	653.95(13)	653.58(38)
$Plane_{N(1)Si(1)O(1)Ca(1)}$-$Plane_{N(2)Si(2)O(1)Ca(1)}$ fold angle	14.58(4)	17.20(11)
$Plane_{Ca_2N_2}$-$Plane_{N_2Si_2OCa}$ fold angle	48.608(12)	48.17(3)
$Plane_{C(17)\text{-}C(22)}$-$Plane_{C(17)\text{-}C(22)}$ fold angle	152.95(7)	151.29(19)
N(2)-Ca(1)-Ca(1)*-N(2)*	168.54(5)	168.8(1)
Ca(1)-N(2)-N(2)*-Ca(1)*	169.39(4)	196.6(1)

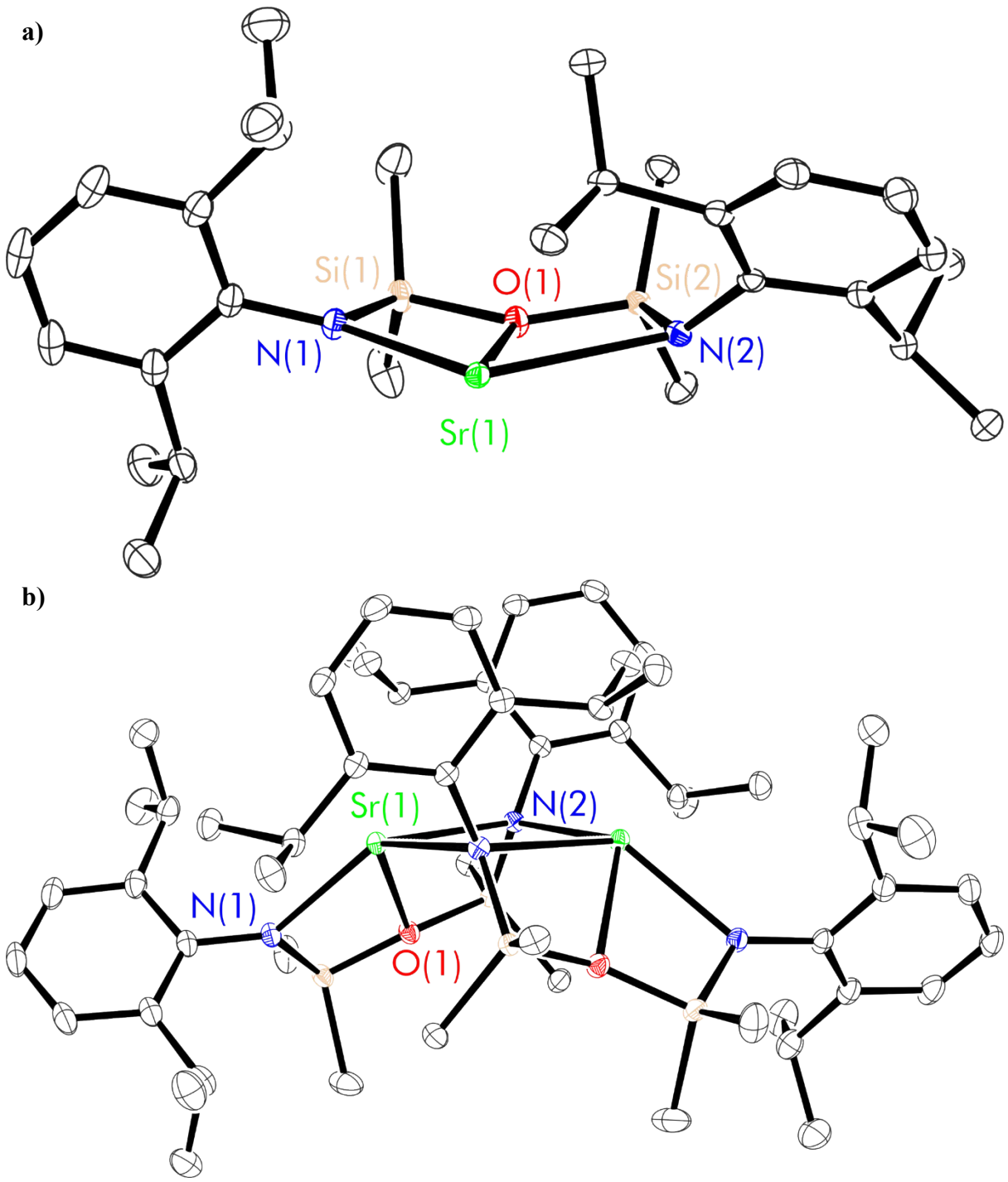

Figure S49 Thermal displacement ellipsoid drawing (30% probability) of $[(^{NON\text{-}Dipp}L)Sr]_2$ (**3**) grown from benzene; **a)** asymmetric unit **b)** full dimeric structure generated by a (–X+1, Y, –Z+1/2) symmetry operation. All hydrogen atoms omitted for clarity.

Table S5 Experimental metrical parameters (bond lengths in Å and angles in °) for $[(^{NON\text{-}Dipp}L)Sr]_2$ crystallised from benzene and *n*-hexane. * refers to symmetry related atoms.

Parameter	$[(^{NON\text{-}Dipp}L)Sr]_2 \cdot C_6H_6$	$[(^{NON\text{-}Dipp}L)Sr]_2 \cdot C_6H_{14}$
Sr(1)-N(1)	2.473(1)	2.477(2)
Sr(1)-N(2)	2.798(1)	2.782(2)
Sr(1)-N(2)*	2.541(1)	2.552(1)
Sr(1)-O(1)	2.5086(9)	2.502(1)
Sr(1)-C(17)*	3.029(1)	3.029(2)
Sr(1)-C(18)*	3.183(1)	3.168(2)
N(1)-Si(1)	1.679(1)	1.679(2)
N(2)-Si(2)	1.695(1)	1.694(2)
O(1)-Si(1)	1.668(1)	1.670(1)
O(1)-Si(2)	1.651(1)	1.651(1)
Sr(1)-Sr(1)*	3.9504(8)	3.9479(9)
N(1)-Sr(1)-N(2)	119.22(3)	119.25(5)
N(1)-Sr(1)-N(2)*	133.79(4)	133.55(5)
N(2)-Sr(1)-N(2)*	84.44(3)	84.36(5)
N(1)-Sr(1)-O(1)	61.81(3)	61.91(5)
N(2)-Sr(1)-O(1)	58.61(3)	58.77(4)
N(2)-Sr(1)-O(1)*	116.03(3)	114.88(5)
Σ{∠Sr(1)}	574.01(8)	572.720(12)
Si(1)-O(1)-Sr(1)	98.70(4)	98.79(6)
Si(2)-O(1)-Sr(1)	105.55(4)	105.34(6)
Si(1)-O(1)-Si(2)	151.32(6)	149.89(9)
Σ{∠O(1)}	355.59(8)	354.020(12)
C(5)-N(1)-Sr(1)	136.04(8)	134.4(1)
C(5)-N(1)-Si(1)	122.94(8)	124.9(1)
Sr(1)-N(1)-Si(1)	99.74(5)	99.49(8)
Σ{∠N(1)}	358.72(12)	358.79(16)
Sr(1)-N(2)-Sr(1)*	95.31(3)	95.40(5)
Sr(1)-N(2)-C(17)	121.86(7)	121.9(1)
Sr(1)-N(2)-Si(2)	93.24(4)	93.44(6)
Sr(1)-N(2)-C(17)*	95.75(7)	95.3(1)
Sr(1)-N(2)-Si(2)*	120.84(5)	120.33(8)
C(17)-N(2)-Si(2)	127.21(8)	127.7(1)
Σ{∠N(2)}	654.21(14)	654.07(18)
$Plane_{N(1)Si(1)O(1)Sr(1)}$-$Plane_{N(2)Si(2)O(1)Sr(1)}$ hinge angle	13.04(4)	14.44(6)
$Plane_{Sr_2N_2}$-$Plane_{N_2Si_2OSr}$ hinge angle	51.228(12)	51.864(18)
$Plane_{C(17)\text{-}C(22)}$-$Plane_{C(17)\text{-}C(22)}$ hinge angle	22.66(8)	23.26(11)
N(2)-Sr(1)-Sr(1)*-N(2)* torsion	172.13(5)	172.30(7)
Sr(1)-N(2)-N(2)*-Sr(1)* torsion	172.84(4)	173.00(6)

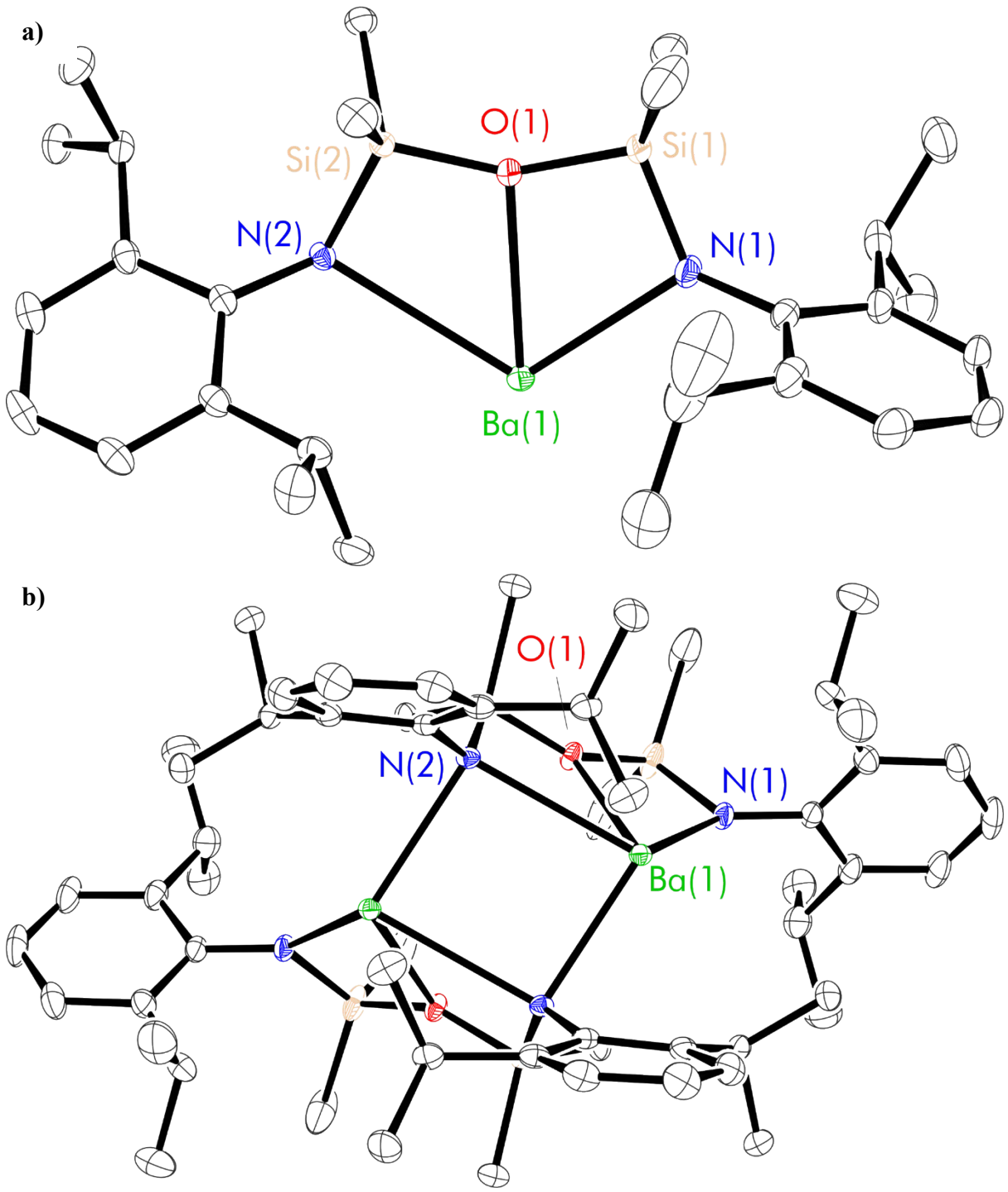

Figure S50 Thermal displacement ellipsoid drawing (30% probability) of $[(^{NON\text{-}Dipp}L)Ba]_2$ grown from benzene (**4**); **a)** asymmetric unit **b)** full dimeric structure generated by a (–X+1, Y, –Z+1/2) symmetry operation. All hydrogen atoms omitted for clarity.

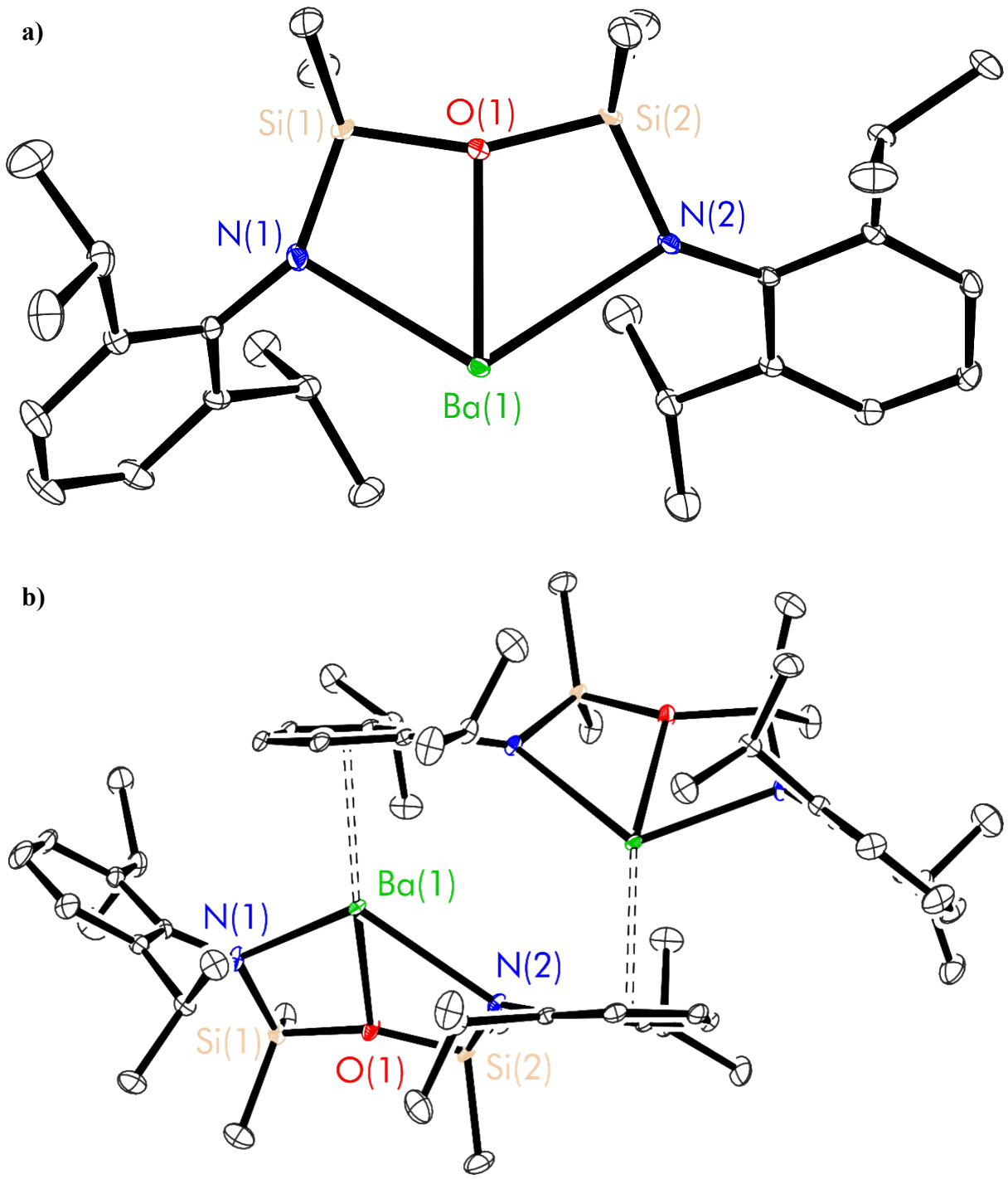

Figure S51 Thermal displacement ellipsoid drawing (30% probability) of $[(^{NON\text{-}Dipp}L)Ba]_2$ grown from hexane (**4a**); **a)** asymmetric unit **b)** full dimeric structure generated by a (–X+1, Y, –Z +3/2) symmetry operation. All hydrogen atoms omitted for clarity.

Table S6 Experimental metrical parameters (bond lengths in Å and angles in °) for $[(^{NON\text{-}Dipp}L)Ba]_2$ crystallised from benzene (**4**) and *n*-hexane (**4a**). * refers to symmetry related atoms.

Parameter	$[(^{NON\text{-}Dipp}L)Ba]_2 \cdot C_6H_6$ (**4**)	$[(^{NON\text{-}Dipp}L)Ba]_2$ (**4b**)
Ba(1)-N(1)	2.582(1)	2.569(2)
Ba(1)-N(2)	2.970(1)	2.799(1)
Ba(1)-N(2)*	2.714(1)	3.702(2)
Ba(1)-O(1)	2.672(1)	2.651(1)
Ba(1)-C(17)*	3.113(1)	3.095(2)
Ba(1)-C(18)*	3.223(1)	3.088(2)
Ba(1)-Centroid$_{C(17)\text{-}C(22)}$*	3.9203(7)	2.8618(7)
Ba(1)-Plane$_{C(17)\text{-}C(22)}$*	2.551(2)	2.8498(7)
N(1)-Si(1)	1.666(1)	1.661(1)
N(2)-Si(2)	1.697(1)	1.701(2)
O(1)-Si(1)	1.662(1)	1.664(1)
O(1)-Si(2)	1.647(1)	1.650(1)
Ba(1)-Ba(1)*	4.1561(8)	4.7644(6)
N(1)-Ba(1)-N(2)	112.61(4)	114.57(5)
N(1)-Ba(1)-N(2)*	122.09(4)	140.79(4)
N(2)-Ba(1)-N(2)*	86.00(4)	80.32(4)
N(1)-Ba(1)-O(1)	58.41(4)	58.43(4)
N(2)-Ba(1)-O(1)	54.62(3)	56.59(4)
N(2)-Ba(1)-O(1)$_{inter}$	108.33(4)	118.73(4)
N(1)-Ba(1)-Centroid$_{C(17)\text{-}C(22)}$*	137.82(4)	112.49(4)
N(2)-Ba(1)-Centroid$_{C(17)\text{-}C(22)}$*	106.98(3)	128.01(3)
O(1)-Ba(1)-Centroid$_{C(17)\text{-}C(22)}$*	152.99(3)	151.65(3)
Σ{∠Ba(1)}	542.06(9)	621.74(10)
Si(1)-O(1)-Ba(1)	98.65(5)	99.07(6)
Si(2)-O(1)-Ba(1)	107.18(5)	103.47(6)
Si(1)-O(1)-Si(2)	150.32(7)	157.43(9)
Σ{∠O(1)}	356.15(10)	359.970(12)
C(5)-N(1)-Ba(1)	125.2(1)	110.3(1)
C(5)-N(1)-Si(1)	128.3(1)	143.9(1)
Ba(1)-N(1)-Si(1)	102.02(6)	102.36(7)
Σ{∠N(1)}	355.52(15)	356.56(16)
Ba(1)-N(2)-Ba(1)*	93.85(4)	93.22(4)
Ba(1)-N(2)-C(17)	124.13(9)	129.6(1)
Ba(1)-N(2)-Si(2)	94.26(5)	96.42(6)
Ba(1)-N(2)-C(17)*	92.58(8)	53.75(8)
Ba(1)-N(2)-Si(2)*	119.45(6)	146.01(7)
C(17)-N(2)-Si(2)	129.0(1)	132.8(1)
Σ{∠N(2)}	653.27(18)	358.82(15)

Table S7 Comparison of experimental metrical parameters for $[(^{NON\text{-}Dipp}L)Ae]_2{\cdot}C_6H_6$ (Ae = Mg, Ca, Sr and Ba). * refers to symmetry related atoms. Metrics for $[(^{NON\text{-}Dipp}L)Mg]_2{\cdot}C_6H_6$ (**1**) reproduced from reference 12.

Interatomic distances / Å	$[(^{NON\text{-}Dipp}L)Mg]_2$ (**1**)	$[(^{NON\text{-}Dipp}L)Ca]_2$ (**2**)	$[(^{NON\text{-}Dipp}L)Sr]_2$ (**3**)	$[(^{NON\text{-}Dipp}L)Ba]_2$ (**4**)
Ae(1)-N(1)	1.987(1)	2.340(1)	2.473(1)	2.582(1)
Ae(1)-N(2)	3.551(1)	2.686(1)	2.798(1)	2.970(1)
Ae(1)-N(2)*	1.999(1)	2.3787(9)	2.541(1)	2.714(1)
Ae(1)-O(1)	2.066(1)	2.3494(8)	2.5086(9)	2.672(1)
Ae(1)-C(17)*	2.877(1)	3.000(1)	3.029(1)	3.113(1)
Ae(1)-C(18)*	3.284(1)	3.269(1)	3.183(1)	3.223(1)
N(1)-Si(1)	1.687(1)	1.684(1)	1.679(1)	1.666(1)
N(2)-Si(2)	1.687(1)	1.698(1)	1.695(1)	1.697(1)
O(1)-Si(1)	1.707(1)	1.6694(9)	1.668(1)	1.662(1)
O(1)-Si(2)	1.692(1)	1.6542(9)	1.651(1)	1.647(1)
Ae(1)-Ae(1)*	4.1130(9)	3.7151(8)	3.9504(8)	4.1561(8)
Bond Angles / °	**$[(^{NON\text{-}Dipp}L)Mg]_2$ (1)**	**$[(^{NON\text{-}Dipp}L)Ca]_2$ (2)**	**$[(^{NON\text{-}Dipp}L)Sr]_2$ (3)**	**$[(^{NON\text{-}Dipp}L)Ba]_2$ (4)**
N(1)-Ae(1)-N(2)	125.62(4)	126.01(3)	119.22(3)	112.61(4)
N(1)-Ae(1)-N(2)*	143.05(5)	134.41(4)	133.79(4)	122.09(4)
N(2)-Ae(1)-N(2)*	86.69(4)	85.31(3)	84.44(3)	86.00(4)
N(1)-Ae(1)-O(1)	76.33(4)	65.77(3)	61.81(3)	58.41(4)
N(2)-Ae(1)-O(1)	50.80(3)	61.91(3)	58.61(3)	54.62(3)
N(2)-Ae(1)-O(1)*	126.25(5)	120.43(3)	116.03(3)	108.33(4)
Σ{∠Ae(1)}	345.63(8)	593.84(8)	574.01(8)	542.06(9)
Si(1)-O(1)-Ae(1)	92.46(5)	97.70(4)	98.70(4)	98.65(5)
Si(2)-O(1)-Ae(1)	128.70(6)	104.94(4)	105.55(4)	107.18(5)
Si(1)-O(1)-Si(2)	138.51(6)	151.14(5)	151.32(6)	150.32(7)

Σ{∠O(1)}	369.67(10)	353.78(7)	355.59(8)	356.15(10)
C(5)-N(1)-Ae(1)	137.79(9)	141.05(7)	136.04(8)	125.2(1)
C(5)-N(1)-Si(1)	126.18(9)	120.61(8)	122.94(8)	128.3(1)
Ae(1)-N(1)-Si(1)	95.90(5)	97.62(5)	99.74(5)	102.02(6)
Σ{∠N(1)}	359.87(14)	359.2(1)	358.72(12)	355.52(15)
Ae(1)-N(2)-Ae(1)*	91.25(4)*	94.16(3)	95.31(3)	93.85(4)
Ae(1)-N(2)-C(17)	116.80(7)*	121.44(6)	121.86(7)	124.13(9)
Ae(1)-N(2)-Si(2)	70.72(4)*	91.01(4)	93.24(4)	94.26(5)
Ae(1)-N(2)-C(17)*	113.44(8)	101.34(6)	95.75(7)	92.58(8)
Ae(1)-N(2)-Si(2)*	118.48(6)	121.89(5)	120.84(5)	119.45(6)
C(17)-N(2)-Si(2)	127.41(9)	124.11(7)	127.21(8)	129.0(1)
Σ{∠N(2)}	359.33(16)	653.9(1)	654.21(14)	653.27(18)
$Plane_{N(1)Si(1)O(1)Ae(1)}$-$Plane_{N(2)Si(2)O(1)Ae(1)}$ hinge angle	13.03	14.58(4)	13.04(4)	8.56(5)
N(2)-Ae(1)-Ae(1)*-N(2)* torsion	156.11(6)	168.54(5)	172.13(5)	174.02(5)

Table S8 Comparison of experimental metrical parameters (bond lengths in Å and angles in °) for $[(^{NON\text{-}Dipp}L)Ae]_2$ (Ae = Ca (**2**), Sr (**3**) and Ba (**4a**)) crystallised from *n*-hexane. * refers to symmetry related atoms.

Interatomic Distances	$[(^{NON\text{-}Dipp}L)Ca]_2$ (**2**)	$[(^{NON\text{-}Dipp}L)Sr]_2$ (**3**)	$[(^{NON\text{-}Dipp}L)Ba]_2$ (**4a**)
Ae(1)-N(1)	2.349(3)	2.477(2)	2.569(2)
Ae(1)-N(2)	2.700(3)	2.782(2)	2.799(1)
Ae(1)-N(2)*	2.386(3)	2.552(1)	3.702(2)
Ae(1)-O(1)	2.344(2)	2.502(1)	2.651(1)
Ae(1)-C(17)*	3.009(3)	3.029(2)	3.095(2)
Ae(1)-C(18)*	3.268(3)	3.168(2)	3.088(2)
Ae(1)-$Centroid_{C(17)\text{-}C(22)}$	3.9770(15)	3.900(9)	2.8618(7)
Ae(1)-$Plane_{C(17)\text{-}C(22)}$	2.289(5)	2.380(3)	2.8498(7)
N(1)-Si(1)	1.685(3)	1.679(2)	1.661(1)
N(2)-Si(2)	1.701(2)	1.694(2)	1.701(2)
O(1)-Si(1)	1.673(3)	1.670(1)	1.664(1)
O(1)-Si(2)	1.657(3)	1.651(1)	1.650(1)
Ae(1)-Ae(1)*	3.7311(9)	3.9479(9)	4.7644(6)
Bond Angles / °	$[(^{NON\text{-}Dipp}L)Ca]_2$ (**2b**)	$[(^{NON\text{-}Dipp}L)Sr]_2$ (**3b**)	$[(^{NON\text{-}Dipp}L)Ba]_2$ (**4b**)
N(1)-Ae(1)-N(2)	125.5(1)	119.25(5)	114.57(5)
N(1)-Ae(1)-N(2)*	135.8(1)	133.55(5)	140.79(4)
N(2)-Ae(1)-N(2)*	85.32(9)	84.36(5)	80.32(4)
N(1)-Ae(1)-O(1)	65.82(9)	61.91(5)	58.43(4)
N(2)-Ae(1)-O(1)	61.95(8)	58.77(4)	56.59(4)
N(2)-Ae(1)-O(1)*	119.65(9)	114.88(5)	118.73(4)
N(1)-Ae(1)-$CentroidC_{(17)\text{-}C(22)}$*	131.36(8)	136.80(5)	112.49(4)
N(2)-Ae(1)-$Centroid_{C(17)\text{-}C(22)}$*	102.69(6)	103.95(4)	128.01(3)
O(1)-Ae(1)-$Centroid_{C(17)\text{-}C(22)}$*	161.49(7)	158.65(4)	151.65(3)
Σ{∠Ae(1)}	594.04(23)	572.720(12)	621.74(10)
Si(1)-O(1)-Ae(1)	97.8(1)	98.79(6)	99.07(6)
Si(2)-O(1)-Ae(1)	105.2(1)	105.34(6)	103.47(6)
Si(1)-O(1)-Si(2)	148.9(2)	149.89(9)	157.43(9)
Σ{∠O(1)}	351.90(24)	354.020(12)	359.970(12)
C(5)-N(1)-Ae(1)	139.1(2)	134.4(1)	110.3(1)
C(5)-N(1)-Si(1)	123.1(3)	124.9(1)	143.9(1)
Ae(1)-N(1)-Si(1)	97.3(1)	99.49(8)	102.36(7)
Σ{∠N(1)}	359.50(37)	358.79(16)	356.56(16)
Ae(1)-N(2)-Ae(1)*	94.18(9)	95.40(5)	93.22(4)
Ae(1)-N(2)-C(17)	121.4(2)	121.9(1)	129.6(1)
Ae(1)-N(2)-Si(2)	90.6(1)	93.44(6)	96.42(6)
Ae(1)-N(2)-C(17)*	101.3(2)	95.3(1)	53.75(8)
Ae(1)-N(2)-Si(2)*	120.6(1)	120.33(8)	146.01(7)

C(17)-N(2)-Si(2)	125.5(2)	127.7(1)	132.8(1)
Σ{∠N(2)}	653.58(38)	654.07(18)	358.82(15)
$Plane_{N(1)Si(1)O(1)Ae(1)}$-$Plane_{N(2)Si(2)O(1)Ae(1)}$ fold angle	17.20(11)	14.44(6)	6.89(6)
N(2)-Ae(1)-Ae(1)*-N(2)* torsion	168.8(1)	172.30(7)	138.93(5)

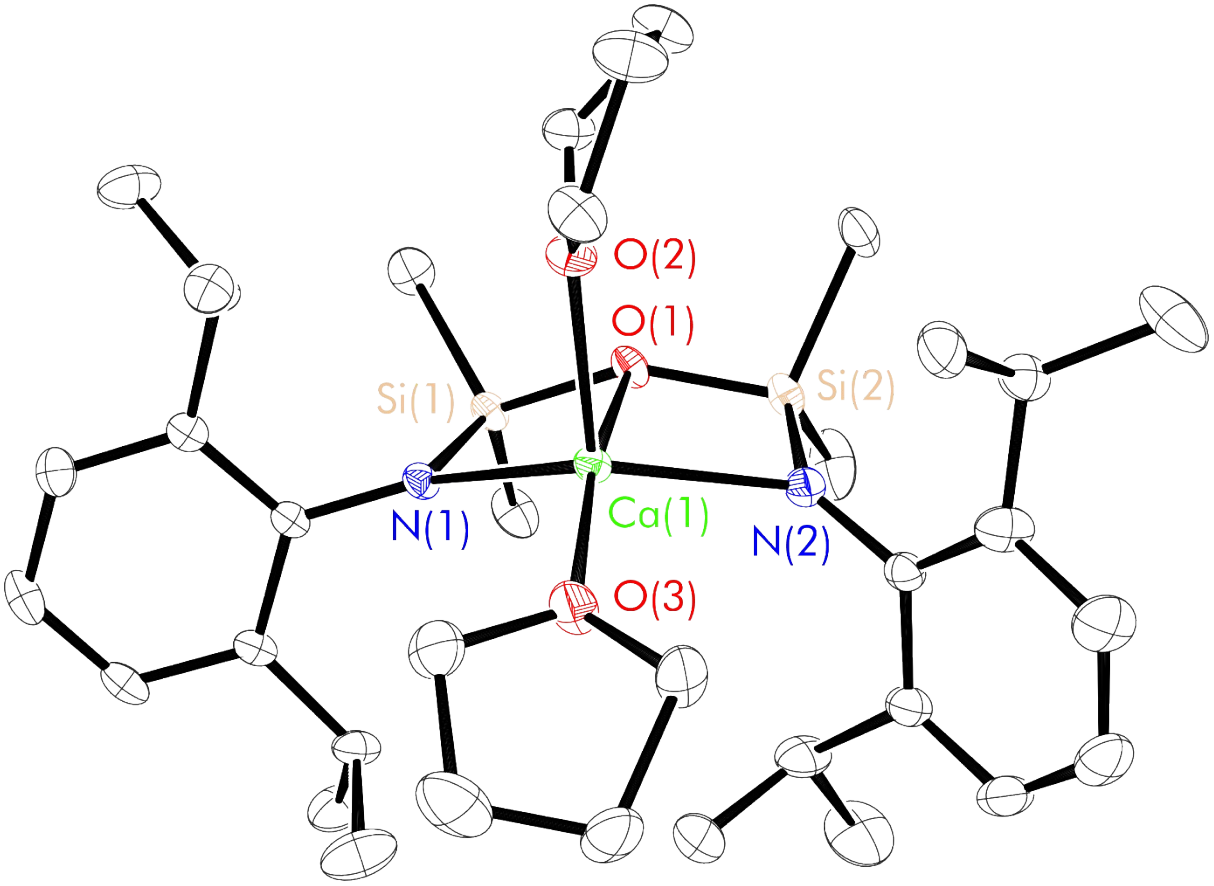

Figure S52 Thermal displacement ellipsoid drawing (30% probability) of [($^{NON\text{-}Dipp}$L)Ca(thf)$_2$] (**5**) All hydrogen atoms omitted for clarity.

Table S9 Experimental metrical parameters (bond lengths in Å and angles in °) for [($^{NON\text{-}Dipp}$L)Ca(thf)$_2$] (**5**).

Ca(1)-N(1)	2.313(1)
Ca(1)-N(2)	2.285(1)
Ca(1)-O(1)	2.490(1)
Ca(1)-O(2)	2.337(1)
Ca(1)-O(3)	2.323(1)
N(1)-Ca(1)-N(2)	119.59(5)
N(1)-Ca(1)-O(1)	65.01(5)
N(1)-Ca(1)-O(2)	110.01(5)
N(1)-Ca(1)-O(3)	107.46(5)
N(2)-Ca(1)-O(1)	65.84(4)
N(2)-Ca(1)-O(2)	108.32(5)
N(2)-Ca(1)-O(3)	114.23(5)
O(1)-Ca(1)-O(2)	96.51(4)
O(1)-Ca(1)-O(3)	168.52(5)
O(2)-Ca(1)-O(3)	94.28(5)
Σ{∠Ca(1)}	1049.77(15)
C(1)-N(1)-Ca(1)	124.5(1)
C(1)-N(1)-Si(1)	135.7(1)
Ca(1)-N(1)-Si(1)	99.46(7)
Σ{∠N(1)}	359.66(16)
C(17)-N(2)-Ca(1)	136.2(1)
C(17)-N(2)-Si(2)	123.6(1)
Ca(1)-N(2)-Si(2)	99.70(6)
Σ{∠N(2)}	359.5(15)
Si(1)-O(1)-Ca(1)	93.05(5)
Si(2)-O(1)-Ca(1)	92.75(5)
Si(1)-O(1)-Si(2)	147.42(8)
Σ{∠O(1)}	333.22(11)
$Plane_{N(1)Si(1)O(1)Ca(1)}$-$Plane_{N(2)Si(2)O(1)Ca(1)}$ fold angle	144.8629(4)

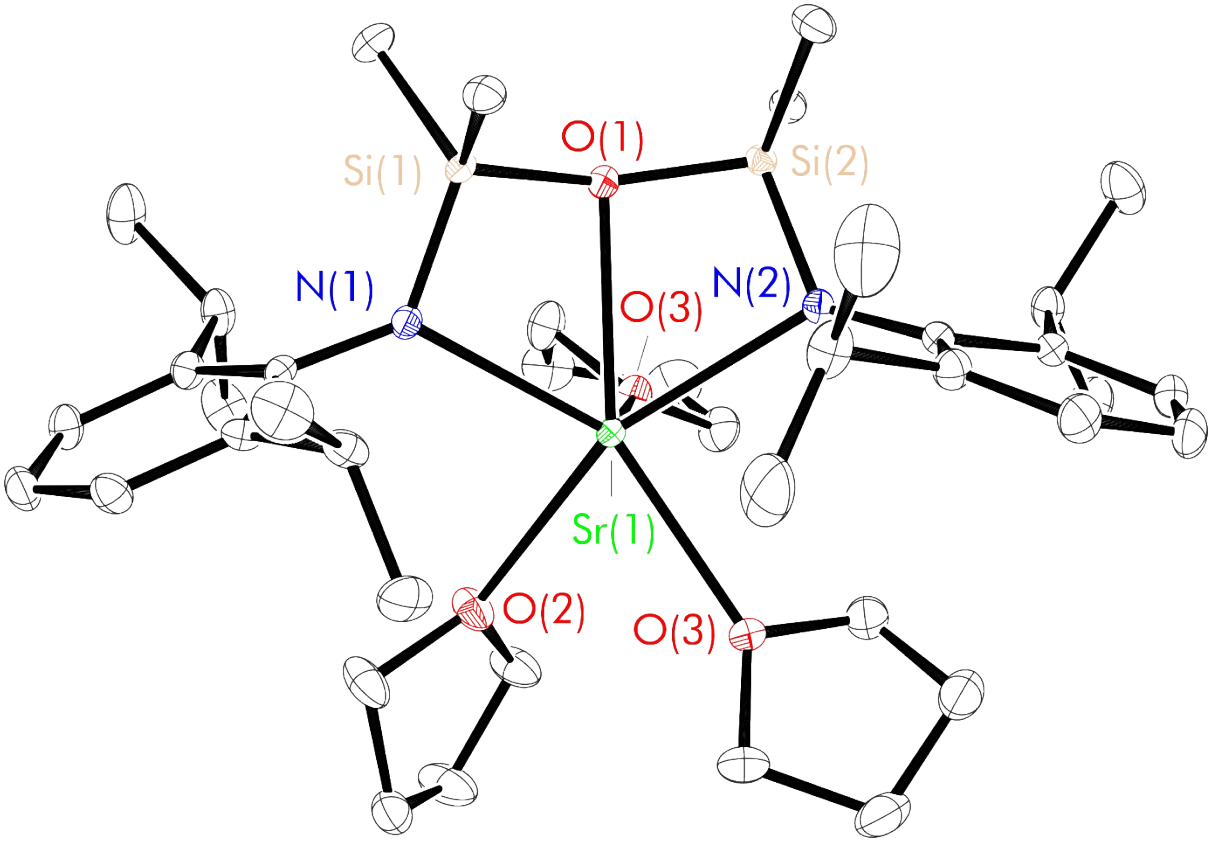

Figure S53 Thermal displacement ellipsoid drawing (30% probability) of [($^{NON\text{-}Dipp}$L)Sr(thf)$_3$] (**6**) All hydrogen atoms omitted for clarity.

Table S10 Experimental metrical parameters (bond lengths in Å and angles in °) for [($^{NON\text{-}Dipp}$L)Sr(thf)$_3$] (**6**).

Sr(1)-N(1)	2.564(2)
Sr(1)-N(2)	2.507(3)
Sr(1)-O(1)	2.627(2)
Sr(1)-O(2)	2.557(4)
Sr(1)-O(3)	2.510(3)
Sr(1)-O(4)	2.591(2)
N(1)-Sr(1)-N(2)	114.48(8)
N(1)-Sr(1)-O(1)	60.40(8)
N(1)-Sr(1)-O(2)	87.1(1)
N(1)-Sr(1)-O(3)	90.95(8)
N(1)-Sr(1)-O(4)	157.73(9)
N(2)-Sr(1)-O(1)	60.62(7)
N(2)-Sr(1)-O(2)	147.1(1)
N(2)-Sr(1)-O(3)	107.96(8)
N(2)-Sr(1)-O(4)	87.71(8)
O(1)-Sr(1)-O(2)	147.4(1)
O(1)-Sr(1)-O(3)	83.31(7)
O(1)-Sr(1)-O(4)	137.03(8)
O(2)-Sr(1)-O(3)	95.5(1)
O(2)-Sr(1)-O(4)	73.8(1)
O(3)-Sr(1)-O(4)	73.80(8)
Σ{∠Sr(1)}	1524.89(34)
C(1)-N(1)-Sr(1)	132.2(2)
C(1)-N(1)-Si(1)	127.7(2)
Sr(1)-N(1)-Si(1)	98.3(1)
Σ{∠N(1)}	358.2(3)
C(17)-N(2)-Sr(1)	131.4(2)
C(17)-N(2)-Si(2)	128.8(2)
Sr(1)-N(2)-Si(2)	99.7(1)
Σ{∠N(2)}	359.9(3)
Si(1)-O(1)-Sr(1)	96.2(1)
Si(2)-O(1)-Sr(1)	95.8(1)
Si(1)-O(1)-Si(2)	148.2(2)
Σ{∠O(1)}	340.2(2)
$Plane_{N(1)Si(1)O(1)Sr(1)}$-$Plane_{N(2)Si(2)O(1)Sr(1)}$ fold angle	150.09(11)

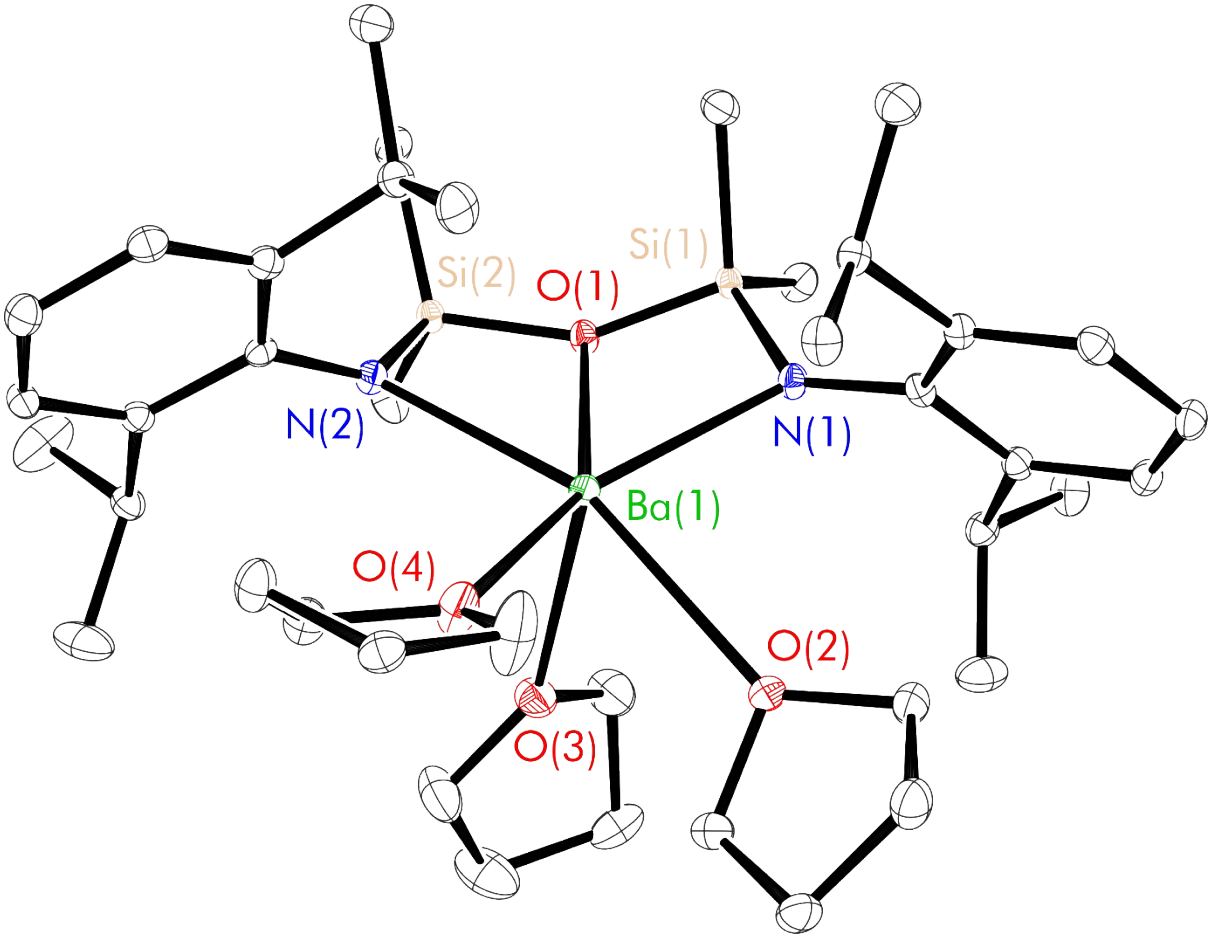

Figure S54 Thermal displacement ellipsoid drawing (30% probability) of [($^{NON\text{-}Dipp}$L)Ba(thf)$_3$] (**7**) All hydrogen atoms omitted for clarity.

Table S11 Experimental metrical parameters (bond lengths in Å and angles in °) for [($^{NON\text{-}Dipp}$L)Ba(thf)$_3$] (**7**).

Ba(1)-N(1)	2.619(2)
Ba(1)-N(2)	2.676(3)
Ba(1)-O(1)	2.889(3)
Ba(1)-O(2)	2.838(3)
Ba(1)-O(3)	2.689(2)
Ba(1)-O(4)	2.772(3)
N(1)-Ba(1)-N(2)	109.33(8)
N(1)-Ba(1)-O(1)	55.74(7)
N(1)-Ba(1)-O(2)	85.59(8)
N(1)-Ba(1)-O(3)	105.62(8)
N(1)-Ba(1)-O(4)	146.94(8)
N(2)-Ba(1)-O(1)	55.88(7)
N(2)-Ba(1)-O(2)	161.11(8)
N(2)-Ba(1)-O(3)	88.44(8)
N(2)-Ba(1)-O(4)	97.81(8)
O(1)-Ba(1)-O(2)	132.92(7)
O(1)-Ba(1)-O(3)	88.65(7)
O(1)-Ba(1)-O(4)	153.58(8)
O(2)-Ba(1)-O(3)	76.08(8)
O(2)-Ba(1)-O(4)	72.77(8)
O(3)-Ba(1)-O(4)	93.33(8)
Σ{∠Ba(1)}	1523.79(30)
C(1)-N(1)-Ba(1)	123.1(2)
C(1)-N(1)-Si(1)	130.9(2)
Ba(1)-N(1)-Si(1)	104.0(1)
Σ{∠N(1)}	358.0(3)
C(17)-N(2)-Ba(1)	117.7(2)
C(17)-N(2)-Si(2)	134.8(2)
Ba(1)-N(2)-Si(2)	103.7(1)
Σ{∠N(2)}	356.2(3)
Si(1)-O(1)-Ba(1)	94.3(1)
Si(2)-O(1)-Ba(1)	96.0(1)
Si(1)-O(1)-Si(2)	151.0(2)
Σ{∠O(1)}	341.3(2)
$Plane_{N(1)Si(1)O(1)Ba(1)}$-$Plane_{N(2)Si(2)O(1)Ba(1)}$ fold angle	159.23(12)

Table S12 Comparison of experimental metrical parameters (bond lengths in Å and angles in °) for [($^{NON\text{-}Dipp}$L)Ae(thf)$_n$] (Ae = Mg and Ca, n = 2; Ae = Sr and Ba, n = 3). [($^{NON\text{-}Dipp}$L)Mg(thf)$_2$] metrics reproduced from reference 16.

Metric	[($^{NON\text{-}Dipp}$L)Mg(thf)$_2$]	[($^{NON\text{-}Dipp}$L)Ca(thf)$_2$] (**5**)	[($^{NON\text{-}Dipp}$L)Sr(thf)$_3$] (**6**)	[($^{NON\text{-}Dipp}$L)Ba(thf)$_3$] (7)
Ae(1)-N(1)	2.040(2)	2.313(1)	2.564(2)	2.619(2)
Ae(1)-N(2)	2.041(2)	2.285(1)	2.507(3)	2.676(3)
Ae(1)-O(1)	2.308(2)	2.490(1)	2.627(2)	2.889(3)
Ae(1)-O(2)	2.065(2)	2.337(1)	2.557(4)	2.838(3)
Ae(1)-O(3)	2.047(2)	2.323(1)	2.510(3)	2.689(2)
Ae(1)-O(4)	-	-	2.591(2)	2.772(3)
N(1)-Ae(1)-N(2)	129.1(1)	119.59(5)	114.48(8)	109.33(8)
N(1)-Ae(1)-O(1)	71.75(8)	65.01(5)	60.40(8)	55.74(7)
N(1)-Ae(1)-O(2)	109.86(9)	110.01(5)	87.1(1)	85.59(8)
N(1)-Ae(1)-O(3)	104.51(9)	107.46(5)	90.95(8)	105.62(8)
N(1)-Ae(1)-O(4)	-	-	157.73(9)	146.94(8)
N(2)-Ae(1)-O(1)	71.77(8)	65.84(4)	60.62(7)	55.88(7)
N(2)-Ae(1)-O(2)	108.44(9)	108.32(5)	147.1(1)	161.11(8)
N(2)-Ae(1)-O(3)	106.22(9)	114.23(5)	107.96(8)	88.44(8)
N(2)-Ae(1)-O(4)	-	-	87.71(8)	97.81(8)
O(1)-Ae(1)-O(2)	96.57(8)	96.51(4)	147.4(1)	132.92(7)
O(1)-Ae(1)-O(3)	171.26(9)	168.52(5)	83.31(7)	88.65(7)
O(1)-Ae(1)-O(4)	-	-	137.03(8)	153.58(8)
O(2)-Ae(1)-O(3)	92.13(9)	94.28(5)	95.5(1)	76.08(8)
O(2)-Ae(1)-O(4)	-	-	73.8(1)	72.77(8)

O(3)-Ae(1)-O(4)	-	-	73.80(8)	93.33(8)
Σ{∠Ae(1)}	1061.61(28)	1049.77(15)	1524.89(34)	1523.79(30)
C(1)-N(1)-Ae(1)	132.5(2)	124.5(1)	132.2(2)	123.1(2)
C(1)-N(1)-Si(1)	128.8(2)	135.7(1)	127.7(2)	130.9(2)
Ae(1)-N(1)-Si(1)	98.7(1)	99.46(7)	98.3(1)	104.0(1)
Σ{∠N(1)}	360.0(3)	359.66(16)	358.2(3)	358.0(3)
C(17)-N(2)-Ae(1)	132.5(2)	136.2(1)	131.4(2)	117.7(2)
C(17)-N(2)-Si(2)	128.4(2)	123.6(1)	128.8(2)	134.8(2)
Ae(1)-N(2)-Si(2)	98.8(1)	99.70(6)	99.7(1)	103.7(1)
Σ{∠N(2)}	359.7(3)	359.5(15)	359.9(3)	356.2(3)
Si(1)-O(1)-Ae(1)	89.90(9)	93.05(5)	96.2(1)	94.3(1)
Si(2)-O(1)-Ae(1)	89.82(9)	92.75(5)	95.8(1)	96.0(1)
Si(1)-O(1)-Si(2)	143.6(1)	147.42(8)	148.2(2)	151.0(2)
Σ{∠O(1)}	323.22(16)	333.22(11)	340.2(2)	341.3(2)
$Plane_{N(1)Si(1)O(1)Ae(1)}$-$Plane_{N(2)Si(2)O(1)Ae(1)}$ fold angle	143.92(9)	144.8629(4)	150.09(11)	159.23(12)

a)

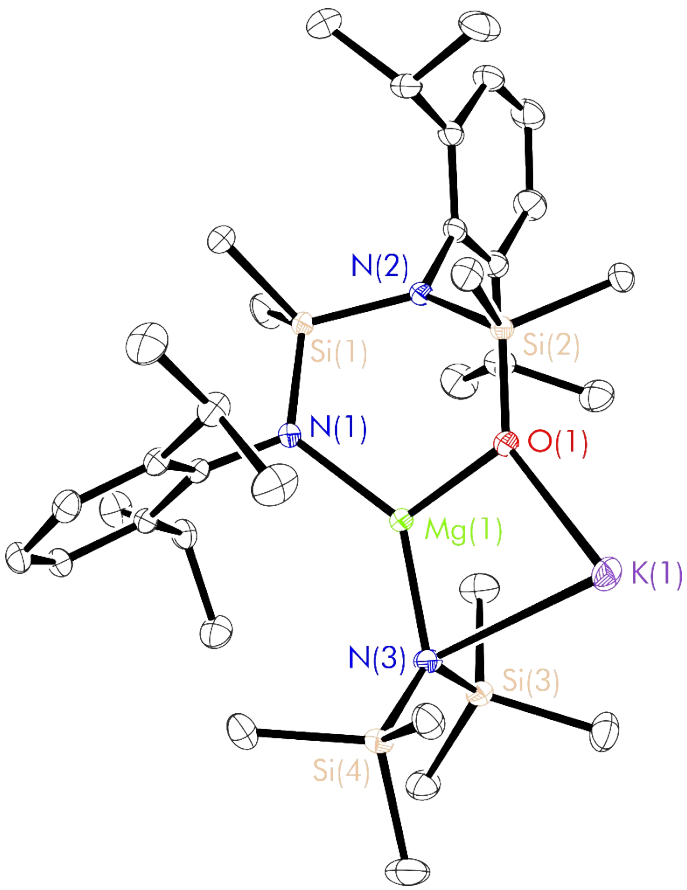

b)

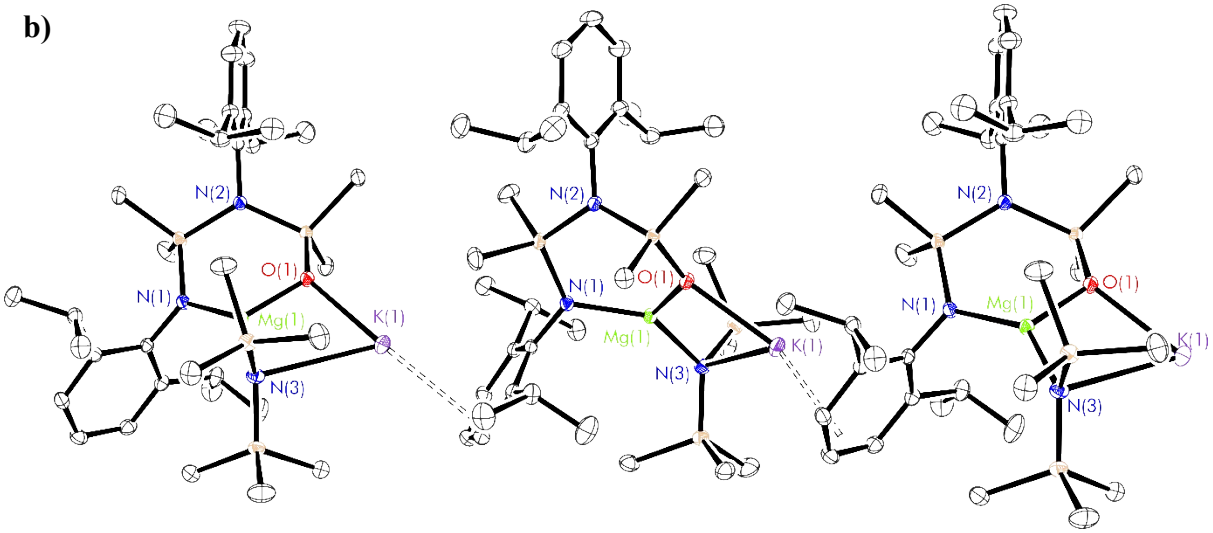

Figure S55 Thermal displacement ellipsoid drawings (30% probability) of **a)** The asymmetric unit and **b)** extended polymeric structure of $[(^{NNO\text{-}Dipp}L)Mg(\mu\text{-}N'')K]_n$ (**8**). All hydrogen atoms omitted for clarity.

Table S13 Experimental metrical parameters (bond lengths in Å and angles in °) for [($^{NNO\text{-}Dipp}$L)Mg(μ-N")K]$_n$ (**8**).

Mg(1)-N(1)	2.002(1)
Mg(1)-N(2)	3.333(1)
Mg(1)-N(3)	2.021(1)
Mg(1)-O(1)	1.899(1)
K(1)-N(3)	3.205(1)
K(1)-O(1)	2.588(1)
K(1)-Centroid$_{C(1)\text{-}C(6)}$	3.033(1)
K(1)-H(14A)	2.7726(3)
K(1)-H(34A)	2.9150(4)
K(1)-H(34C)	3.0104(4)
Mg(1)-K(1)	3.4417(5)
N(1)-Mg(1)-N(3)	138.09(6)
N(1)-Mg(1)-O(1)	107.64(5)
N(3)-Mg(1)-O(1)	112.38(5)
Σ{∠Mg(1)}	358.11(9)
N(3)-K(1)-O(1)	67.47(4)
N(3)-K(1)-Centroid$_{C(1)\text{-}C(6)}$	142.94(3)
O(1)-K(1)-Centroid$_{C(1)\text{-}C(6)}$	144.76(3)
Σ{∠K(1)}	355.17(6)

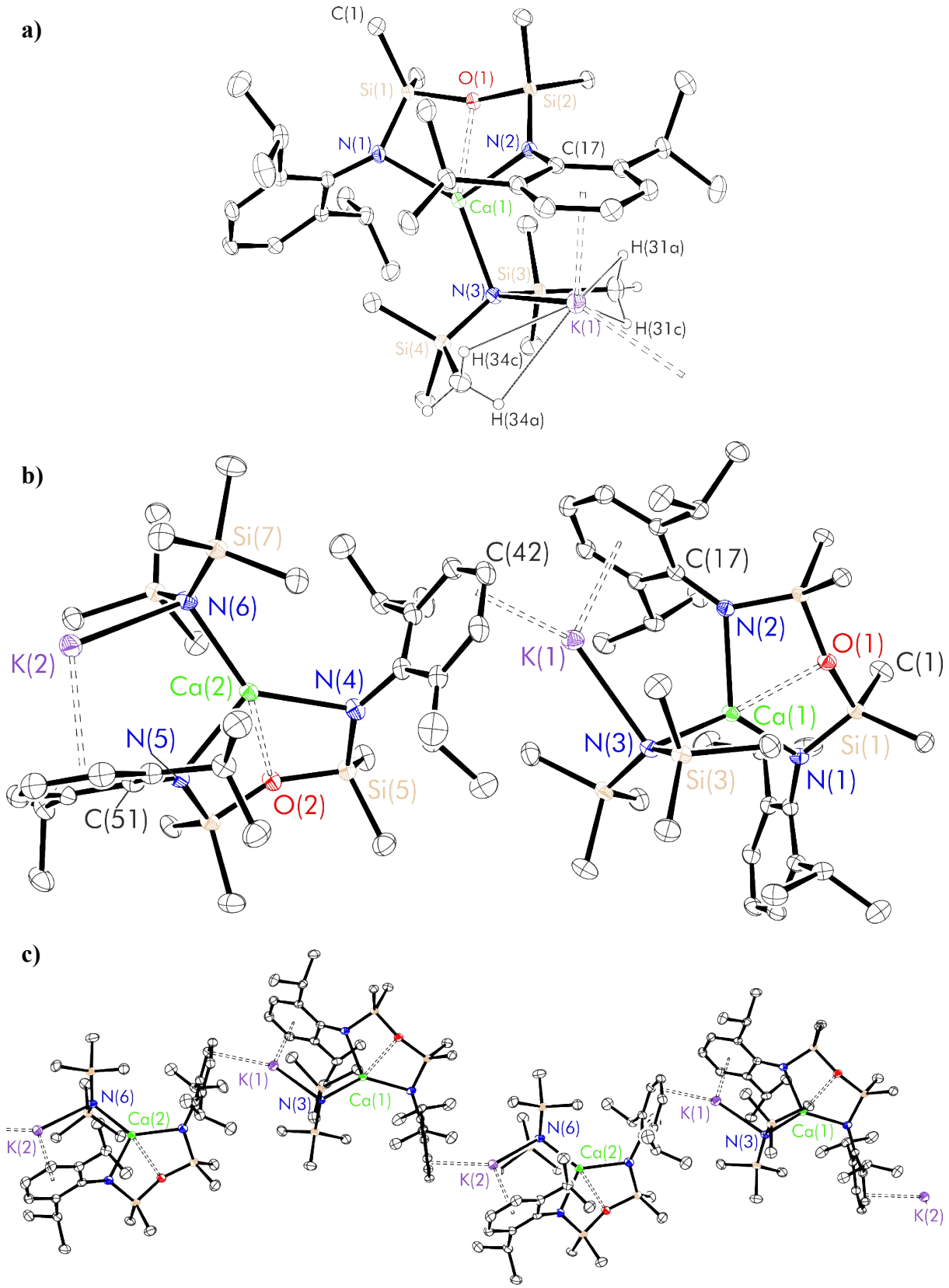

Figure S56 Thermal displacement ellipsoid drawings (30% probability) of **a)** one monomeric [($^{NON\text{-}Dipp}$L)Ca(μ-N")K] unit **b)** full dimeric [($^{NON\text{-}Dipp}$L)Ca(μ-N")K]$_2$ asymmetric unit and **c)** extended polymeric structure [($^{NON\text{-}Dipp}$L)Ca(μ-N")K]$_n$ (**9**). All hydrogen atoms (excluding selected atoms in a)) omitted for clarity.

Table S14 Experimental metrical parameters (bond lengths in Å and angles in °) for [($^{NON\text{-}Dipp}$L)Ca(μ-N")K]$_n$ (**9**). Representative metrics from one [($^{NON\text{-}Dipp}$L)Ca(μ-N")K] molecule are presented.

Ca(1)-N(1)	2.342(2)
Ca(1)-N(2)	2.365(2)
Ca(1)-N(3)	2.365(2)
Ca(1)-O(1)	2.443(1)
K(1)-N(3)	2.924(2)
K(1)-Centroid$_{C(17)\text{-}C(22)}$	2.9507(10)
K(1)-Centroid$_{C(41)\text{-}C(43)}$	2.9668(16)
K(1)-H(31A)	2.9964(6)
K(1)-H(31C)	2.9156(6)
K(1)-H(34A)	2.8283(5)
K(1)-H(34B)	2.7428(5)
Ca(1)-K(1)	4.1338(8)
N(1)-Ca(1)-N(2)	121.24(6)
N(1)-Ca(1)-N(3)	135.71(7)
N(2)-Ca(1)-N(3)	102.97(6)
N(1)-Ca(1)-O(1)	65.01(6)
N(2)-Ca(1)-O(1)	65.17(6)
N(3)-Ca(1)-O(1)	147.95(6)
Σ{∠Ca(1)}	638.05(15)
N(3)-K(1)-Centroid$_{C(17)\text{-}C(22)}$	114.00(4)
N(3)-K(1)-Centroid$_{C(41)\text{-}C(43)}$	136.18(6)
Centroid$_{C(17)\text{-}C(22)}$-K(1)-Centroid$_{C(41)\text{-}C(43)}$	107.11(4)
Σ{∠K(1)}	357.29(8)
Ca(1)-N(1)-C(5)	124.9(1)
Ca(1)-N(1)-Si(1)	98.79(8)
C(5)-N(1)-Si(1)	135.9(2)
Σ{∠N(1)}	359.59(24)
Ca(1)-N(2)-C(17)	128.5(1)
Ca(1)-N(2)-Si(2)	97.53(8)
C(17)-N(1)-Si(2)	133.3(2)
Σ{∠N(2)}	359.33(24)
Ca(1)-O(1)-Si(1)	95.43(7)
Ca(1)-O(1)-Si(2)	95.19(7)

Si(1)-O(1)-Si(2)	155.0(1)
Σ{∠O(1)}	345.62(14)
Ca(1)-N(3)-K(1)	102.17(7)
Ca(1)-N(3)-Si(3)	102.68(9)
Ca(1)-N(3)-Si(4)	109.99(9)
K(1)-N(3)-Si(3)	102.94(8)
K(1)-N(3)-Si(4)	98.97(8)
Si(3)-N(3)-Si(4)	135.4(1)
Σ{∠N(3)}	652.15(21)
$Plane_{N(1)Si(1)O(1)Ca(1)}$-$Plane_{N(2)Si(2)O(1)Ca(1)}$ fold angle	29.82(8)

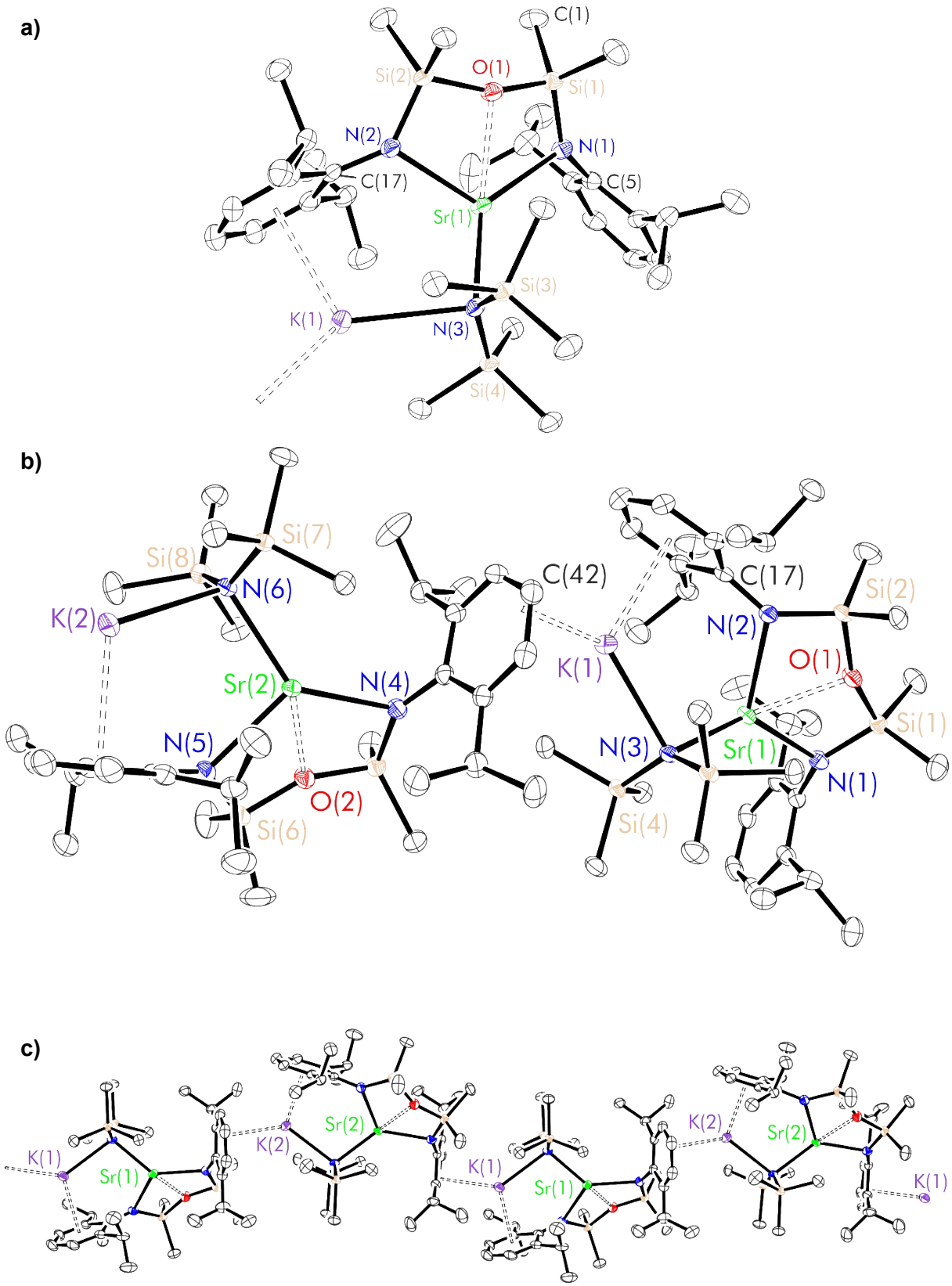

Figure S57 Thermal displacement ellipsoid drawings (30% probability) of **a)** one monomeric [($^{NON\text{-}Dipp}$L)Sr(μ-N")K] unit **b)** full dimeric [($^{NON\text{-}Dipp}$L)Sr(μ-N")K]$_2$ asymmetric unit sn **c)** extended polymeric structure of [($^{NON\text{-}Dipp}$L)Sr(μ-N")K]$_n$ (**10**). All hydrogen atoms excluded for clarity.

Table S15 Experimental metrical parameters (bond lengths in Å and angles in °) for [($^{NON\text{-}Dipp}$L)Sr(μ-N")K]$_n$ (**10**). Representative metrics from one [($^{NON\text{-}Dipp}$L)Sr(μ-N")K] molecule are presented.

Sr(1)-N(1)	2.524(3)
Sr(1)-N(2)	2.533(3)
Sr(1)-N(3)	2.525(3)
Sr(1)-O(1)	2.539(2)
K(1)-N(3)	2.892(3)
K(1)-Centroid$_{C(17)\text{-}C(22)}$	2.982(2)
K(1)-Centroid$_{C(40)\text{-}C(43)}$	2.9655(2)
K(1)-H(29A)	2.9156(9)
K(1)-H(29B)	2.8594(10)
K(1)-H(32A)	2.9907(7)
K(1)-H(32B)	2.8396(8)
Sr(1)-K(1)	4.2341(9)
N(1)-Sr(1)-N(2)	119.8(1)
N(1)-Sr(1)-N(3)	135.2(1)
N(2)-Sr(1)-N(3)	100.4(1)
N(1)-Sr(1)-O(1)	60.85(9)
N(2)-Sr(1)-O(1)	61.29(9)
N(3)-Sr(1)-O(1)	139.94(9)
Σ{∠Sr(1)}	617.48(23)
N(3)-K(1)-Centroid$_{C(17)\text{-}C(22)}$	112.36(8)
N(3)-K(1)-Centroid$_{C(41)\text{-}C(43)}$	1346.41(9)
Centroid$_{C(17)\text{-}C(22)}$-K(1)-Centroid$_{C(40)\text{-}C(43)}$	109.73(7)
Σ{∠K(1)}	354.68(14)
Sr(1)-N(1)-C(5)	116.1(2)
Sr(1)-N(1)-Si(1)	99.1(1)
C(5)-N(1)-Si(1)	144.7(3)
Σ{∠N(1)}	359.90(37)
Sr(1)-N(2)-C(17)	121.8(2)
Sr(1)-N(2)-Si(2)	98.4(1)
C(17)-N(1)-Si(2)	138.0(3)
Σ{∠N(2)}	358.20(37)
Sr(1)-O(1)-Si(1)	98.9(1)
Sr(1)-O(1)-Si(2)	98.9(1)

Si(1)-O(1)-Si(2)	158.7(2)
Σ{∠O(1)}	356.50(24)
Sr(1)-N(3)-K(1)	102.6(1)
Sr(1)-N(3)-Si(3)	103.7(1)
Sr(1)-N(3)-Si(4)	108.6(1)
K(1)-N(3)-Si(3)	102.5(1)
K(1)-N(3)-Si(4)	102.1(1)
Si(3)-N(3)-Si(4)	133.4(2)
Σ{∠N(3)}	652.9(3)
$Plane_{N(1)Si(1)O(1)Sr(1)}$-$Plane_{N(2)Si(2)O(1)Sr(1)}$ hinge angle	16.33(15)

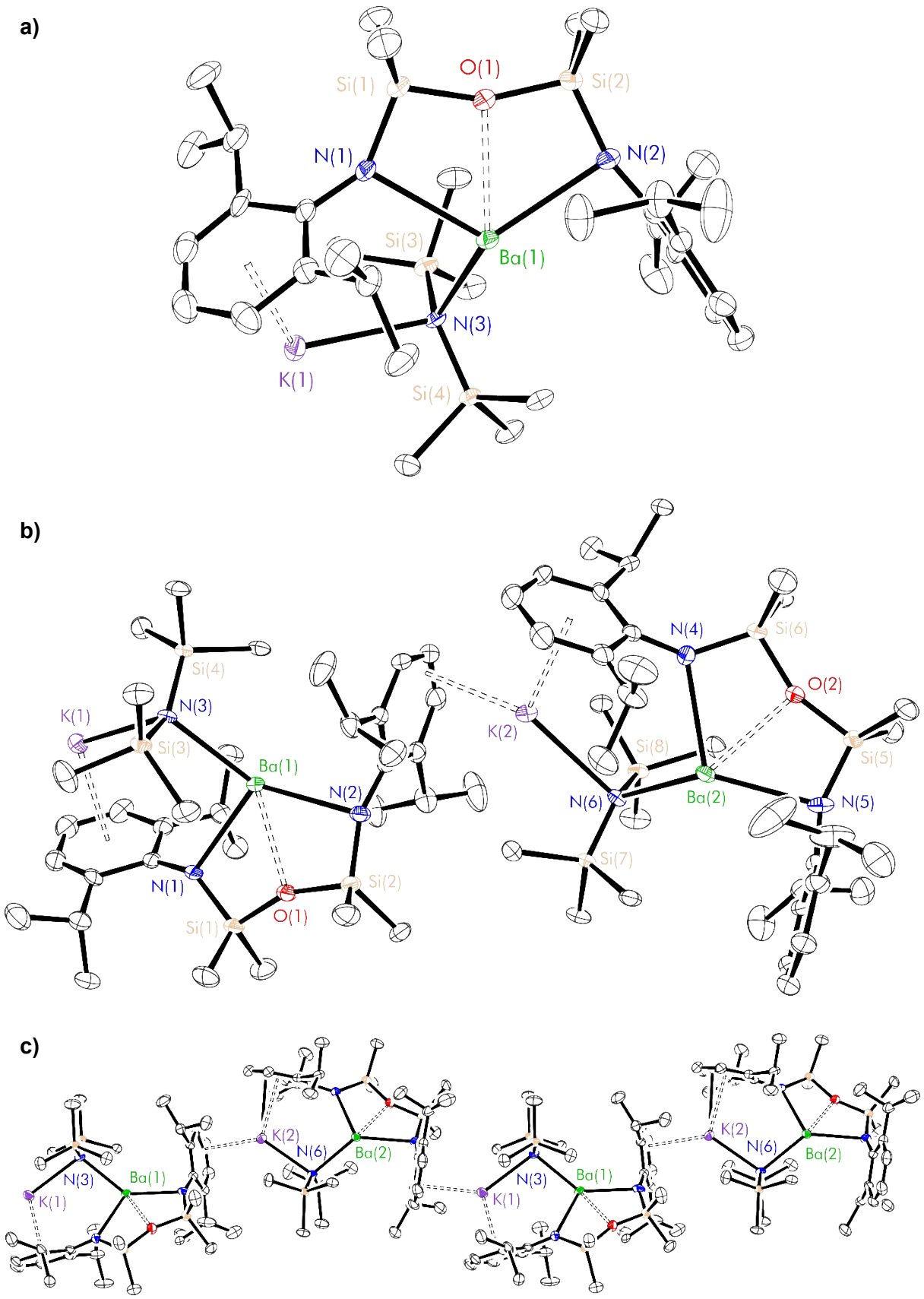

Figure S58 Thermal displacement ellipsoid drawings (30% probability) of **7** **a)** one monomeric [($^{NON\text{-}Dipp}$L)Ba(μ-N")K] unit **b)** full dimeric [($^{NON\text{-}Dipp}$L)Ba(μ-N")K]$_2$ asymmetric unit and **c)** extended polymeric structure [($^{NON\text{-}Dipp}$L)Ba(μ-N")K]$_n$ (**11**). All hydrogen atoms excluded for clarity.

Table S16 Experimental metrical parameters (bond lengths in Å and angles in °) for [($^{NON\text{-}Dipp}$L)Ba(μ-N")K]$_n$ (**11**). Representative metrics from one [($^{NON\text{-}Dipp}$L)Ba(μ-N")K] molecule are presented.

Ba(1)-N(1)	2.698(8)
Ba(1)-N(2)	2.741(8)
Ba(1)-N(3)	2.707(7)
Ba(1)-O(1)	2.673(5)
K(1)-N(3)	2.876(7)
K(1)-Centroid$_{C(17)\text{-}C(22)}$	2.972(5)
K(1)-Centroid$_{C(40)\text{-}C(43)}$	2.996(6)
K(1)-H(29A)	2.887(2)
K(1)-H(29B)	2.884(2)
K(1)-H(32A)	2.779(2)
K(1)-H(32B)	2.914(2)
Ba(1)-K(1)	4.444(2)
N(1)-Ba(1)-N(2)	114.4(2)
N(1)-Ba(1)-N(3)	97.6(2)
N(2)- Ba(1)-N(3)	134.5(2)
N(1)-Ba(1)-O(1)	57.4(2)
N(2)-Ba(1)-O(1)	57.4(2)
N(3)-Ba(1)-O(1)	135.6(2)
Σ{∠Ba(1)}	596.9(5)
N(3)-K(1)-Centroid$_{C(17)\text{-}C(22)}$	110.12(18)
N(3)-K(1)-Centroid$_{C(41)\text{-}C(43)}$	136.2(2)
Centroid$_{C(17)\text{-}C(22)}$-K(1)-Centroid$_{C(40)\text{-}C(43)}$	112.32(16)
Σ{∠K(1)}	358.6(3)
Ba(1)-N(1)-C(5)	117.2(6)
Ba(1)-N(1)-Si(1)	99.3(4)
C(5)-N(1)-Si(1)	141.8(7)
Σ{∠N(1)}	358.3(10)
Ba(1)-N(2)-C(17)	97.5(6)
Ba(1)-N(2)-Si(2)	98.4(4)
C(17)-N(1)-Si(2)	158.5(7)
Σ{∠N(2)}	354.4(10)
Ba(1)-O(1)-Si(1)	101.3(3)

Ba(1)-O(1)-Si(2)	100.8(3)
Si(1)-O(1)-Si(2)	157.6(5)
Σ{∠O(1)}	359.7(7)
Ba(1)-N(3)-K(1)	105.4(2)
Ba(1)-N(3)-Si(3)	105.2(2)
Ba(1)-N(3)-Si(4)	106.4(3)
K(1)-N(3)-Si(3)	101.9(3)
K(1)-N(3)-Si(4)	100.3(3)
Si(3)-N(3)-Si(4)	134.4(4)
Σ{∠N(3)}	653.6(7)
$Plane_{N(1)Si(1)O(1)Ba(1)}$-$Plane_{N(2)Si(2)O(1)Ba(1)}$ hinge angle	6.5(4)

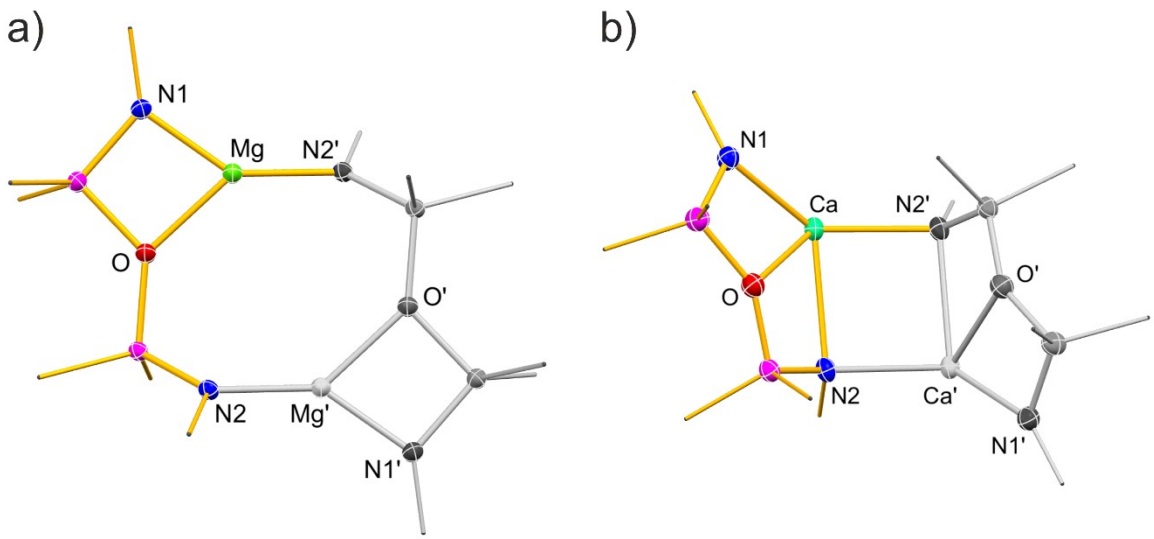

Figure S59 Core crystallographic units of a) complex **1** and b) complex **2**.

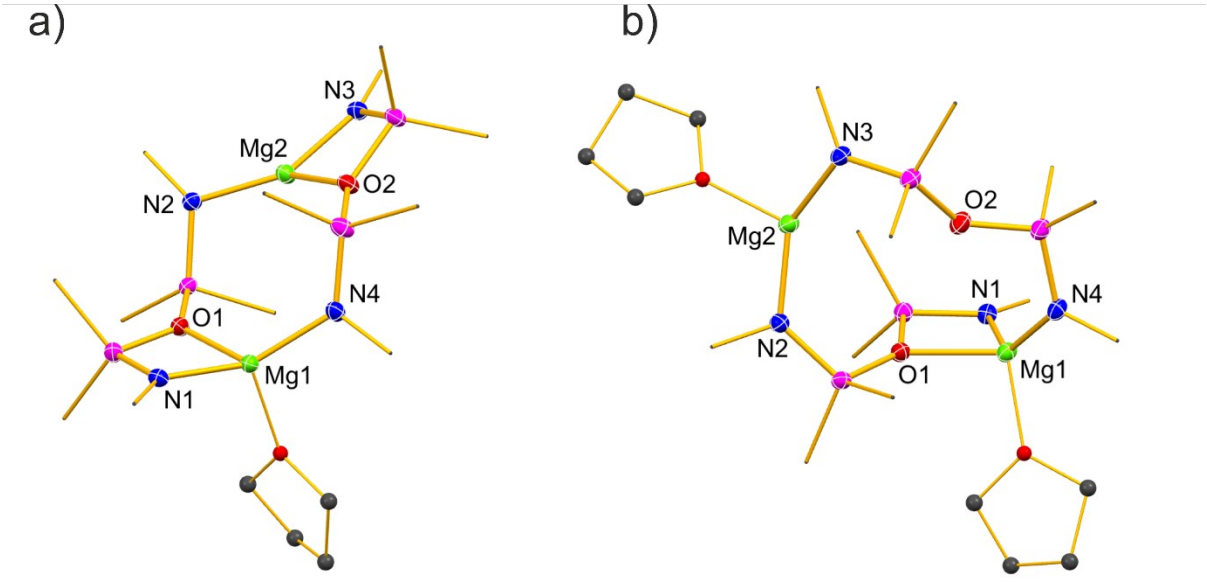

Figure S60 Core crystallographic units of a) complex **1·thf** and b) complex **1·thf$_2$**.

Table S17 Comparison of average experimental metrical parameters (bond lengths in Å and angles in °) for [($^{NON\text{-}Dipp}$L)Ae(μ-N")K]$_n$ (Ae = Ca, Sr and Ba). Representative metrics from one [($^{NON\text{-}Dipp}$L)Ae(μ-N")K] molecule in the asymmetric unit of each compound is presented.

	[($^{NON\text{-}Dipp}$L)Ca(μ-N")K]$_n$ (**9**)	[($^{NON\text{-}Dipp}$L)Sr(μ-N")K]$_n$ (**10**)	[($^{NON\text{-}Dipp}$L)Ba(μ-N")K]$_n$ (**11**)
Ae(1)-N(1)	2.342(2)	2.524(3)	2.698(8)
Ae(1)-N(2)	2.365(2)	2.533(3)	2.741(8)
Ae(1)-N(3)	2.365(2)	2.525(3)	2.707(7)
Ae(1)-O(1)	2.443(1)	2.539(2)	2.673(5)
K(1)-N(3)	2.924(2)	2.892(3)	2.876(7)
K(1)-Centroid$_{C(17)\text{-}C(22)}$	2.9507(10)	2.982(2)	2.972(5)
K(1)-Centroid$_{C(41)\text{-}C(43)}$	2.9668(16)	2.9655(2)	2.996(6)
K(1)-H(31A)	2.9964(6)	2.9156(9)	2.887(2)
K(1)-H(31C)	2.9156(6)	2.8594(10)	2.884(2)
K(1)-H(34A)	2.8283(5)	2.9907(7)	2.779(2)
K(1)-H(34B)	2.7428(5)	2.8396(8)	2.914(2)
Ae(1)-K(1)	4.1338(8)	4.2341(9)	4.444(2)
N(1)-Ae(1)-N(2)	121.24(6)	119.8(1)	114.4(2)
N(1)-Ae(1)-N(3)	135.71(7)	135.2(1)	97.6(2)
N(2)-Ae(1)-N(3)	102.97(6)	100.4(1)	134.5(2)
N(1)-Ae(1)-O(1)	65.01(6)	60.85(9)	57.4(2)
N(2)-Ae(1)-O(1)	65.17(6)	61.29(9)	57.4(2)
N(3)-Ae(1)-O(1)	147.95(6)	139.94(9)	135.6(2)
ΣX-Ae(1)-X	638.05(15)	617.48(23)	596.9(5)
N(3)-K(1)-Centroid$_{C(17)\text{-}C(22)}$	114.00(4)	112.36(8)	110.12(18)
N(3)-K(1)-Centroid$_{C(40)/C(41)\text{-}C(43)}$	136.18(6)	1346.41(9)	136.2(2)
Centroid$_{C(17)\text{-}C(22)}$-K(1)-Centroid$_{C(40)/C(41)\text{-}C(43)}$	107.11(4)	109.73(7)	112.32(16)
ΣX-K(1)-X	357.29(8)	354.68(14)	358.6(3)
Ae(1)-N(1)-C(5)	124.9(1)	116.1(2)	117.2(6)
Ae(1)-N(1)-Si(1)	98.79(8)	99.1(1)	99.3(4)
C(5)-N(1)-Si(1)	135.9(2)	144.7(3)	141.8(7)
ΣX-N(1)-X	359.6(2)	359.9(4)	358.3(10)
Ae(1)-N(2)-C(17)	128.5(1)	121.8(2)	97.5(6)
Ae(1)-N(2)-Si(2)	97.53(8)	98.4(1)	98.4(4)
C(17)-N(1)-Si(2)	133.3(2)	138.0(3)	158.5(7)
ΣX-N(2)-X	359.3(2)	358.2(4)	354.4(10)
Ae(1)-O(1)-Si(1)	95.43(7)	98.9(1)	101.3(3)

Ae(1)-O(1)-Si(2)	95.19(7)	98.9(1)	100.8(3)
Si(1)-O(1)-Si(2)	155.0(1)	158.7(2)	157.6(5)
ΣX-O(1)-X	345.62(14)	356.50(24)	359.7(7)
Ae(1)-N(3)-K(1)	102.17(7)	102.6(1)	105.4(2)
Ae(1)-N(3)-Si(3)	102.68(9)	103.7(1)	105.2(2)
Ae(1)-N(3)-Si(4)	109.99(9)	108.6(1)	106.4(3)
K(1)-N(3)-Si(3)	102.94(8)	102.5(1)	101.9(3)
K(1)-N(3)-Si(4)	98.97(8)	102.1(1)	100.3(3)
Si(3)-N(3)-Si(4)	135.4(1)	133.4(2)	134.4(4)
ΣX-N(3)-X	652.15(21)	652.9(3)	653.6(7)
$Plane_{N(1)Si(1)O(1)Ae(1)}$-$Plane_{N(2)Si(2)O(1)Ae(1)}$ fold angle	29.82(8)	16.33(15)	6.5(4)

IV References

1 B. J. Cosier and A. M. Glazer, *J. Appl. Crystallogr.*, 1986, **19**, 105–107.

2 *CrysAlisPRO, Journal, Oxford Diffraction / Agilent Technologies UK Ltd.*

3 A. Altomare, G. Cascarano, C. Giacovazzo and A. Guagliardi, *J. Appl. Crystallogr.*, 1993, **26**, 343–350.

4 L. Palatinus and G. Chapuis, *J. Appl. Crystallogr.*, 2007, **40**, 786–790.

5 G. M. Sheldrick, *Acta Crystallogr. A*, 2015, **71**, 3–8.

6 L. J. Farrugia, *J. Appl. Crystallogr.*, 2012, **45**, 849–854.

7 P. W. Betteridge, J. R. Carruthers, R. I. Cooper, K. Prout and D. J. Watkin, *J. Appl. Crystallogr.*, 2003, **36**, 1487–1487.

8 G. M. Sheldrick, *Acta Crystallogr. Sect. C Struct. Chem.*, 2015, **71**, 3–8.

9 O. V. Dolomanov, L. J. Bourhis, R. J. Gildea, J. A. K. Howard and H. Puschmann, *J. Appl. Crystallogr.*, 2009, **42**, 339–341.

10 L. J. Farrugia, *J. Appl. Crystallogr.*, 1997, **30**, 565–565.

11 D. B. Leznoff, G. Mund, K. C. Jantunen, P. H. Bhatia, A. J. Gabert and R. J. Batchelor, *J. Nucl. Sci. Technol.*, 2002, **39**, 406–409.

12 A. O'Reilly, M. D. Haynes, Z. R. Turner, C. L. McMullin, S. Harder, D. O'Hare, J. R. Fulton and M. P. Coles, *Chem. Commun.*, 2024, **60**, 7204–7207.

13 P. P. Power, *Inorg. Synth.*, 2018, **37**, 24–26.

14 B. A. Vaartstra, J. C. Huffman, W. E. Streib and K. G. Caulton, *Inorg. Chem.*, 1991, **30**, 121–125.

15 A. Bowles, Y. Liu, M. Stevens, I. Vitorica-Yrezabal, C. McMullin and F. Ortu, *Chem. Eur. J.*, 2023, **29**, e202301850.

16 R. J. Schwamm, J. R. Harmer, M. Lein, C. M. Fitchett, S. Granville and M. P. Coles, *Angew. Chemie Int. Ed.*, 2015, **54**, 10630–10633.